Lejla Zubcevic

Structure and Function of Bacterial

ION CHANNELS

Submitted in partial fulfilment of

the requirements for the degree of

Doctor of Philosophy

Wolfson College

University of Oxford

September 2012

Declaration

The work described in this thesis was carried out in the laboratory of Dr. Stephen Tucker in the Department of Physics, at the University of Oxford between October 2008 and September 2012. All work within this thesis is entirely my own unless otherwise stated in the text. This work has not previously been submitted for any other degree at the University of Oxford or any other university.

Lejla Zubcevic

September 2012

Abstract

KirBac channels are prokaryotic homologs of eukaryotic inwardly-rectifying potassium channels, which have served as models for gaining insight into the structure of eukaryotic channels. This thesis focuses on the structure-function relationship in these channels. The first part of this study concerns a novel KirBac channel, KirBac9.2, which contains a unique amino acid sequence in the place of the canonical GYG selectivity filter. Although expressed and purified in a stable and functional form, the protein did not form well-diffracting crystals. Functional studies suggest that KirBac9.2 is non-selective for monovalent cations and a random mutagenesis screen identified a number of activatory mutants in the cytoplasmic domains of the channel. A full electrophysiological investigation of KirBac9.2 channel function is beyond the scope of this study. However, initial studies suggest that it is possible to record currents from KirBac9.2 channels reconstituted into lipid bilayers. The second part of this thesis investigates KirBac3.1, which is a classical KirBac channel containing the consensus GYG sequence for potassium selectivity. Five high resolution structures of a mutant channel are reported, which suggest a new feature in the gating mechanism of KirBac3.1 where a rotation of the cytoplasmic domains is linked to a change in the electrostatic environment of the cytoplasmic cavity. In addition, a functional study of the KirBac3.1 showed that the channel is highly pH sensitive.

Acknowledgements

First and foremost, I owe gratitude to my supervisor Dr. Stephen Tucker, for his continued support and encouragement, as well as, at times, superhuman patience. I am particularly grateful for the financial support at the final stages of my DPhil, as well as the many hours spent critically reading this manuscript. My past and present colleagues also deserve a mention: Dr. Vass Bavro for help and advice on the crystallography projects and his displays of startling and entertaining originality; Chetan Sharma for scientific chats and for educating my palate; Matthias Schmidt for tips on PyMol and other computational tools as well as the many invitations to fancy events; Drs. Giovanna Bucci and Lijun Shang for help and advice on electrophysiological experiments; Lauriane Angue, Emma Sadler and Firdaus Abd Wahab for various helpful discussions on ion channels and experimental techniques; the honorary member of the group, Amadeus Stevenson, for providing superb computational assistance and for the many hours of interdisciplinary banter. I am also deeply indebted to the laboratory of Professor Fran Ashcroft, in particular to Drs. Christophe Girard, Constantina Fotinou and Heidi De Wet whose experience and knowledge greatly helped at the initial stages of my DPhil. I also owe gratitude to Professor Colin Nichols at the Washington University in St. Louis for allowing me to visit and conduct radioactive flux experiments in his laboratory, and to Drs. Shizhen Wang, Nazz DAvanzo and Sun Joo Lee for their scientific input, as well as for making my stay in St. Louis pleasant. I have very much appreciated interactions with Dr. Edward Lowe, who on numerous occasions helped with various aspects of my crystallography projects and Dr. Simon Newstead, who volunteered both his advice and equipment for the thermostability assays. Dr. Joao Muniz deserves much credit for assisting with X-ray data collection, and for, together with Dr. Vass Bavro, undertaking the refinement of the KirBac3.1 structures. Many thanks to my Oxford family, for everything: Hannah Sleven, Merilin Kiviorg, Gayle Lonergan, Nora Markova, Laurence Gillen, Tim Power, Ian Bellman, Ivo Vlaev and Thomas Kaufmann. Finally, I am grateful to my parents for their understanding and support, but most of all for ever being the voice of reason.

List of Abbreviations

BSA Bovine Serum Albumin

CAPSO 3-Cyclohexylamino-2-HydroxyPropane-1-Sulfonic-Acid

CHAPS 3-3-Colamidopropyl-Dimethylammonio-1-Propane Sulfate

DDAO N,N-Dimethyldecylamine-N-Oxide

DDM Dodecyl-beta-Maltoside

DEND Developmental Delay Epilepsy Neonatal Diabetes

DM Decyl-beta-Maltoside

DMPC 1,2-Dihexanoyl-sn-Glycero-3-Phosphocholine

DPhPC 1,2-Diphytanoyl-sn-Glycero-3-PhosphoCholine

EDTA Ethylene-Diamine-Tetraacetic Acid

EGTA Ethylene-Glycol-Tetraacetic Acid

Fos-MEA 10 Fos-Methylethanolamine 10

Fos12 Fos Choline 12

GPCR G-protein Coupled Receptor

GUV Giant Unilammelar Vesicle

HEGA-10 Decanoyl-N-Hydroxyethylglucamide

HEGA-8 Octanoyl-N-Hydroxyethylglucamide

HEPES 4-2-HydroxyEthyl-1-Piperazine Ethane Sulfonic acid

IPTG Isopropyl-beta-D-galactopyranoside

LDAO n-Dodecyl-N,N-dimethylamine-N-Oxide

LF12 LysoFos Choline 12

MEGA-10 Decanoyl-N-Methylglucamide

MEGA-8 Octanoyl-N-Methylglucamide

MES 2-N-Morpholino Ethanesulfonic Acid

Na Cholate 3,7,12-Trihydroxy-5-cholanoic acid, monosodium salt

Na-dodecanoyl Sarcosine N-Methyl-N-1-Oxododecyl-Glycine, sodium salt

NMDG N-Methyl-D-Glucamine

OTM n-Octyl-beta-D-Thiomaltopyranoside

PEG PolyEthylene Glycol

PIP2 Phosphatidylionsitol 4,5-bisphosphate

POPE 1-Hexadecanoyl-2-Octadecenoyl-sn-Glycero-3-Phosphoethanolamine

POPG 1-Hexadecanoyl-2-Octadecenoyl-sn-Glycero-3-Phospho-1-Glycerol

PVDF Polyvinylidene Flouride

SeSAME Seizures, Sensineural deafness, Ataxia, Mental retardation and Electrolyte imbalance

TBST Tris Buffered Saline-TWEEN

TetraDM Tetradecyl Maltoside

TriDM Tridecyl Maltoside

Tris Trisaminomethane

TRITON-X Polyethylene Glycol p-1,1,3,3-Tetramethylbutyl-Phenyl-Ether

UDM Undecyl Maltoside

Zwittergent n-Tetradecyl-N,N-Dimethyl-3-Ammonio-1-Propanesulfate

Contents

Chapter 1

Introduction

1.1 Potassium Channels

Ion channels are integral membrane proteins that form aqueous pores in the plasma membranes of cells in order to facilitate the passage of charged, inorganic ions. This movement of ions across the membrane underlies all forms of electrical activity as well as many ion transport pathways.

This thesis will focus on a subset of ion channels whose fundamental purpose is to allow rapid and selective permeation of potassium ions across the cell membrane. The extent of evolutionary conservation within the K^+ channel family is remarkably high and all potassium channels, prokaryotic and eukaryotic alike, share the basic structural elements that provide selectivity for potassium ions and a pathway across the membrane.

The first potassium channel to be cloned was the voltage-gated *Shaker* channel, isolated from the genome of the fruit fly, *Drosophila melanogaster* [1]. The identification of this gene allowed cloning of many other homologous voltage-gated channels. In addition, the high homology that exists between the pore-forming domains of potassium channels also led to identification of other classes of channels, such as the calcium-activated Big Potassium (BK) channel [2], the Inwardly Rectifying K^+ (Kir) channels and the two-pore K^+channel family. [3, 4, 5, 6]. These findings pointed to a modular design of potassium channels, where the highly conserved pore domains could be fused to a number of different regulatory domains, such as voltage sensing domains of K_V channels, calcium binding domains of BK, and the cytoplasmic domains of Kir channels (Figure 1.1).

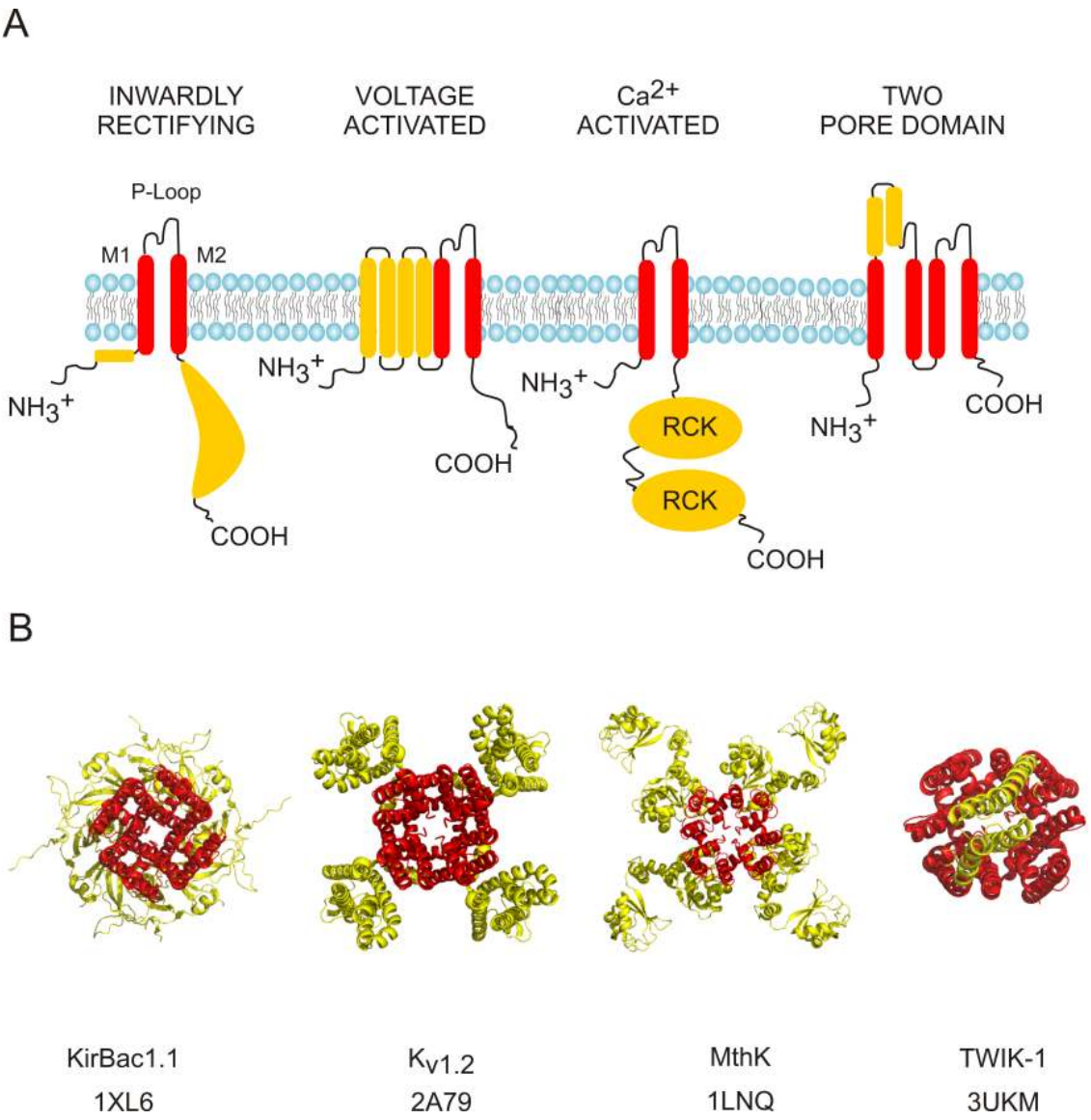

Figure 1.1: *Modular design of potassium channels. The conserved transmembrane domains and the P-loop containing the selectivity filter can be fused to a number of regulatory domains to result in potassium channels with different functional properties.* ***A*** *Shows the topology of a single subunit of inwardly rectifying (Kir), voltage gated (K_V), the calcium-activated MthK and the two-pore-domain (K2P) potassium channels with the conserved pore-forming regions coloured in red and the regulatory domains coloured in yellow.* ***B*** *A top-view of the tetrameric assemblies of a Kir channel (PDB 21XL6), the voltage gated $K_V1.2$ channel (PDB 2A79), the calcium-activated MthK channel (PDB 1LNQ) and the two-pore domain TWIK-1 channel (PDB ID 3UKM). The pore-forming regions are colorued in red, while the regulatory domains are coloured in yellow.*

1.1.1 Selectivity in Potassium Channels

The first atomic structure of a potassium ion channel was the KcsA channel from *Streptomyces lividans* [7]. Because of the high sequence homology of the transmembrane domains to eukaryotic K^+ channels, KcsA became a model for K^+ channel pore structure [8, 9, 10]

and more importantly provided the structural basis for understanding the principles of ionic selectivity.

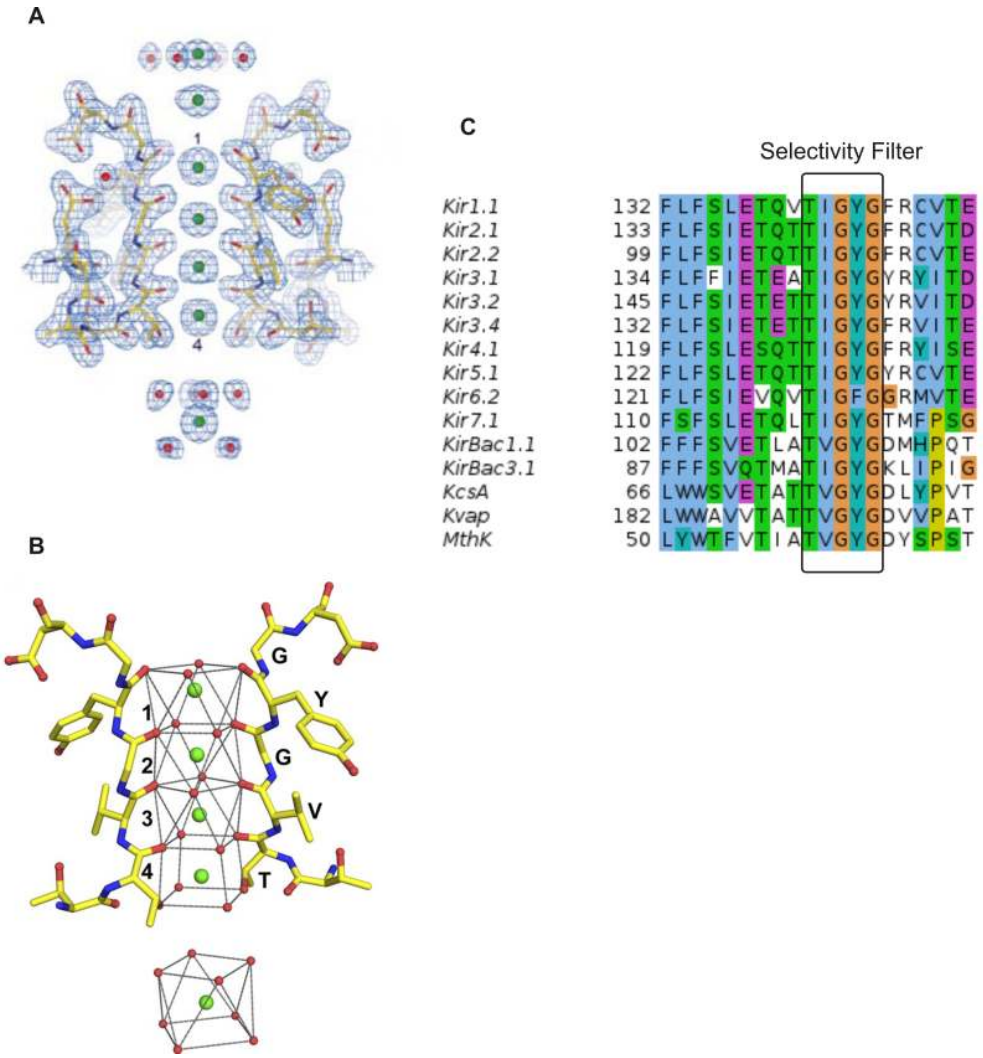

Figure 1.2: *The structural basis for potassium channel selectivity.* ***A*** *The electron density in the selectivity filter region of KcsA as observed in the high resolution structure [11]. The $2F_0$-F_c map is contoured at 2σ. Potassium ions (green spheres) are hydrated (water molecules shown as red spheres) before entering the narrow selectivity filter region. Figure adapted from [11]* ***B*** *Ionic coordination in the selectivity filter of a potassium channel. Potassium ions (green spheres) are coordinated by the carbonyl oxygens of the peptide backbone (oxygen atoms coloured in red). The potassium ion outside the selectivity filter is coordinated by eight water molecules (red spheres). The carbonyl oxygens of the TVGYG motif coordinate potassium ions by mimicking their hydration shell. Figure adapted from [12]* ***C*** *Conservation of the selectivity filter region (boxed) in different types of potassium channels.*

In solution, a potassium ion is surrounded by a shell of water molecules. The ion in this hydrated state is too large to pass through the selectivity filter of the channel, and must therefore shed these water molecules prior to entering the selectivity filter. The carbonyl

oxygens that form the backbone of the T(V/I)GYG motif mimic the hydration shell of the ion, and thereby compensate for the energetic cost of dehydration [11]. A sodium ion has a smaller ionic radius than potassium, but its charge density is higher which means that it attracts a bigger hydration shell. Consequently, the energy required to dehydrate the sodium ion is higher than that required to remove the hydration shell of a potassium ion [13]. So, a combination of its physicochemical properties result in sodium being less permeant than potassium: firstly, the energetic cost of dehydration of sodium is high, and secondly, once dehydrated, the sodium ion is too small to be coordinated by the potassium channel selectivity filter pore in a manner which would sufficiently compensate for the energy expended on dehydration.

Alterations of the selectivity filter motif can affect the permeability of the channel to different ions and point mutations in this region have been found to render the filter non-selective, i.e. enable permeation of most monovalent cations [14]. It is interesting to note that mutations of the GYG motif can result in a non-selective channel, but never in a channel which is exclusively selective for another ion. Indeed, the selectivity filters of the non-selective cyclic nucleotide-gated (CNG) channel as well as that of the NaK channel [15, 16] are homologous to the potassium selective filters. However, substitution of the crucial GYG residues with other amino acids renders these channels non-selective (Figure 1.3).

Potassium channel pores are occupied by multiple potassium ions simultaneously, which form a queue in the selectivity filter that is pushed forward when a new ion enters the pore [17]. The selectivity filter has multiple binding sites for potassium ions, but only two are thought to be occupied at any one time, eg. sites 1 and 3 or sites 2 and 4 (Figure 1.2 A and B). The rapid permeation of potassium ions through the filter is facilitated by the electrostatic repulsion between the ions themselves [18]. This mechanism of permeation appears to be universal to all potassium channels.

By contrast, the recently solved structures of the prokaryotic Na_VAb [19], Na_VRh [20] and Na_VMs [21] sodium channels indicate that the selectivity filter contains only one sodium coordination site and that sodium ions may permeate in a semi-hydrated form, with only one of the glutamate residues in the filter interacting with the ion directly while the remaining three glutamate sidechains coordinate its hydration shell [19]. However, the mechanism of sodium channel selectivity is still not fully understood as a structure with sodium ions coordinated in the selectivity filter is yet to be solved.

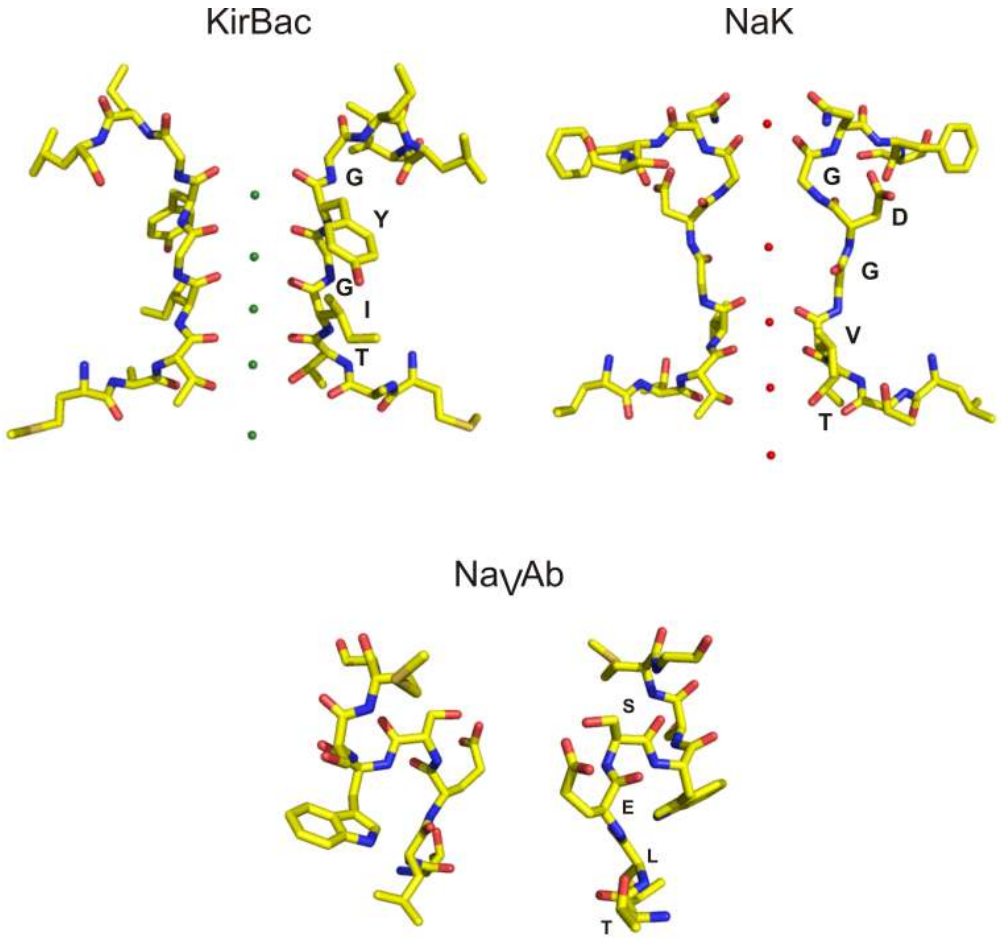

Figure 1.3: *Comparison of the selectivity filters of a K^+ channel, the non-selective NaK channel and a prokaryotic Na^+ channel. K^+ ions are shown as green spheres, and Na^+ ions as red spheres. The selectivity filter sequences of a potassium channel and the non-selective NaK channel differ only in the substitution of a tyrosine with an aspartate. The substitution results in a loss of ionic coordination sites and renders the channel permeable to both sodium and potassium ions. The selectivity filter of the voltage-gated sodium channel from Arcobacter butzleri, $Na_V Ab$, is substantially different, most notably for containing fewer ionic coordination sites. It is thought that the glutamate coordinates a partially hydrated sodium ion as it permeates the filter, and that the ion is fully rehydrated as it passes by the backbone carbonyl groups of the leucine residue. No sodium ions have been resolved in the selectivity filter [19].*

1.1.2 Origins of the Resting Membrane Potential

The cell membrane potential is the difference in electric potential across the membrane. Chemical gradients across the membrane are fundamentally important for the establishment of this potential difference and they arise through the activity of the Na^+-K^+ATPase, which ensures that the $[Na^+]_{IN}$ is lower than $[Na^+]_{OUT}$, whilst $[K^+]_{IN}$ is higher than $[K^+]_{OUT}$. The presence of K^+ selective leak channels in the membrane then allows the flow of K^+ ions down its chemical gradient, and it is this efflux of positively charged ions that generates an intracellular environment which is more negative than the outside, consequently resulting in a transmembrane potential.

The resting membrane potential is the equilibrium condition where the electrical potential is balanced by the chemical potential. The equilibrium potential (E_X), also known as the reversal potential, can be quantified for each type of ion using the Nernst Equation which makes it possible to calculate theoretical reversal potentials if the ionic concentrations are known:

$$E_X = \frac{RT}{zF} ln \left(\frac{[C_{out}]}{[C_{in}]} \right)$$

where R is the ideal gas constant, T is the temperature in Kelvin, z is the valence of the ionic species and F is Faraday's constant. The membrane potential is given by the Goldman equation as an average of each contributing ion's reversal potential which also takes into account the relative permeabilities ($\frac{P_X}{P_{tot}}$) of these ions across the membrane.

$$E_m = \frac{P_{K^+}}{P_{tot}} E_K + \frac{P_{Na^+}}{P_{tot}} E_{Na} + \frac{P_{Cl^-}}{P_{tot}} E_{Cl}$$

Because of the K^+ selective leak channels found in most cells this equilibrium depends significantly on the potassium gradient across the membrane, and the resting potential for most cells is close to the reversal potential (E_K) for potassium ions (-70mV).

1.1.3 The Inwardly Rectifying (Kir) Potassium Channels

Most ion channels have a fixed conductance and function as resistors in the cell membrane. According to Ohm's law $V = IR$, which means that most channels, when open, have a linear current/voltage relationship. However, Kir channels are unique in that their current/voltage behaviour is non-linear: during hyperpolarisation the inward currents are significantly larger than the outward currents at corresponding depolarising voltages.

However, in living cells their main role is to mediate outward potassium currents. When open at rest, Kir channels maintain the membrane voltage close to the potassium Nernst potential (-60mV to –90mV). However, due to their rectifying properties, during depolarisation following influx of sodium ions, eg. during an action potential, they are effectively closed in spite of the fact that the membrane potential under these conditions favours efflux of potassium ions. This prevents the channel short circuiting the action potential during depolarisation. Interestingly, this rectification is not intrinsic to the pore of the channel, but mediated by a voltage dependent block by intracellular magnesium ions and polyamines [22].

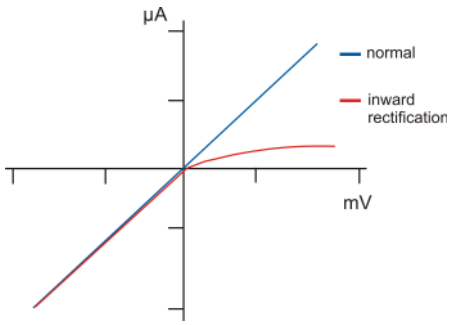

Figure 1.4: *A schematic of a current-voltage relationship in a fixed-conductance channel (normal) and an inward rectifying channel (inward rectification). Inwardly rectifying channels produce larger currents at hyperpolarising voltages than at corresponding depolarising voltages. Therefore, their current-voltage relationship is non-linear.*

1.1.3.1 Kir Channel Superfamily

The eukaryotic Kir family consists of 7 subfamilies. There is a high degree of conservation within the family, but nevertheless they all display distinct functional profiles that have evolved to fulfil their individual purposes in the cells and tissues where they are expressed.

Kir1.1, or the ROMK (Renal Outer Medullary K^+ channel) was the first Kir channel to be cloned and is expressed primarily in the kidney where it is involved in K^+ homeostasis. Kir1.1 is a pH dependent [23, 24, 25] channel, and mutations in the *KCNJ1* gene have been found to cause Type II Bartter's syndrome, a severe renal disorder [26, 27].

By contrast, the Kir2.x family are strongly rectifying channels. They are expressed ubiquitously, in particular in the nervous system and in the heart. Mutations in Kir2.x channels have been found to cause Andersen's syndrome, which is a complex multisystem disorder that affects many different tissues [28, 29].

The Kir3.x family, also known as GIRK (G-Protein activated Inward Rectifier K^+ channels) are strongly rectifying channels that are activated by G-protein$\beta\gamma$ subunits [30, 31]. They are found in the heart and the brain as well as in endocrine tissues. Mutations in Kir3.4 that result in loss of selectivity have been identified in aldosterone-secreting adenomas which increase secretion of aldosterone and cause severe hypertension [32]. However, it appears that the severity of the symptoms as well as the appearance of adenomas correlates with the type and the severity of the mutation [33].

The Kir4.x family are weak rectifiers with a strong pH dependence [34, 35]. They are mainly expressed in non-excitable tissues, such as glial cells and the kidney. SeSAME syndrome, another complex multisystem disorder, which causes a number of severe neurological symptoms and renal dysfunction, is caused by loss-of-function mutations in the Kir4.1 channel [36, 37, 38]. Furthermore, it has been suggested that Kir4.1 is the target of an autoimmune response in a subgroup of multiple sclerosis patients [39].

Kir5.1 is the only member of the Kir family that does not appear to form functional homotetramers. It is typically found in a heterotetrameric assembly with members of the Kir4.x family [40, 41, 42]. Although no disease-causing mutation has been identified in Kir5.1, it has been shown that disruptions of this gene in mice can result in a severe renal phenotype [43].

Kir6.x channels coassemble with the sulfonylurea receptor (SUR) to form K_{ATP} channels [6]. These ATP-sensitive channels play a crucial role in linking the metabolic state of the cell to membrane excitability. Kir6.2 channels are expressed in neurons as well as in the pancreas, and activatory mutations in the *KCNJ11* gene have been shown to cause several types of neonatal diabetes, often linked with severe neurological symptoms such as in the DEND syndrome [44, 45, 46].

Kir7.1 channels are mainly expressed in the brain, and their defining feature is a very low single channel conductance [5]. Mutations in the *KCNJ13* gene that affect the selectivity of the channel have been found to cause the Snowflake Vitreoretinal Degeneration, a hereditary disorder causing early-onset cataract and retinal detachment [47].

1.1.3.2 Kir Channel Structure

Kir channels are comprised of four subunits which assemble around a central pore to form a tetrameric channel. Each monomer consists of an N-terminus, an amphipathic helix termed "slide helix", the outer transmembrane helix, the pore-helix, selectivity filter, the inner helix, the C-linker and the cytoplasmic domain (Shown in Figure 1.5).

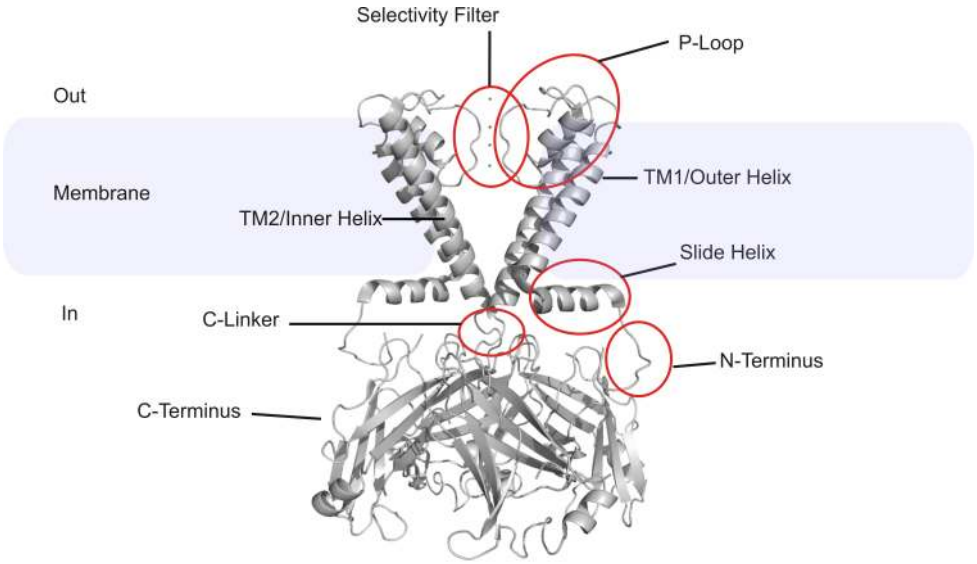

Figure 1.5: *The architecture of a Kir channel. For ease of viewing, two transmembrane subunits have been removed. Potassium ions in the selectivity filter are shown as green spheres. The transmembrane and cytoplasmic domains are linked by a short positively charged sequence called the C-linker, which is involved in PIP_2 binding [48, 49].*

The transmembrane domains provide the passageway for ions through the cell membrane. Negatively charged residues in the inner helix are responsible for polyamine and magnesium block that underlies inward rectification in strong rectifiers [50, 51, 52, 53]. During depolarisation, when the membrane potential favours efflux of positive ions, polyamines and magnesium block the conductive path by binding in the transmembrane pore of the channel thereby preventing efflux of potassium ions.

The cytoplasmic domains form an extended pore and facilitate inward rectification by concentrating polyamines in the cytoplasmic cavity. Negatively charged residues in the cytoplasmic cavity also appear to control the conductance levels of the channels by increasing the local concentration of potassium ions [54, 55, 56, 57, 58, 59]. The cytoplasmic domains of Kir channels contain the binding sites for modulators such as G$\beta\gamma$ and sodium [30, 31, 49].

1.1.3.3 Gating

The transition between the open and closed states of the channel in response to modulating stimuli is known as "gating". Gating of Kir channels is modulated by a number of factors, such as pH, lipids and lipid-like molecules, intracellular sodium and G-proteins.

The first channel to be crystallised in an open conformation was the calcium activated MthK from *Methanobacterium thermoautotrophicum* [60, 61]. Comparison of its structure with that of the closed conformation of the KcsA channel suggested that the opening of the helix bundle crossing relied on bending of the inner helices at a conserved "glycine hinge" residue [62]. Subsequent studies of other potassium channels showed similar mechanisms of opening, suggesting that the bending of the inner helices around the conserved glycine residue is a universal feature of gating. This will be addressed in more detail in Chapter 4.

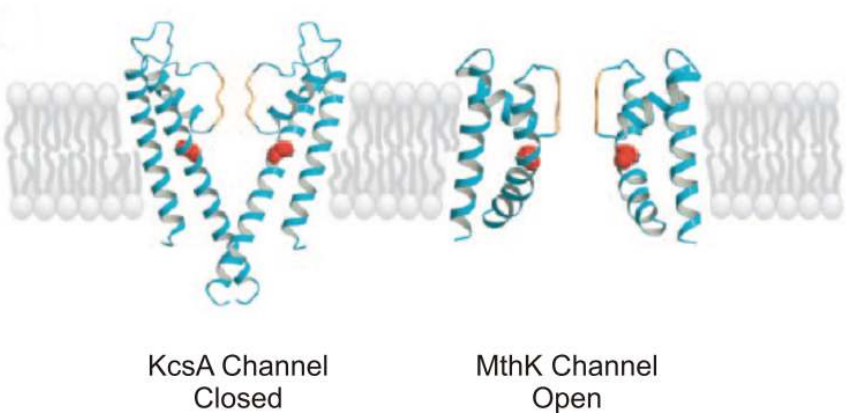

Figure 1.6: *A comparison of the pore-forming domains of KcsA in the closed state and MthK in the open state. Gating at the helix bundle gate depends on bending of the inner helix (TM2) at a conserved "glycine hinge" residue (red spheres). Figure adapted from [63]*

1.1.3.4 Regulation by pH

All Kir channels are pH sensitive in that their activity is inhibited by low intracellular pH. However, only a few are sensitive to changes in the physiological range of pH: Kir1.1, Kir4.1 and the heteromeric Kir4.1/5.1. Hence, these channels are defined as pH sensitive [64, 65, 66, 35, 25, 67, 68]. It has been suggested that the pH sensitivity relies on multiple titratable sidechains within the cytoplasmic domains [65]. However, the molecular mechanisms underlying this pH regulation are not yet fully understood.

1.1.3.5 Regulation by PIP_2

Phosphatidylinositol 4,5-bisphosphate (PIP_2) is an anionic phospholipid found at the inner leaflet of the plasma membrane and is required for the function of all Kir channels [69], as well as many other eukaryotic channels and transporters [70, 71, 72, 73, 74, 75, 76].

The requirement for PIP_2 is thought to have two reasons. Firstly, PIP_2 is only found in the plasma membrane which means that unwanted channel activity can be avoided during trafficking in the ER and the Golgi apparatus, where the membranes lack PIP_2. Secondly, the concentration of PIP_2 is linked to the activity of Phospholipase C, an enzyme activated by various G-protein coupled receptors (GPCRs). An increase in PLC enzymatic activity depletes the membranes of PIP_2 and thereby reduces Kir channel activity. This therefore provides a link between the activity of Kir channels and GPCRs.

Recent crystal structures of Kir2.2 [48] and the heteromeric Kir3.2/3.4 [49] have demonstrated that the binding site for PIP_2 is at the interface between the transmembrane and the cytoplasmic domains, in the region known as the C-linker. The charged residues of the C-linker region play a crucial role in the binding of PIP_2 .

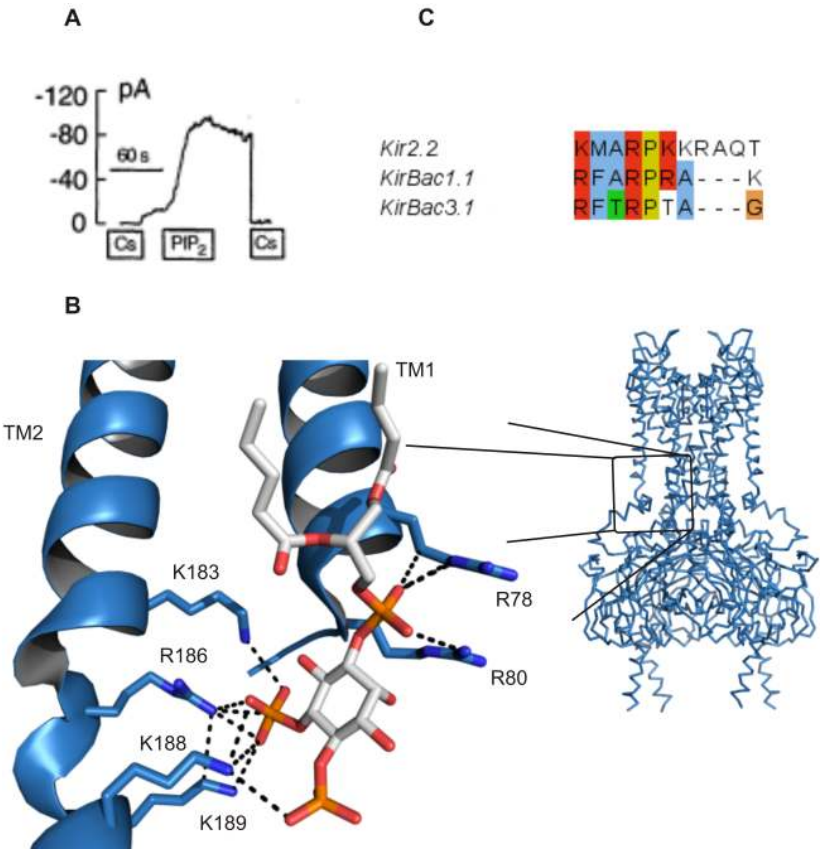

Figure 1.7: *Kir channels and PIP_2.* ***A*** *The requirement for PIP_2 for channel activity observed in inside-out excised patch experiments. Following excision of a patch, channel activity decreased due to wash-out of native PIP_2 from the membrane. Perfusion of the patch with a buffer containing PIP_2 resulted in channel currents which could be blocked by caesium. Adapted from [70].* ***B*** *The PIP_2 binding site in Kir2.2 (PDB 3SPI). The structure of the tetrameric channel is shown on the right side of the figure. A close-up of the C-linker (enclosed in the black box on the tetrameric structure) is shown in the centre of the figure. PIP_2 is shown as sticks, and coloured according to atom type: carbon, grey; oxygen, red; phosphorus, orange. The molecule is coordinated by the positively charged residues K183, R186, K188, K189 (all shown as sticks). The dashes represent the interactions that are involved in binding PIP_2.* ***C*** *The alignment compares the sequences of the eukaryotic Kir2.2 C-linker with that of the prokaryotic KirBac1.1 and KirBac3.1 channels, which are shorter and lack some of the charged residues that are involved in binding PIP_2.*

1.2 Prokaryotic Kir (KirBac) Channels

In 2001, Durell and Guy reported the existence of a family of prokaryotic channels with a high overall homology to eukaryotic Kir channels [77]. These were referred to as KirBac channels. At the time of their discovery, structural studies of eukaryotic membrane proteins still presented a big challenge. In 2003 a structure of the soluble C-terminal domain assembly of a eukaryotic channel had been solved [58], but it was still unknown how the transmembrane domains were coupled to this cytoplasmic assembly.

The ability to express and purify these prokaryotic homologs soon resulted in crystal structures of KirBac1.1 in 2003 [78], and KirBac3.1 in 2004 [79]. In particular the structure of KirBac1.1 was important as it provided the first full image of an inward rectifier, and showed how the transmembrane domains are coupled to the cytoplasmic assembly through the slide helix. These structures gave, for the first time, a scaffold for building full molecular models of eukaryotic Kir channels and made it possible to begin to relate structural and functional studies in this family of K^+ channels.

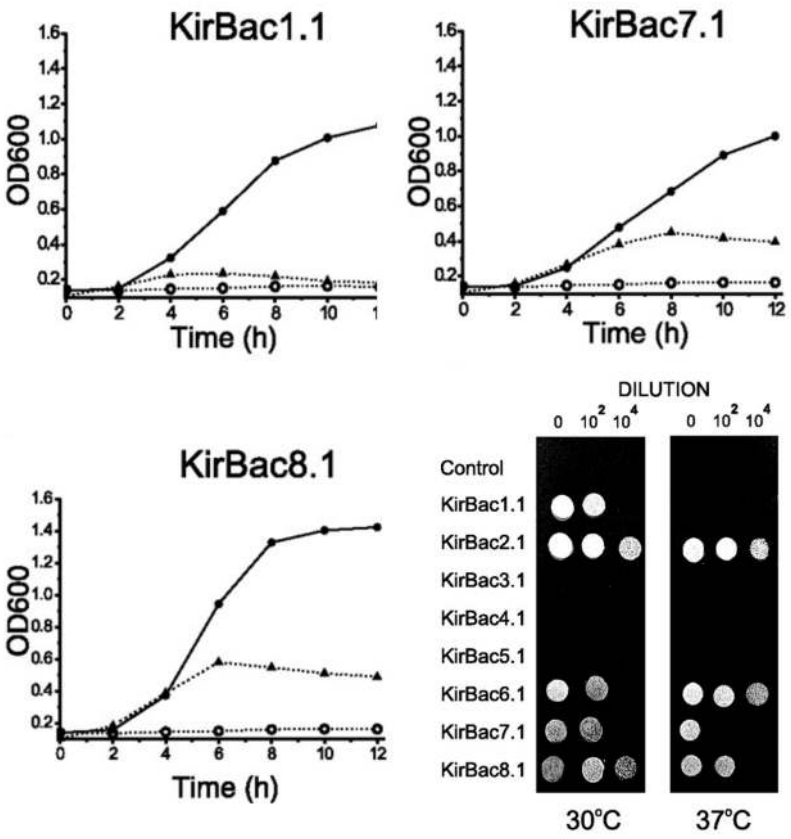

Figure 1.8: *Functional studies of KirBac channels. The complementation assays showed functional variety within the members of the family. Droptests show that KirBac3.1, KirBac4.1 and KirBac5.1 could not support growth of K^+ auxotrophic E.coli, while KirBac1.1, KirBac7.1and KirBac8.1 showed robust activity. Growth curves of KirBac1.1, KirBac7.1 and KirBac8.1 showed an improvement in growth upon lowering of growth temperature. Solid line represents 30°C, while the dashed line with a triangle mark shows growth at 37°C. Figure adapted from [80].*

1.2.1 Functional studies of KirBac channel

Initially, the only functional assays available for studying KirBac channels were genetic complementation assays, which employ K^+ auxotrophic strains of *E. coli* to probe channel function. A study of eight KirBac channels (KirBac1.1-KirBac8.1) using this genetic complementation assay suggested that there is distinct functional variety within the KirBac family [80]. These results revealed that KirBac3.1, KirBac4.1 and KirBac5.1 were apparently non-functional in *E. coli*. By contrast, expression of KirBac1.1, KirBac7.1 and KirBac8.1 was found to be toxic to the cells, due to high levels of activity (Figure 1.8).

Subsequent success in electrophysiological studies of KirBac channels has been limited, since the expression of functional prokaryotic channels has proven difficult in heterologous expression systems, such as cultured mammalian cells and oocytes. However, reconstitution of purified protein into lipid bilayers and liposomes resulted in a series of successful functional studies of the KirBac1.1 channel [81, 82, 83, 84, 85]. These studies involved both rubidium uptake assays, as well as patch clamp studies of the channel-containing liposomes.

As predicted by the complementation experiments, KirBac1.1 exhibited robust levels of activity. Interestingly, the activity of the channel was found to be strongly inhibited, not activated, by PIP_2 (Figure 1.9B). Electrophysiological experiments revealed that KirBac1.1 is not blocked by polyamines, and consequently does not exhibit rectification (Figure 1.9A). However, a point mutation in the inner helix, TM2, which introduces an aspartate in the place of an isoleucine at the "rectification control site" turns the channel into a strong rectifier (Figure 1.10).

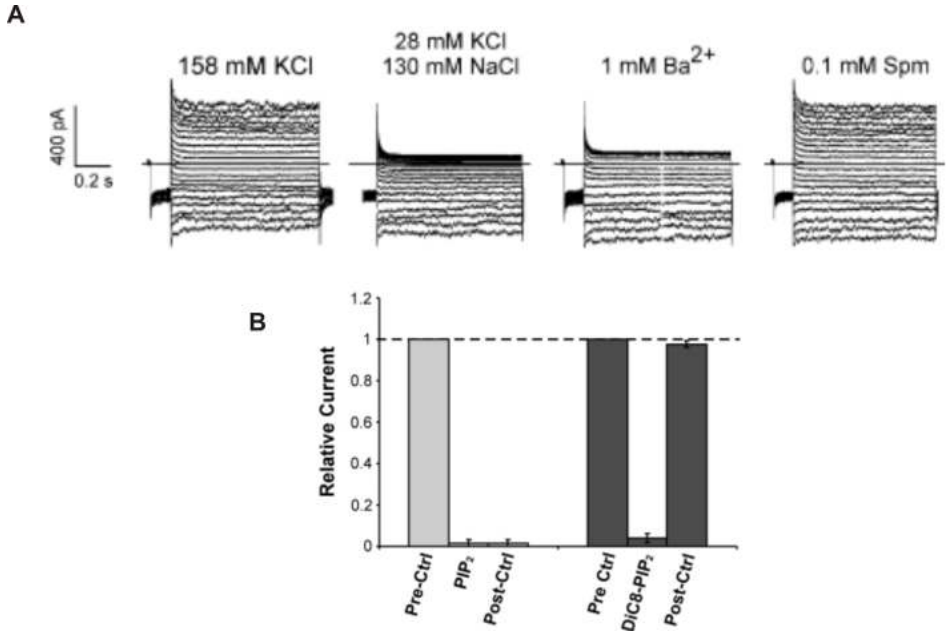

Figure 1.9: *Electrophysiological studies of the wild-type KirBac1.1 reconstituted into liposomes.* ***A*** *Representative currents from an inside-out patch of giant liposomes reconstituted with KirBac1.1. The channel conducts potassium in preference to sodium. The currents are blocked by Ba^{2+}, but not by spermine.* ***B*** *The bars represent the data from recordings in the presence of PIP_2 and its synthetic, water-soluble analogue, diC8-PIP_2. The pre-control bars represent the currents recorded before the application of PIP_2. The PIP_2 and diC8-PIP_2 bars represent currents after perfusion of the patch with buffers containing 5μM PIP_2 and diC8-PIP_2 respectively. Post-control bars represent the currents recorded after wash-out of PIP_2 and diC8-PIP_2. Figure adapted from [81].*

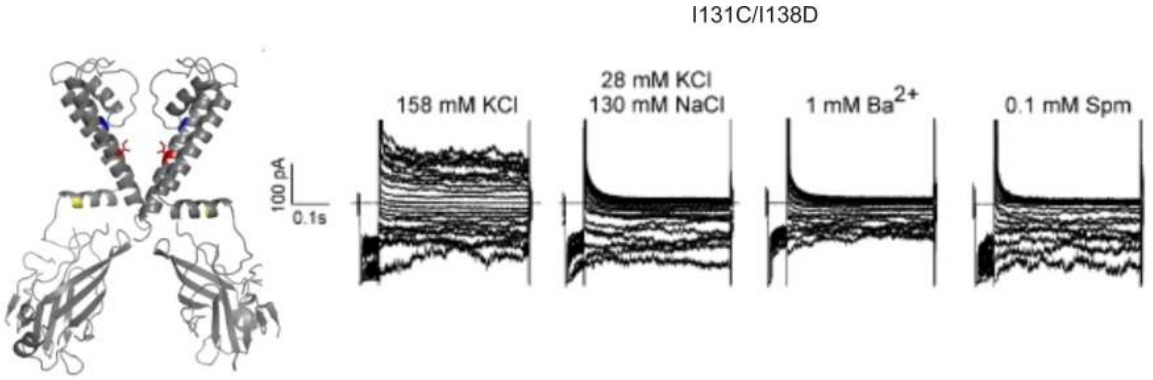

Figure 1.10: *Introducing an aspartate in the inner helix of the KirBac1.1 turns the channel into an inward rectifier, which exhibits voltage dependent block by spermine. The location of the I138D mutation is shown on the KirBac1.1 structure as red sticks. The tetramer-stabilising mutation I131C is shown in blue. The right-side panel shows representative currents from an inside-out patch of giant liposomes reconstituted with KirBac1.1 I131C/I138D mutant. The channel currents are inhibited both by Ba^{2+} and spermine. Figure adapted from [81].*

1.3 Novel KirBac Channels

KirBac channels are defined by their homology to eukaryotic Kir channels, both in the selectivity filter and the transmembrane and the cytoplasmic domains. However, a novel group of KirBac channels with unique P-loop sequences was previously identified in the Tucker Laboratory. They were identified from a BLAST search of the Integrated Microbial Genomes (IMG) Database, using the KirBac1.1 sequence as a query. Their respective genes were isolated from the native organisms by PCR of genomic DNA, and subsequently sequenced in order to confirm that no sequencing errors of the genomic DNA had occurred. These channels retained a high homology (~80%) to other KirBac channels, but their selectivity filter sequences deviated significantly from the canonical K^+ channel GYG motif. Their existence suggests that the Kir channel architecture can be adapted for permeation of ions other than potassium.

The KirBac9.1 gene was isolated from *Anaeromyxobacter dehalogenans 2CP-C*, a metal-reducing bacterium found in uranium-containing soil [86]. KirBac9.2 was found in the closely related *Anaeromyxobacter sp. FW109-5*, while KirBac11.1 was isolated from *Gemmatimonas aurantiaca T-27T*. Little is known about *Gemmatimonas aurantiaca* since its existence was only recently reported, and the T-27T strain is so far the only one that has been successfully cultured [87].

As mentioned above, despite their clear overall homology with other KirBac channels the P-loops of these novel subunit diverge significantly from the canonical T(V/I)GYG motif, as shown in Figure 1.11. The selectivity filter of the KirBac9.2 channel, which contains alanine and proline residues, does not bear any resemblance to any known selectivity filter. The selectivity filter of KirBac9.1 contains glutamate and aspartate residues which are also found in the selectivity filters of sodium and calcium channels. However, it still remains to be investigated whether this channel permeates sodium and calcium ions. The selectivity filter of KirBac11.1 has some similarity to the non-selective NaK channel filter.

Previous complementation data had shown that all three channels, despite their novel selectivity filter sequences could support growth of K^+-auxotrophic *E. coli* to some extent, suggesting that they were, to some extent, permeable to potassium ions. However, since their selectivity filter sequences deviate so dramatically from the consensus GYG motif, it is probable that they may be non-selective.

The existence of these novel KirBac channels suggests a modular evolution of parts of the

channel, possibly to adapt an existing structure to new environmental demands. This is, as mentioned in section 1.1, to some extent observed in the family of voltage-gated ion channels, where the overall architecture ofK_V, Na_V and Ca_V channels is preserved but the pore-forming domains, including the selectivity filter regions, have adapted to select for different ions. However, the homology between the novel KirBac channels and the rest of the KirBac family is much greater, and the differences, unlike between the K_V and Na_V/Ca_V channels, are restricted specifically within the selectivity filter. A full sequence alignment is shown in Figure 1.12.

1.4 Thesis Overview

The aim of this thesis is to provide an investigation into the structure-function relationship in KirBac channels. The initial focus of the research was KirBac9.2. Chapter 2 contains an account of the steps taken to successfully express and purify the protein, as well as documents the attempts to obtain well-diffracting crystals for structural studies. Chapter 3 provides an insight into the functional properties of KirBac9.2, where the selectivity of the channel is investigated using a radioactive tracer flux assay. The chapter also describes the search for activatory mutations, using a random mutagenesis approach. Finally, it reports the steps towards an electrophysiological study of KirBac9.2. Chapter 4 focuses on another, more classical, member of the KirBac family, KirBac3.1. Here, we report five high resolution atomic structures of a double gating mutant (S129R/S205L) obtained by X-ray crystallography. Finally, Chapter 5 describes the approaches taken towards a functional characterisation of KirBac3.1.

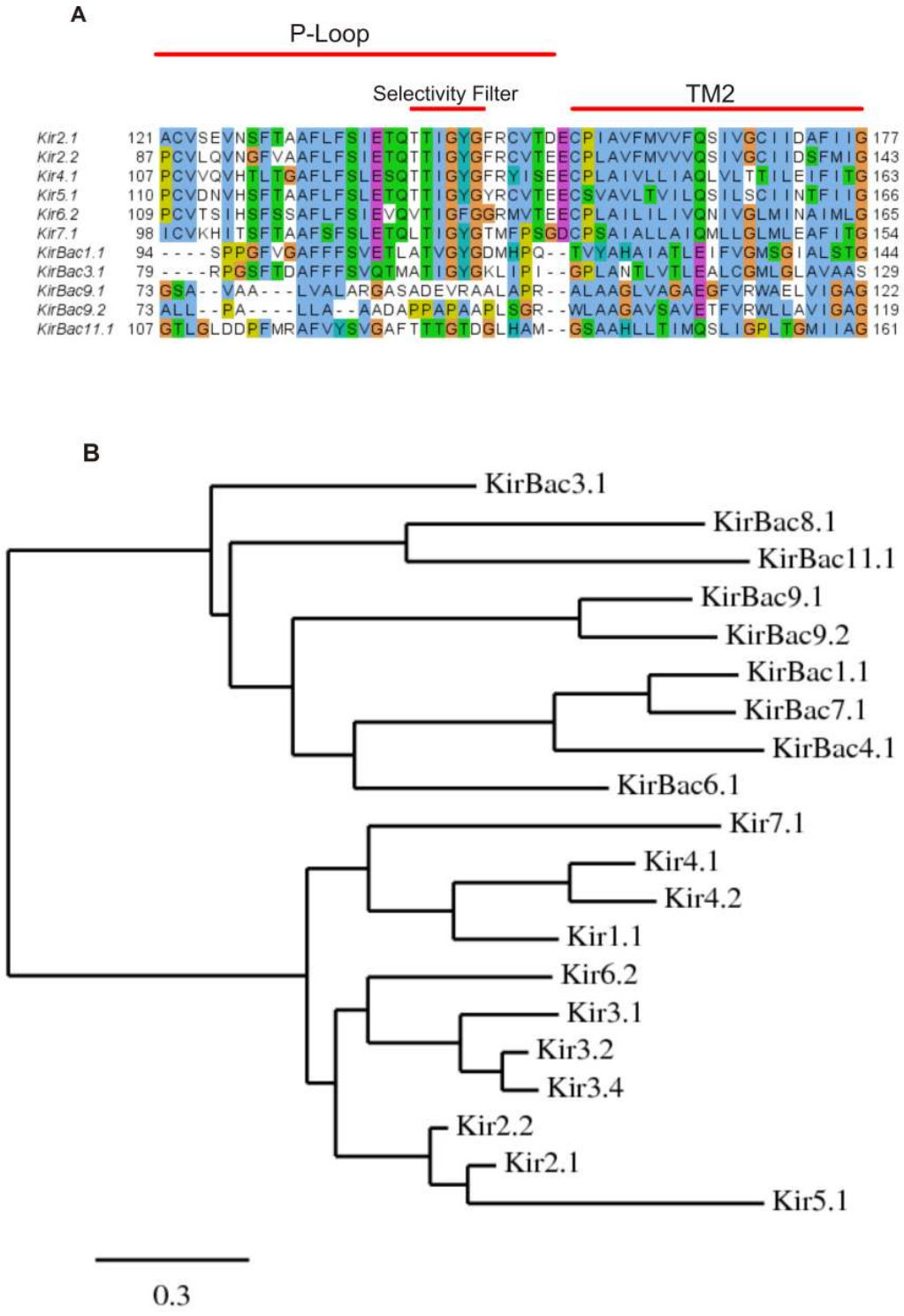

Figure 1.11: ***A*** *An alignment of the selectivity filter regions of the eukaryotic Kir and prokaryotic KirBac channels.* ***B*** *A phylogenetic tree of the eukaryotic and the prokaryotic channels. The dendogram was constructed using an online server at www.Phylogeny.fr. The legend denotes the scale of the phylogenetic distance.*

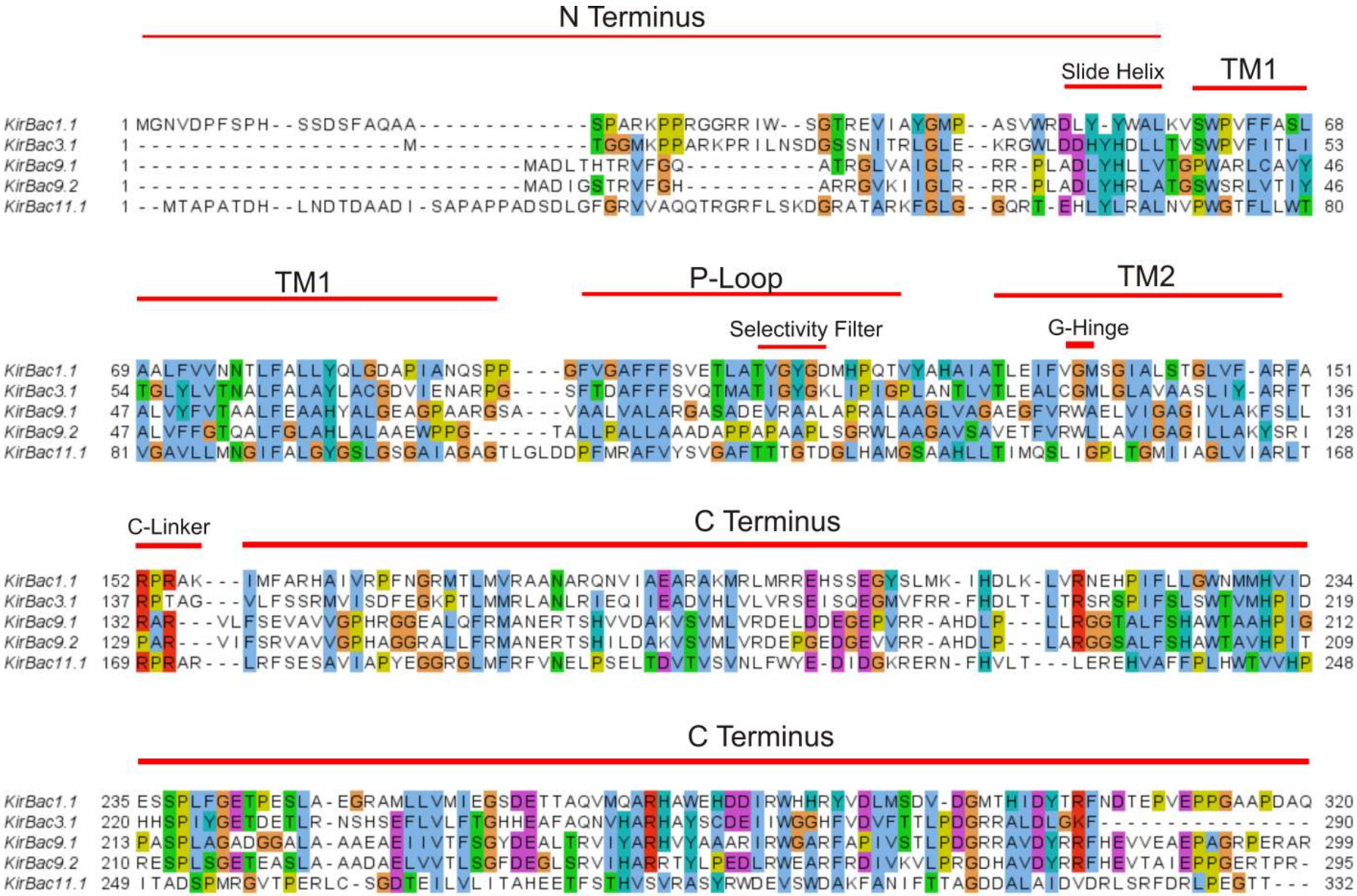

Figure 1.12: *Full alignment of the novel KirBac channels with KirBac1.1 and KirBac3.1.*

Chapter 2

Crystallisation of KirBac9.2, a Novel Prokaryotic Kir Channel

2.1 Introduction

This chapter focuses on the work leading towards solving the atomic structure of the KirBac9.2 channel using X-ray crystallography. X-ray crystallography remains the most powerful and widely used approach for determining high resolution three dimensional structures of proteins. X-rays are short length electromagnetic waves which can be used to resolve the structural details within a protein molecule, such as hydrogen bonds (2-3Å) and covalent bonds (1-2Å) [88]. However, there are several steps that need to be considered between identifying a protein target and successfully solving its structure.

The first hurdle in the process involves expressing and purifying the protein of interest. In the early days of protein research, obtaining proteins for biochemical as well as structural studies meant that large quantities of native tissues had to be processed and the proteins of interest isolated via a number of biochemical steps. However, the advances in molecular genetics made in the last two decades of the $20th$ century revolutionised the field. Genomic sequencing, recombinant protein technology and the development of microbial expression systems have all contributed to the dramatic increase in proteins available for both structural and functional studies [89, 90, 91].

In the field of structural biology, the low cost as well as the ease of manipulation and handling have made *E.coli* the protein expression system of choice [89]. X-ray crystallography in particular demands large quantities of protein for screening of crystallisation conditions.

The more protein that can be purified, the larger the number of conditions that can be screened, and consequently the chances of success are increased. Once expression of the target protein has been achieved, the protein needs to be purified in a stable and, preferably functional form.

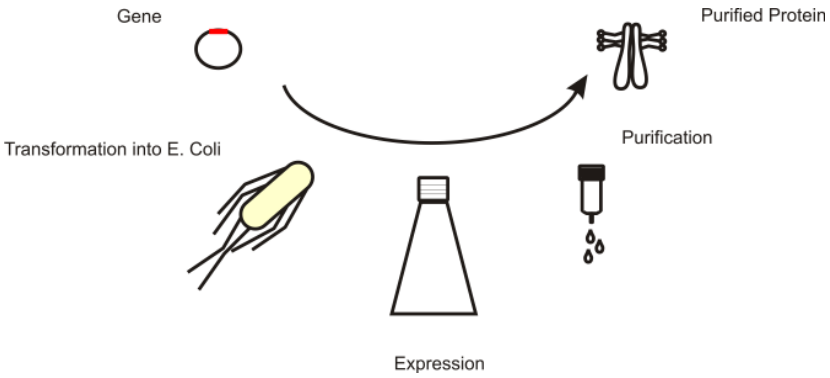

Figure 2.1: *Progress from gene to purified protein. The gene encoding the protein of interest is transformed into E.coli. A culture of the transformed cells is grown, and the expressed protein isolated through a number of purification steps.*

The purity of the protein in crystallographic terms refers both to its chemical purity, i.e. isolating the protein without contaminants, as well as conformational purity, i.e. having a monodisperse protein solution, without aggregates or various oligomeric states and truncations [92, 93]. In the case of membrane proteins, the purification from cells involves extraction with detergent. Not all detergents are suitable for this process, and often the appropriate detergent needs to be identified empirically. Typically, a non-ionic detergent with a large micelle, such as the sugar based Decyl-β-Maltoside (DM), is a good starting point. A larger micelle ensures that the hydrophobic regions of the membrane protein are shielded from the solvent, and thereby prevents the protein from precipitating.

Crystallisation involves transition of the protein molecules from a soluble to a solid state [94]. In practice, this is achieved by placing a saturated protein sample into a crystallisation liquor made up of precipitants, buffers and salts that will promote formation of nuclei and crystal growth. The role of crystallisation buffers is to influence hydration and solubility of protein molecules, as well as the electrostatic interaction between them. Screening of crystallisation buffers is the most time consuming aspect of X-ray crystallography as it is impossible to predict in advance which crystallisation buffers will have a beneficial effect on

the ability of a given protein to crystallise. Vapour diffusion is the most common method of crystallisation, where the concentrated protein sample is mixed with a crystallisation buffer and placed over a well containing a larger volume of the same buffer in a sealed container. As the difference of vapour pressure in the well and in the drop leads to equilibration, the water is drawn out of the crystallisation drop. This then leads to a supersaturated protein solution, which is a term to describe a non-equlibrium state where for a brief period the protein in solution has exceeded its limit of solubility. In order for the equilibrium to be established, the protein must come out of solution, either in the form of amorphous or crystalline precipitation [95]. Crystallisation can be refined by creating secondary screens, also known as 'grid screens', based on conditions which produce promising results, i.e. crystalline precipitation. The buffers in a grid screen are designed to expand the initial condition by varying the precipitants and their concentration, the pH and salt type and content. Addition of small molecules, the so called 'additives' to the crystallisation buffers can also benefit the crystallisation process [96].

In the case of membrane proteins, the choice of crystallisation detergent can be of crucial importance. Often, a membrane protein will be most stable and most soluble when it is solubilised in a detergent with a large micelle. However, large micelles in crystallisation can prove problematic as they may act to occlude parts of the protein which could otherwise be engaging in crystal contacts. This can lead to crystals that diffract poorly, as the contacts between molecules are lacking or weak. Choosing a detergent that forms small micelles can dramatically improve the quality of crystals. Unfortunately, small micelle detergents cannot be applied to all proteins, as they will often cause precipitation. Stability of a given protein in different types of detergent is another parameter that needs to be determined empirically [97].

In order to obtain structural data from a protein crystal, the sampe is bombarded by X-rays and their scattering is recorded in the form of a diffraction pattern which carries information about the position of atoms within the structure of the protein. The relationship between the position of a reflection on a diffraction pattern and the resolution of the data is inverse, so that low resolution data is found near the centre of the diffraction image and the resolution increases the further reflections are removed from the centre [88, 98, 99]. Diffraction data should be of 4Å resolution or better to build an accurate atomic model of a protein molecule.

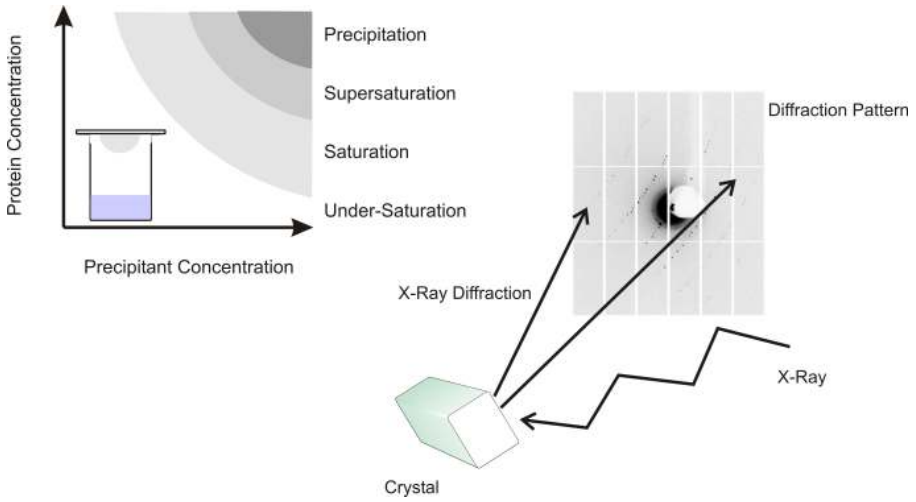

Figure 2.2: *Crystals are grown using the principle of vapour diffusion. Crystals appear when the drop has reached supersaturatioin, as shown in the phase diagram. Crystals are bombarded with X-rays and the resulting diffraction is recorded on a detector.*

2.2 Materials and Methods

2.2.1 Cloning and Codon Optimisation of KirBac9.2

The wild-type KirBac9.2 gene was isolated from the genomic DNA of *Anaeromyxobacter sp.* (strain Fw109-5) by PCR by Dr. Stephen Tucker. A gene encoding the same amino acid sequence, but with the codons optimised for expression in *E.coli* was synthesised by Genscript Ltd. The new gene also contained a thrombin cleavage site (LVPRGS sequence) and a 6xHis affinity purification tag. The codon optimised KirBac9.2 was cloned into a pQE60Lac vector.

2.2.2 Expression of KirBac9.2

The codon optimised KirBac9.2 in the pQE60Lac vector was transformed into Rosetta pLysS *E.coli* (Novagen), and plated on carbenicillin (0.05 mg/ml) and chloramphenicol (0.03 mg/ml) Luria Broth agar plates. One colony was picked to inoculate starting culture, which was grown overnight. 0.5L Luria Broth (Sigma Aldrich) in a 2L baffled conical flask containing antibiotics was inoculated with 10ml starting culture. The cells were grown at 37°C with shaking (220rpm) until the optical density (OD600) reached 0.4, after which they were transferred to 19°C . Once the cells reached OD600 0.85, expression was induced with 0.5mM Isopropyl-β-D-thiogalactopyranoside (IPTG). Cultures were grown at 19°C overnight. Cells were harvested by centrifugation for 15 minutes at 12,000 RCF at 4°C (Beckmann JLA8.1 rotor). Pellets were collected, weighed and frozen at –80°C for storage.

2.2.3 Purification of KirBac9.2

Pellets were resuspended in 25ml per 5g bacterial pellet in a buffer of 50mM Tris pH 7.8, 150mM NaCl, complemented with one tablet of EDTA free protease cocktail (Roche), 2μg/ml DNAseI (Sigma Aldrich) and 0.5mg/ml lysozyme (Fluka). The resuspension was passed through a cell distruptor 4-6 times (Stansted Fluid Power Ltd) at a pressure of ~ 12000psi.

2.2.3.1 Preparation of Membranes

The lysate was centrifuged for 10 minutes at 7,000 RCF to remove large debris and unbroken cells. Supernatant was transferred into ultracentrifuge tubes, and spun at 200,000 RCF for

90 minutes. Membrane pellets were resuspended and washed in 50mM Tris pH7.8, 1M NaCl before being centrifuged for another hour at 200,000 RCF. An additional wash cycle was preformed in 50mM Tris pH 7.8, 150mM NaCl. Resuspension of membranes was aided by a small acrylic painting brush. The washed membranes were weighed and resuspended in 20 ml per gram membranes 50mM Tris pH 7.8, 150mM NaCl, 30mM Dodecyl-β-Maltoside (DDM) (Affymetrix) .

2.2.3.2 Solubilisation and Purification

The membranes resuspended in detergent buffer were incubated for 3 hours, on a rotating wheel at 4°C. Following solubilisation, the membranes were centrifuged at 70,000 RCF for 30 minutes to remove debris and unsolubilised material. To the cleared solubilised membranes 10mM imidazole was added before they were loaded on cobalt TALON affinity resin (Takara). The cobalt acts to bind specifically to the C-terminal 6xHistidine tag, thereby isolating the KirBac9.2 channel from the rest of the proteins solubilised from the membrane fraction [100]. Before loading the solubilised membranes, TALON resin was pre-equilibrated in 50mM Tris pH 7.8, 150mM NaCl, 10mM imidazole. 1ml resin slurry was used per 1.5g washed membranes. The binding was performed overnight on a rotating wheel at 4°C. The unbound material was removed by gravity flow using a 50ml column (BioRad) The resin was washed with 25 times column volume of each of the following wash buffers: Wash 1. 50mM Tris pH 7.8, 150mM NaCl, 10mM imidazole, 2mM DDM; Wash 2. 50mM Tris pH 7.8, 500mM NaCl, 20mM imidazole, 2mM DDM; Wash 3. Tris pH 7.8, 150mM NaCl, 80mM imidazole, 2mM DDM

The channel was finally eluted from the TALON resin in 30ml elution buffer consisting of: 50mM Tris pH 7.8, 150mM NaCl, 400mM imidazole, 1mM DDM.

2.2.3.3 Gel Electrophoresis and Western Blotting

Samples and protein standards (Novex Sharp Pre-Stained Protein Standard, Invitrogen) were loaded onto a SDS gel (12-14% Bis-Tris, Invitrogen) and the gel was run at 200V for 40 minutes. Gels were stained by SafeStain (Invitrogen).

Where indicated, the protein bands were transferred from the gel to a PVDF (polyvinylidene fluoride) membrane using iBlot Dry Blotting System (Invitrogen) for western blotting.

The membranes were incubated in TBST buffer (50mM Tris pH 7.8, 150mM NaCl, 0.05% Tween 20) complemented with 5% skimmed milk powder for 1 hour at room temperature. Following incubation, the membranes were washed twice in TBST buffer. Anti-His antibody (anti-His (C-terminal) antibody, Alkaline Phosphatase conjugated, Invitrogen) was diluted (1μl in 2000μl) in TBST buffer. The PVDF membranes were incubated with the antibody for 2 hours at room temperature. The excess antibody was removed by washing the membranes three times in TBST buffer. The visualisation of the his-tagged protein was performed by application of a chemiluminescent Alkaline Phosphatase substrate (Novex AP Chemiluminescent Substrate) directly to the PVDF membranes.

2.2.3.4 Size Exclusion Chromatography

The eluate was concentrated on a 100kDa cut-off filtration device (Millipore) and filtered through a 0.22μm membrane (Millipore) to remove any precipitation. Following filtration, the protein was loaded onto a size exclusion column (Superdex 200, 10/300 Tricorn column, GE Healthcare), equilibrated with 50mM Tris pH 7.8, 150mM NaCl, 1mM DDM, to remove aggregates and isolate the tetrameric channel. The profile was monitored at 280nm absorbance (Unicorn software, ÄKTA, GE Healthcare). All buffers were filtered through a 0.22μm membrane (Milipore) and degassed using a vacuum pump for 60 minutes. The tetrameric channel eluted at ~ 12ml with a 0.5ml/min flow rate.

2.2.4 Crystallisation of KirBac9.2

The pure tetrameric protein was concentrated to 2.5 mg / ml - 25 mg / ml. Concentration was determined by absorption at 280nm using a Nanodrop spectrophotometer (Thermo Scientific). The protein was filtered through a 0.22 μm membrane prior to crystallisation.

The initial screening included commercial screens from Molecular Dimensions and Hampton Research designed for membrane proteins. These were 'MemGold', 'MembFac' and 'MemSys' from Molecular Dimensions and 'Detergent Screen' and 'Additive Screen' from Hampton Research. All primary screening was done using the sitting drop diffusion method in 96-well double-drop plates (Molecular Dimensions). Each chamber has a large well, containing the reservoir solution and two small crystal growth wells. The experimental set-up typically involved pipetting 100μl crystallisation buffer into the reservoir by hand, and using the Mosquito

robot (TTP Lab Tech) to aliquot the protein and crystallisation buffer into the crystal growth wells [101]. The crystallisation drops contained 150nl protein and 150nl buffer in the top well, and 150nl protein and 300nl buffer in the bottom well. The plates were incubated at room temperature (22°C). Drops were monitored once a day during the first week, and once a week for the first month for appearance of crystals

2.2.4.1 Optimisation of Initial Screening

After the initial screening, the conditions which favoured crystal formation were isolated, and expanded into grid screens. Each condition was expanded to 24- 48 new conditions, varying the type and concentration of precipitants and salts, as well as varying the pH. In separate experiments, the initial conditions were also expanded by addition of small molecules from the Additive Screen and detergents from the Detergent Screen (Hampton Research). All optimisation experiments were done in hanging drop format, as this was found to be most favourable for crystal growth. The drops were set up in Nextal hanging drop plates (Qiagen) by hand. The wells were filled with 400μl crystallisation buffer. The drop size was kept at 4μl, and unless otherwise stated, contained 1.6μl concentrated protein, 0.4μl additive/detergent and 2μl crystallisation buffer. Where no additive was present, the volume of both protein and buffer was 2μl.

2.2.5 Fluorescent Thermostability Assay

A cysteine mutation was introduced into the KirBac9.2 gene in position T44. The protein was expressed and purified as described previously. 1μl protein at 8 mg / ml was added to 150μl buffer containing 50mM Tris pH 7.8, 150mM NaCl and detergent at 3 times critical micelle concentration (CMC) in a black Nunc plate. Frozen N-[4-(7-diethylamino-4-methyl-3-coumarinyl)phenyl]maleimide dye dissolved in dimethyl formamide to a stock concentration of 4 mg / ml was diluted to 40 μg / ml with the same buffer as the protein, complemented with 1mM DDM. 1.5μl diluted dye was added to the protein, and a clear cover was placed on the plate. Fluorescence emission was measured at 463nm on the SpectraMax plate reader (Molecular Devices) at 30°C. Recordings were made every 5 minutes for 3 hours, with short shaking intervals between each reading [102]. Detergents tested included OTM, LF12, HEGA-8, Na-

Cholate, UDM, MEGA-10, Fos-MEA10, LDAO, Fos12, MEGA-8, TetraDM, Na-dodecanoyl sarcosine, HEGA-10, DDAO, Zwittergent.

2.2.6 Crystallisation in Lipidic Environments

2.2.6.1 Crystallisation in the Lipid Cubic Phase

The protein was concentrated and prepared for crystallisation as described above. The cubic phase experiments were set up according to manufacturer's instructions (NeXtal CubicPhase Qiagen). The crystallisation wells in these plates are treated with a dehydrated layer of monolein, to which 400nl concentrated protein is added. The plate was incubated at room temperature for 3 hours, to allow the lipid layer to swell and begin the spontaneous formation of the lipid cubic phase. Following the incubation, the crystallisation buffers were aliquoted into the reservoirs and then into the crystallisation wells. The plates were sealed and left at 22°C.

2.2.6.2 Crystallisation in Bicelles

To prepare bicelles, 30mg DMPC (Avanti Polar Lipids) and 10mg CHAPS (Sigma Aldrich) were mixed in 1ml filtered milliQ water to form a white suspension. Cycles of heating and cooling were repeated until the suspension became clear. The bicelles were diluted to 40% with water, and the dilution used for crystallisation. The concentrated protein was mixed with the 40% solution of bicelles in ratios 2:1, 3:1 and 4:1. The mixture was used to set up crystallisation experiments.

2.2.7 Crystal Harvesting

Crystals were harvested using nylon loops (Hampton Research) or LithoLoops (Molecular Dimensions). Cryoprotection was achieved by washing the crystal in mother liquor with increased precipitant concentration before flash freezing. Where this was not possible, the altered mother liquor was added directly to the crystallisation drop before the crystal was harvested [103].

2.2.8 Crystal Testing

Diffraction of crystals was recorded at ESRF beamline ID23-2 and at Diamond Lightsource beamlines I02, I03, I04 and I24.

2.2.9 Data Analysis

Diffraction data was analysed using iMosflm [104].

2.2.10 Molecular Biology

2.2.10.1 Chimeras

Chimeric KirBac9.2 and KirBac1.1/3.1 were obtained by overlap extension PCR [105, 106]. Unique restriction enzyme cleavage sites (NcoI/BglII) were introduced at 5' and 3' ends of the fragments and used for cloning into the pQE60Lac vector.

2.2.11 Homology Modelling

A homology model of KirBac9.2 was created using the SWISS-MODEL server [107, 108, 109], with the KirBac3.1 structure as a template (PDB ID: 2WLJ).

2.3 Results and Discussion

2.3.1 Codon Optimisation and Sub-Cloning of KirBac9.2

The initial attempts to express KirBac9.2 using the wild-type DNA sequence isolated from the native organism failed. This native sequence is very GC rich, which could have posed problems during expression in *E.coli* . Codon usage bias can be a significant factor when attempts are made to express a protein in a non-native environment [110]. Therefore, we synthesised a new construct of KirBac9.2 encoding the same amino acid sequence, but with the codons optimised for expression in *E.coli*. The codon optimised KirBac9.2 gene was cloned into a modified pQE60 vector, containing the Lac repressor and therefore more tightly regulated than the standard pQE60 plasmid.

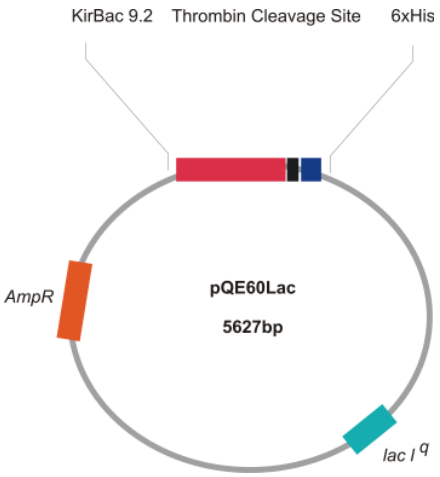

Figure 2.3: *The pQE60Lac plasmid carrying the KirBac9.2 gene for expression. The gene was fused to a thrombin cleavage site as well as a 6xHis affinity tag at the C-terminal end.*

2.3.2 Optimisation of KirBac9.2 Expression

For the purposes of expressing the KirBac9.2, we tested two strains of *E.coli*: the Codon Plus BL21(DE3) RP and the Rosetta BL21(DE3) pLysS. The Codon Plus RP cells contain a plasmid encoding the tRNAs for rarely occurring codons in *E.coli* for arginine (AGA, AGG) and proline (CCC). The Rosetta strains are also designed to supply the cells with codons rarely used in bacteria. They carry a plasmid encoding tRNA for isoleucine (AUA), arginine

(AGG/ AGA), leucine (CUA), proline (CCC) and glycine (GGA). The plasmids encoding the tRNAs for rare codons in both strains carry the choloramphenicol resistance gene.

The expression was tested after 3 hours and 15 hours post-induction growth, at 37 ° C and 19 ° C. It was found that both strains were capable of producing KirBac9.2 (not shown).

2.3.3 Optimisation of KirBac9.2 Purification

Having established that the protein could be expressed, the next step was to optimise its purification. The initial protocol for purification was adapted from the protocols established for the successful purification of KirBac1.1 [78] and KirBac3.1 [79, 111]. These protocols involved breaking the cells and extracting the protein directly from the lysate at room temperature using a maltoside detergent. However, this approach, regardless of the cell line used for expression, resulted in very low, and very unstable yields (shown in Figure 2.4 as Initial Purification).

Possible reasons for the low yield and stability were identified as long exposure to a high temperature and to proteases during the solubilisation step, and potential co-purification with harmful contaminants. To optimise the purification three adjustments to the initial protocol were made:

Firstly, solubilisation was performed at 4 ° C. Secondly, to minimise exposure to proteases, the membrane fraction was isolated before solubilisation. Thirdly, to limit the possibility of contaminants binding to the affinity resin, low concentration of imidazole was added to the binding step. The experiments showed that extracting the protein from isolated membranes resulted in the largest proportion of tetrameric channel. The optimisation results are shown in Figure 2.4. Interestingly, greater protein yields were obtained the Rosetta strain than from the Codon Plus strain (not shown).

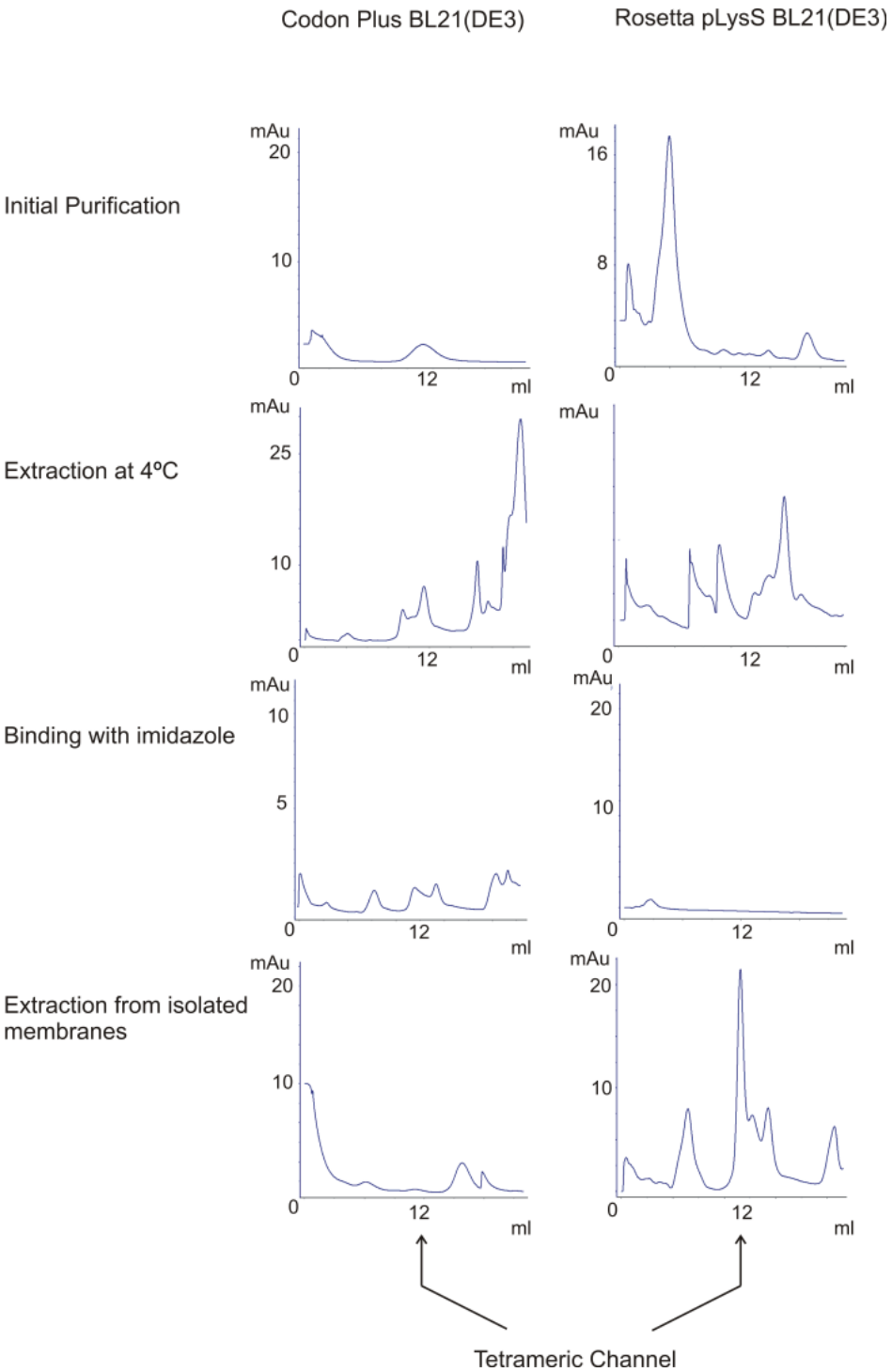

Figure 2.4: *Results of the optimisation of KirBac9.2 purification. Initial purification involves solubilisation from total cell lysate. In the Extraction at 4 °C panel this solubilisation step was performed in a cold room. Binding of the His-tagged protein to Co^{2+} resin was performed in the presence of 10mM imidazole to minimise binding of contaminants. Finally, the membrane fraction was isolated by ultracentrifugation before the solubilisation step was performed. Tetrameric fractions, which on a Superdex200 column (GE Healthcare) elute at ~ 12ml [112, 113], are indicated with an arrow. .*

The final protocol was therefore changed to include a membrane isolation step, followed by extraction at 4 ° C and binding in the presence of 10mM imidazole. Further purification was obtained by washing the membranes: the initial membrane fraction was resuspended once in a high salt buffer, to remove any contaminants loosely attached to the membranes. The wash was repeated in a low salt buffer to remove excess salt that could interfere with the channel. The final result of the optimisation was monodisperse, tetrameric channel that was stable at 4 ° C for >1 week, as shown in Figure 2.5.

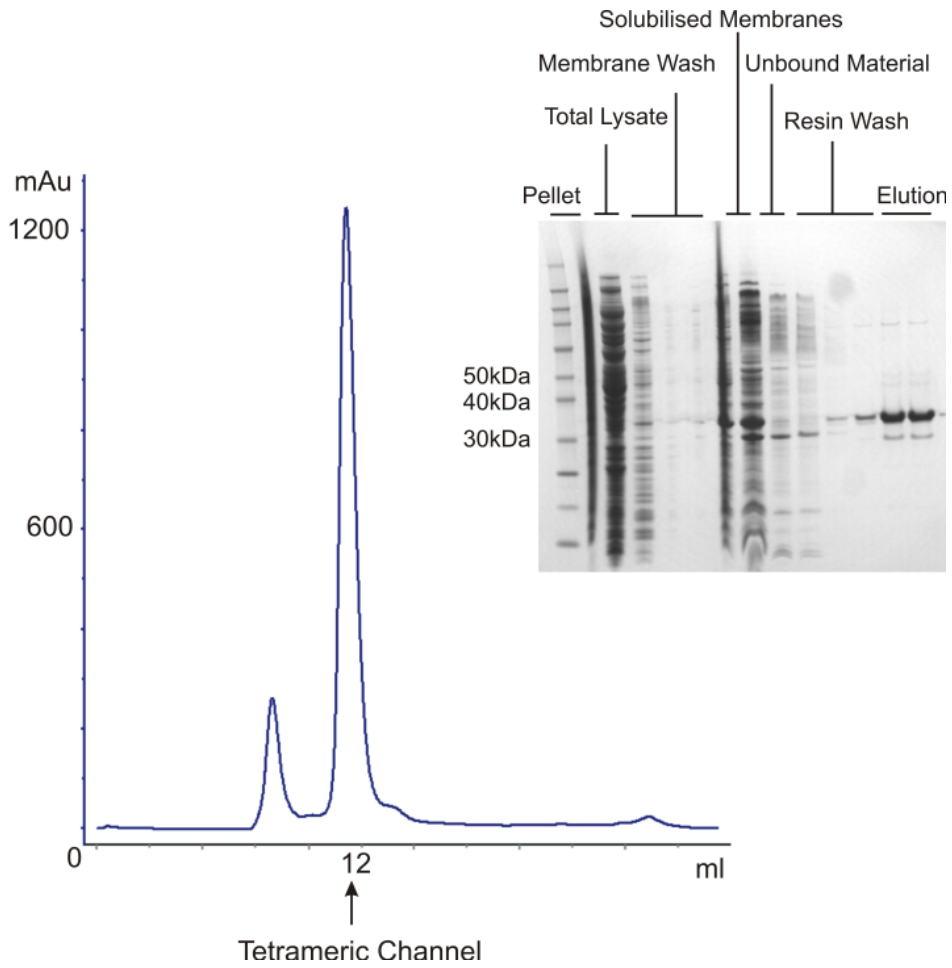

Figure 2.5: *The results of the optimised purification. The channel is purified from isolated and washed membranes and eluted in 0.5mM TriDM. The size exclusion profile shows that the channel is stable in its tetrameric form. The Coomassie stained SDS-PAGE gel shows all purification steps: total harvested bacterial pellet (Pellet), total lysate, the supernatant obtained by ultracentrifugation in the membrane isolation and wash steps (Membrane wash), total contents of solubilised membranes (Solubilised Membranes), material which did not bind to the TALON affinity resin (Unbound Material), the material which was eluted from the column during the resin washing steps (Resin Wash) and the purified protein (Elution).*

2.3.4 Crystallisation of KirBac9.2

2.3.4.1 Choosing a Suitable Crystallisation Detergent

Initially, the protein was purified in TriDM, a maltoside detergent which forms large micelles. This detergent had previously been used for purification and crystallisation of KirBac3.1 and KirBac1.1 [78, 111], and given that it kept the channel stable, seemed a suitable starting point for our structural studies. It was immediately noticed that the protein could be concentrated to extremely high concentrations (in excess of 25 mg / ml) in this detergent without precipitating. However, while screening the commercial crystallisation conditions in 96-well plates, it became apparent that lots of conditions grew gel-like, hexagonal crystals. The diffraction of these crystals, shown in Figure 2.6A, indicated that they were likely to be crystals of detergent. Small molecules, such as salts and detergents, crystallise in small unit cells [88]. On a diffraction pattern, this is reflected in the large distances between the spots. Protein molecules, on the other hand, crystallise in relatively large unit cells, and consequently the spaces between the diffraction spots of these crystals are small.

The large micelle of TriDM, apart from being easily concentrated may also act to prevent the protein molecules from making contact with each other, making it possible to concentrate the protein to such high levels without precipitating [114, 115]. In order to improve on this issue, the effect of other maltoside detergents on the stability of KirBac9.2 was tested and the results are shown in Figure 2.7. Here, the length of the alkyl chain seemed to be important: DM was found to cause precipitation, whereas the channel was stable in DDM. Therefore, DDM was chosen for the next round of crystallisation experiments. The lowest concentration of detergent that prevents aggregation was determined by gel filtration to be 1mM, 5 x critical micelle concentration (CMC) of DDM[116].

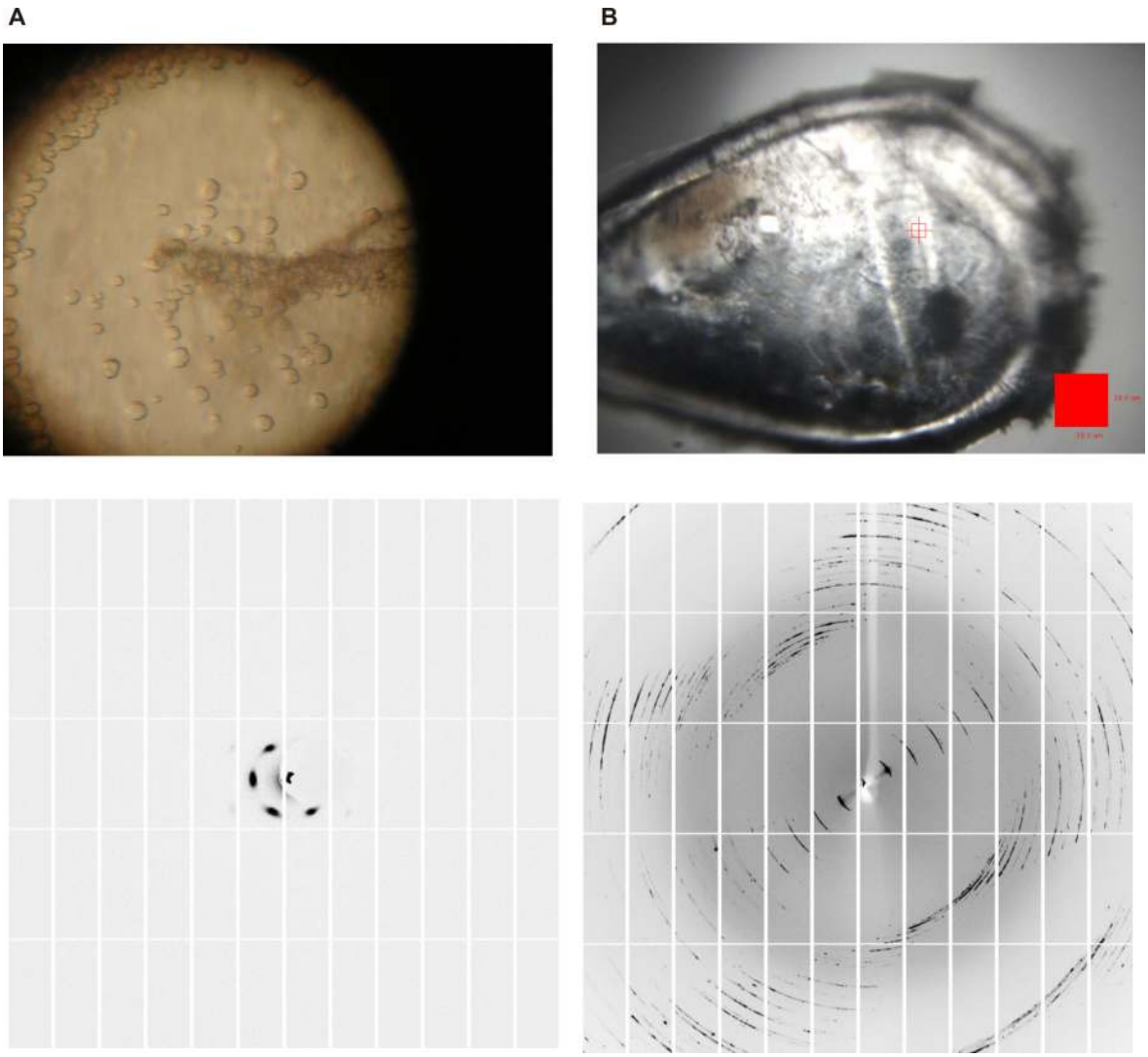

Figure 2.6: *Examples of diffraction of detergent and lipid crystals.* ***A*** *shows detergent crystals grown in TriDM (top panel) and their diffraction (bottom panel). These crystals grew in a large number of conditions in the Memgold, Membfac and Memsys screens when TriDM was used as the crystallisation detergent for KirBac9.2.* ***B*** *Shows an example of possible lipid crystals grown in a lipid cubic phase screen (top panel) and their diffraction (bottom panel). These long, thin crystals appeared in nearly all lipid cubic phase and bicelle crystallisation experiments*

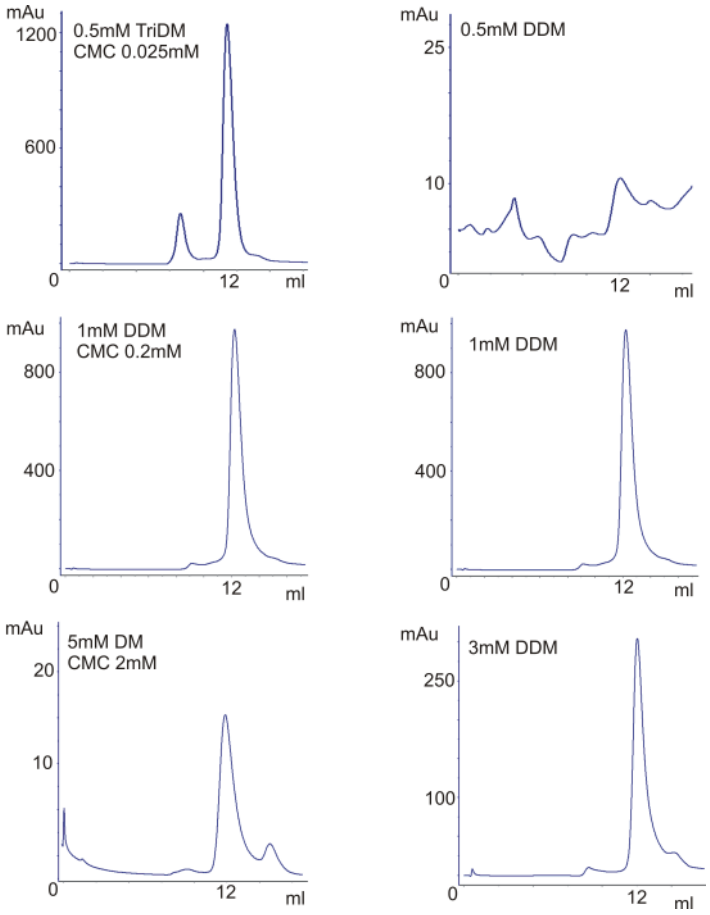

Figure 2.7: *In order to identify a detergent suitable for crystallisation, the oligomeric state of KirBac9.2 was tested on a size exclusion column in the presence of TriDM, DDM and DM. The use of TriDM and DDM both resulted in nice elution profiles. DM caused precipitation and consequently resulted in a much lower protein yield. Because of its smaller micelle size, DDM was chosen over TriDM as the crystallisation detergent. The minimal concentration of DDM required to keep the channel in its tetrameric form (1mM) was determined using a size exculsion column.*

2.3.4.2 Initial Crystallisation Results

There are a number of commercially available crystallisation screens which combine different salts, buffers, precipitants and additives. We initially commenced screening with commercial crystallisation buffers optimised for membrane proteins. The compositions of these buffers have been compiled from data mining available membrane protein crystal structures and the conditions in which successful crystal growth was achieved.

We started by concentrating the protein to 5 - 10mg / ml, and screening its ability to form crystals in the commercial buffers. The experiments were set up on 96-well sitting drop plates, and the drop size varied between 150-400nl. The small volumes were achieved by using Mosquito, a dispensing robot. A number of conditions produced crystalline dust, i.e. a

myriad of microcrystals. These conditions were identified, and in an attempt to grow larger crystals, larger drops were set up in both 24-well sitting drop and hanging drop plates. As the equilibration time is longer for larger volumes, the nucleation process is slowed down, and chances of getting fewer, larger crystals are increased [95]. Indeed, this proved to be the case. Relatively large crystals appeared, and their diffraction patterns indicated that they were likely to be protein, which encouraged further optimisation of crystallisation conditions.

2.3.4.3 Optimising the KirBac9.2 Crystallisation

Inclusion of small molecules in the crystallisation experiments has often proven to improve the diffraction of protein crystals. The nature of these stabilising molecules is vaguely defined, and the commercially available additive screens encompass, among other things, ions, sugars, lipids, reducing agents, chaotropes, cross linkers, amino acids, detergents and volatile organic compounds [117, 118, 119, 120, 121]. Cross screening of additives against the isolated crystallisation conditions was done on 96 well plates, and following identification of additives which produced microcrystals in 96 well plates, larger drops were set up. The best result was obtained from crystals grown in the presence of LysoFoscholine12, a synthetic lipid-like detergent. These crystals diffracted to 12.65Å, which offered some initial encouragement.

2.3.4.4 Analysis of KirBac9.2 Crystal Data

The asymmetric unit within a crystal is the smallest unit of volume that by application of *symmetry* operations can reproduce the unit cell. By contrast, the unit cell is the smallest unit of volume that by application of *translation* can reproduce the entire crystal [88].

The data collected from crystals grown in the presence of LysoFoscholine12 allowed us to calculate the space group and the unit cell. These were estimated to be P 63 and the unit cell dimensions a, b, c= 169.17, 169.17, 309.26. The unit cell is large, and a possible cause for this can be a very large solvent content within the crystal. Membrane protein crystals have a higher solvent content than crystals of soluble proteins, typically around ~70%. High solvent content correlates with poor resolution and quality of diffraction data, since the molecules within the crystal do not form sufficient contacts [114, 98].

One method that reduces the unit cell size and increases the packing density by reducing the solvent content is dehydration of the crystals. This can be done in a number of ways: by "drying" the crystal before flash freezing in liquid nitrogen, or by equilibrating the crystal

with solutions with an increasing concentration of precipitant [122, 123].

Both of these approaches were tried, and indeed both improved the diffraction of the crystals from 13Å to ~9Å, as shown in Figure 2.8B. However, no change was observed in the unit cell size.

Another explanation for the large unit cell could be that the assymetric unit of the crystals containts many copies of the protein. This may indicate the presence of some inherent disorder and flexibility within the protein, which prevents it from staying uniform.

It is interesting to note that the best crystals were obtained with addition of the lipid like detergent LysoFoscholine12. It is commonly accepted that lipids can improve stability of membrane proteins in crystals [97] and we therefore decided to explore a few avenues relating to crystallisation and lipids.

2.3.5 Effects of Lipids on Crystallisation of KirBac9.2

2.3.5.1 Crystallisation with Lipid-like Detergents

The first and most obvious step was to test crystallisation in the presence of other available lipid like detergents. Here we focused primarily on foscholine detergents. These are lipid mimetics, carrying a phosphate head group and a single hydrophobic tail [124].

We tested six different foscholine detergents, FosCholine-12, FosCholine-10, FosCholine-9, FosCholine-8 and LysoFosCholine-10. These were mixed into the concentrated protein solution at 0.5, 1 and 2 x CMC , and the mixture was put through the commercial crystallisation screens. Once the favourable conditions were identified, we designed screens to expand on them and the screening was repeated. Crystals grew in the presence of both FosCholine-12 and FosCholine-10, as well as LysoFosCholine-10. However, in all cases the diffraction quality was comparable to that of the crystals tested previously, as shown in Figure 2.8C, and no change in the unit cell was observed.

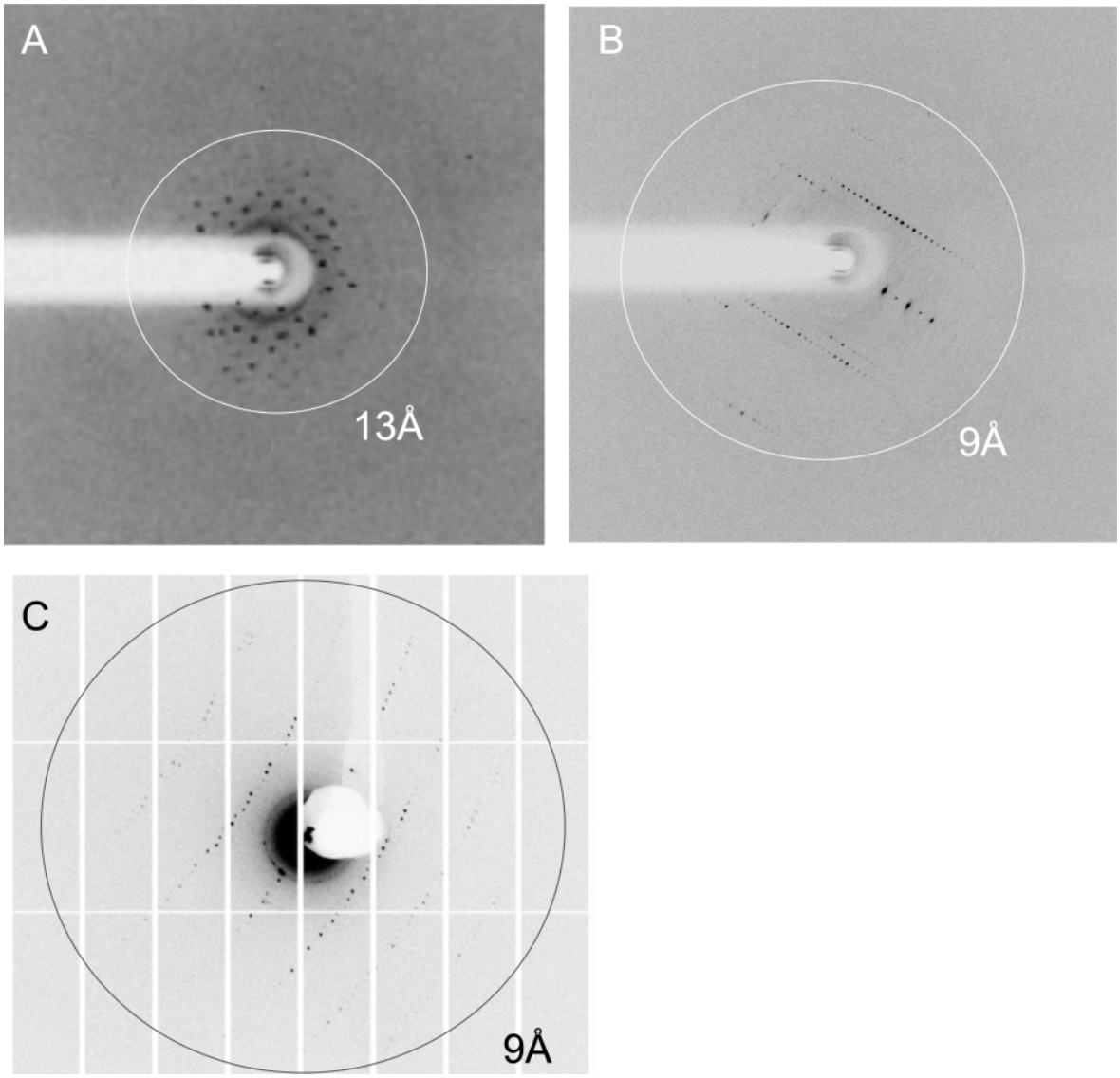

Figure 2.8: ***A*** *and* ***B*** *show diffraction of crystals grown in 50mM Hepes pH7.2, 0.2M NaCl, 22% PEG 550 MME and 1xCMC LysoFoscholine 12.* ***A*** *shows the initial diffraction, and* ***B*** *diffraction of crystals from the same drop that had been dehydrated.* ***C*** *shows diffraction of crystals grown in the same condition, but with 1xCMC Foscholine 10 replacing LysoFoscholine 12.*

2.3.5.2 Crystallisation in the Cubic Phase and Bicelles

Crystallisation in lipidic conditions was also attempted. We tested two methods: crystallisation in the lipid cubic phase and in bicelles.

The lipid cubic phase is a term to describe a particular kind of lipid structure, where lipid molecules form a continuous curved bilayer in three dimensions, separating networks of water channels. When protein is added to these structures, the molecules insert into the bilayer. As the mixture of lipids and protein equilibrates over a well of crystallisation buffers, the curvature of the bilayer is destabilised leading to a phase separation between the curved bilayer and a lamellar lipid structure. The protein concentrates in the lamellar part, where it is also thought to crystallise [125, 126, 127, 128]. Although the exact mechanisms involved are not known, it has been successfully used to crystallise a number of G-protein coupled receptors [129, 130, 131].

Bicelles are small disks, made up of a lipid bilayer and capped with detergent molecules. They have been successfully used to crystallise certain transporters, as well as bacteriorhodopsin [132, 133]. The bilayer-like nature of these structures is thought to be beneficial for crystallisation of membrane proteins as it provides a more native-like environment than detergent micelles.

The results of these two crystallisation methods for KirBac9.2 were similar; both screens produced lots of long, thin needle-like crystals. However, they showed a small-cell diffraction which is suggestive of lipid or detergent crystals. An example of these needle crystals and their diffraction is shown in 2.6B.

2.3.6 Fluorescent Thermal Stability Assay

As the experiments with lipids did not produce any improvements, we next focused on identifying other detergents that would be suitable for crystallisation of KirBac9.2.

Stability is an important parameter in crystallisation of proteins, which is why the choice of detergent is important when working with membrane proteins. Detergents with large micelles, such as DDM, are typically useful for keeping membrane proteins suspended in solution, but their large micelle can interfere with the proteins' ability to crystallise.

To determine whether KirBac9.2 can be stable and soluble in another type of detergent, with a smaller micelle, we employed the fluorescent thermal stability assay [102]. The technique was done with the help and advice of Dr. Simon Newstead. The main principle of this

assay is the use of a thiol-specific fluorochrome, bonded to a cysteine residue buried in the protein. The labelled protein, along with buffer/detergent of interest is then heated to 30 ° C and the fluorescence measured at set time intervals. As the protein unfolds, the fluorescence increases. A detergent which increases the stability of the protein will keep the fluorescence readings at a minimum for the longest time period.

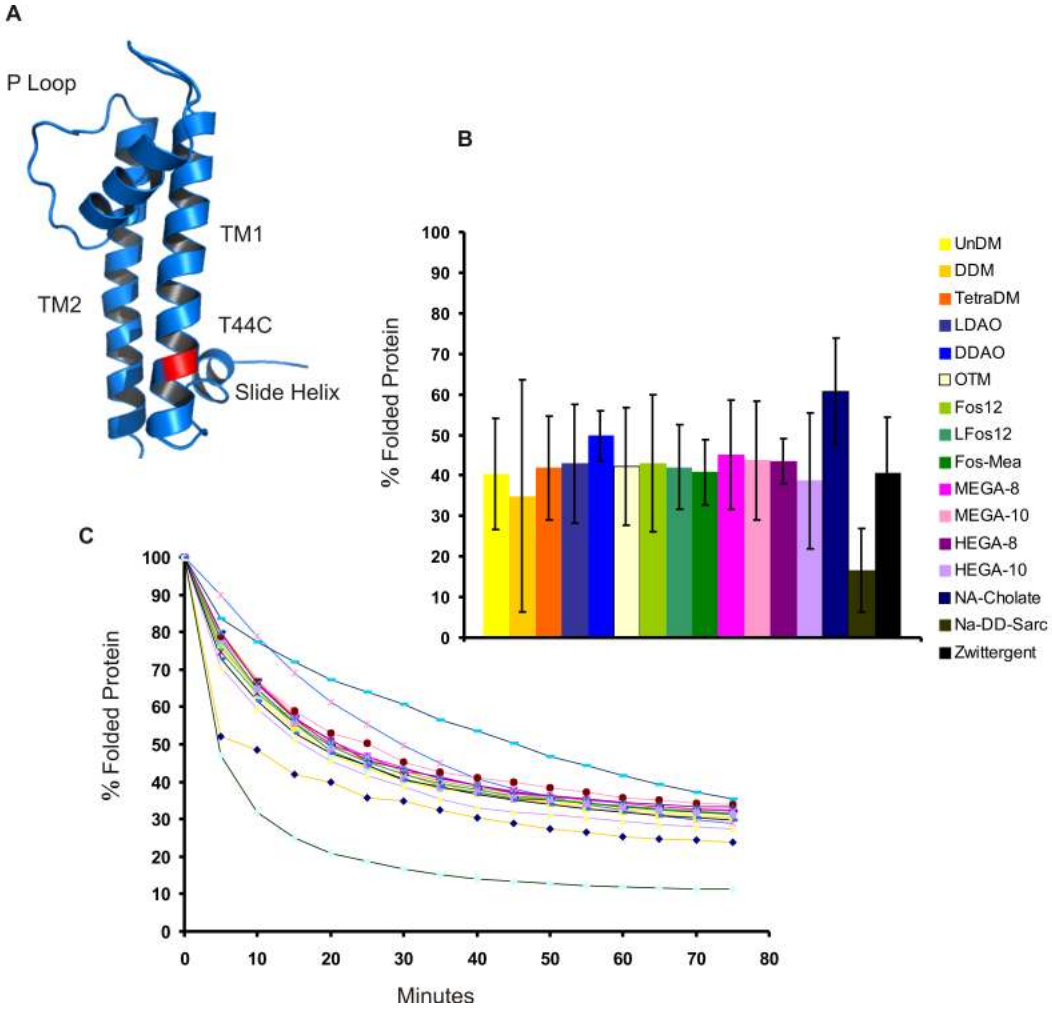

Figure 2.9: *For the assay, a mutation was introduced in KirBac9.2 at position 44.* ***A*** *The presumed location of the mutation is shown on a homology model.* ***B*** *The bar graph represents the percentage of folded protein at t=30 minutes.* ***C*** *A time-course of protein unfolding in the presence of different detergents. At time=0, the folded protein proportion is set to 100%. The percentage of remaining folded protein at each time point was calculated as a fraction of the maximum for the detergent series.*

As KirBac9.2 does not have any native cysteine residues, a point mutation was made in position T44. Based on a homology model of KirBac9.2 created using SWISS-MODEL, residue 44 was found to occur half way up the TM1, and therefore is a suitable candidate

for this type of assay- under folded conditions, it will be shielded by the detergent micelle and the fluorescence background will be minimal. An alignment pointed out the presence of a serine residue in this region in KirBac1.1, which led us to believe that a cysteine mutation in this position would be tolerated in KirBac9.2 (alignment in Figure 1.12). The mutant protein was mixed with N-[4-(7-diethylamino-4-methyl-3-coumarinyl)phenyl]maleimide, and the mixture was pipetted into wells containing 3xCMC detergent. We focused primarily on testing detergents with small micelles, but some larger detergents were also included.

The test was performed twice, from two separate protein preparations and the results are shown in 2.9. Interestingly, the assay suggested that KirBac9.2 was equally stable in DDM as it was in LDAO. LDAO has proven very useful for membrane protein crystallisation, possibly due to the small size of its headgroup and its zwitterionic nature which allow it to pack tighter around the hydrophobic domains of a membrane protein [97].

2.3.6.1 Solubilisation and Purification of KirBac9.2 in LDAO

Due to the apparently improved thermal stability of KirBac9.2 in LDAO, we attempted to use LDAO to solubilise and purifiy KirBac9.2 The initial test using LDAO instead of DDM to solubilise and purify the channel did not yield any tetrameric protein and lots of precipitation was observed.

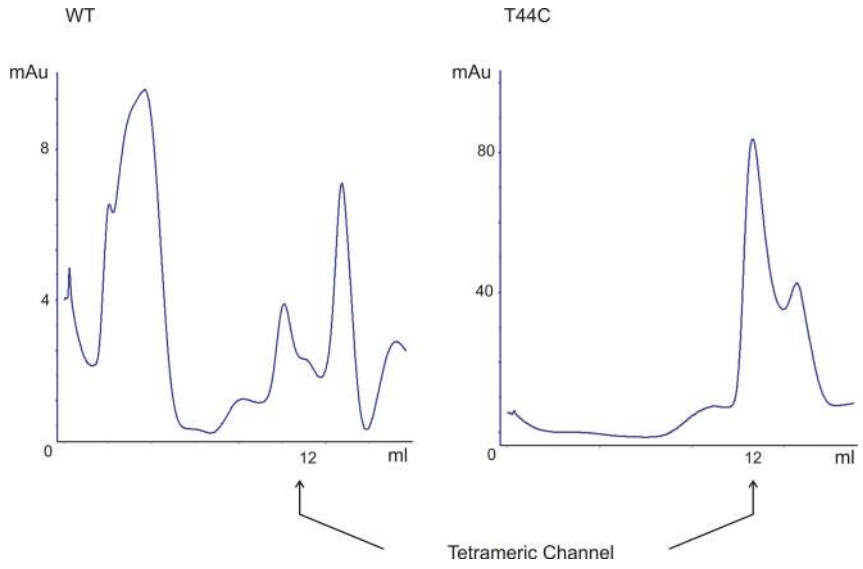

Figure 2.10: *Purification of wild-type KirBac9.2 and the T44C mutant in 5mM LDAO. The tetrameric fraction is indicated with an arrow.*

Since the stability assay was done on protein solubilised with DDM, we repeated the

process using DDM to solubilise the channel and LDAO was used in the purification steps only. However, the channel did not respond well to this treatment. We therefore varied the concentration of LDAO and also small quantities of DDM were added to the buffers. Still, the protein was far from monodisperse and the solutions were prone to precipitation (Results not shown). Finally, after all attempts to purify the wild-type channel in LDAO had failed, the focus was turned to the T44C mutant, which had been used in the stability assays. Indeed, using the cysteine mutant we were able to obtain protein purified in LDAO (2.10). However, it became obvious during concentration of the protein that its stability was compromised by the use of LDAO, and eventhough a small amount of protein could be recovered for use in crystallisation experiments no crystals were ever obtained.

Similar results were achieved with DDAO, Sodium Cholate, MEGA-8, MEGA-10, HEGA-8 and HEGA-10.

2.3.7 Manipulating the construct

2.3.7.1 Truncating the KirBac9.2 Protein

Attempts to crystallise the full length, wild-type protein in both detergent and lipid conditions did not yield crystals of a suitable quality. Furthermore, the data collected from these crystals that did diffract showed that they had a very large unit cell, suggestive of some inherent disorder and flexibility within the channel. This problem could be arising from the flexible N- and C-terminal regions of the channel. The initial structures of KirBac1.1 as well as that of KirBac3.1 were obtained from constructs deleting some of their N- and C-terminal regions. To test whether removing parts of the N-and C-terminal regions might aid the crystallisation of KirBac9.2 we created three truncated constructs, as shown in Figure 2.13.

KirBac9.2 has a short N-terminal, compared to those of KirBac1.1 and KirBac3.1. This short sequence contains one aspartate, which as a charged residue might have a negative effect on the order within the channel. We created a construct deleting the first three residues of the KirBac9.2 sequence (construct ΔN). The ΔN construct did not express as well as the wild-type clone but still produced enough protein for crystallisation trials. Apart from the slightly lower expression, the protein behaved quite similarly to the wild-type, and was not overly prone to aggregation.

Two C-terminal truncations were created, one deleting ten, and the other fifteen terminal amino acids (constructs ΔC10 and ΔC15). The C-terminal sequence of KirBac9.2 contains

many charged residues, which may cause difficulties during crystallisation. The ΔC10 construct was designed to delete five charged residues at the end of the KirBac9.2 sequence, and the ΔC15 construct deleted one further charged residue as well as two prolines. Expression of construct ΔC15 was lower than that of the wild-type and the ΔC10, but still produced a significant amount of protein. Both were put through crystallisation trials. However, crystallisation trials of ΔN, ΔC10 and ΔC15 produced crystals, which were similar in both appearance and quality to those of wild-type.

2.3.7.2 Chimeric Approach

Chimeras of channels have previously been successfully expressed and purified and a crystal structure of a chimera combining the transmembrane domains of a KirBac channel with the cytoplasmic domains of a Kir channel has been solved [134]. KirBac9.2 is highly homologous to other KirBac channels, with the exception of the selectivity filter region. By replacing the intracellular domains of KirBac9.2 with those of either KirBac1.1 or KirBac3.1, we might be able to grow crystals with well ordered lattices and solve the atomic structure of the KirBac9.2 selectivity filter, which is the most intriguing part of this channel.

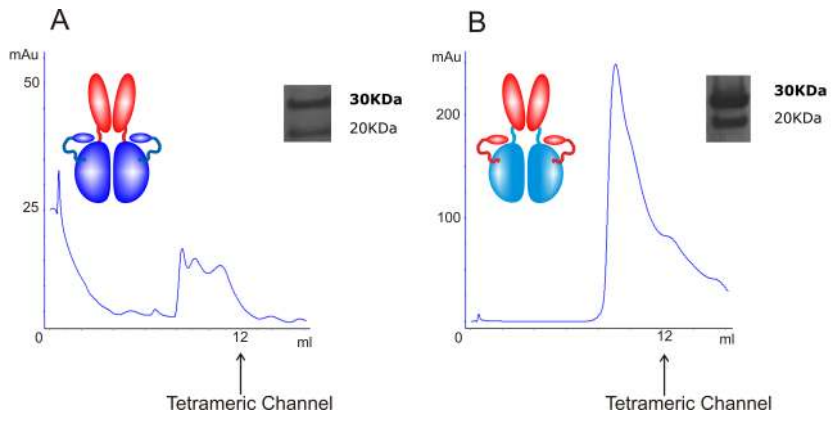

Figure 2.11: *Two of the chimeras showed some expression when tested by Western blot.* ***A*** *the result of western blot and size exclusion analysis of the chimera consisting of the transmembrane regions of KirBac9.2 and KirBac3.1 full N-terminal, slide helix, C-linker and intracellular domains.* ***B*** *shows the equivalent results of a chimera that combines the KirBac9.2 N-terminal, slide helix and the transmembrane domains with the C-linker and cytoplasmic regions of KirBac1.1. Both proteins were prone to aggregation, and no tetrameric channel was obtained from the size exclusion column.*

A number of constructs were made fusing the channels at the interface of the transmembrane and the cytoplasmic regions. A list of chimeras is provided in Figure 2.14B and C.

Expression of the constructs was tested, and the results analysed by western blot and gel filtration where appropriate.

Two of the chimeras appeared to express, but unfortunately neither produced significant quantities of tetrameric protein, as shown in Figure 2.11A and B. The lack of expression that we encountered in this project suggests that KirBac9.2 might be fundamentally different from the other KirBacs.

2.3.7.3 Crystallisation Trials of KirBac9.2 Activatory Mutants

Changes in protein stability as well as potential changes in the conformational state can be favourable for crystal formation. We therefore attempted crystallisation of two activatory mutants of KirBac9.2, S199F and G193C. These were identified in a random mutagenesis approach which is described in Chapter 3.

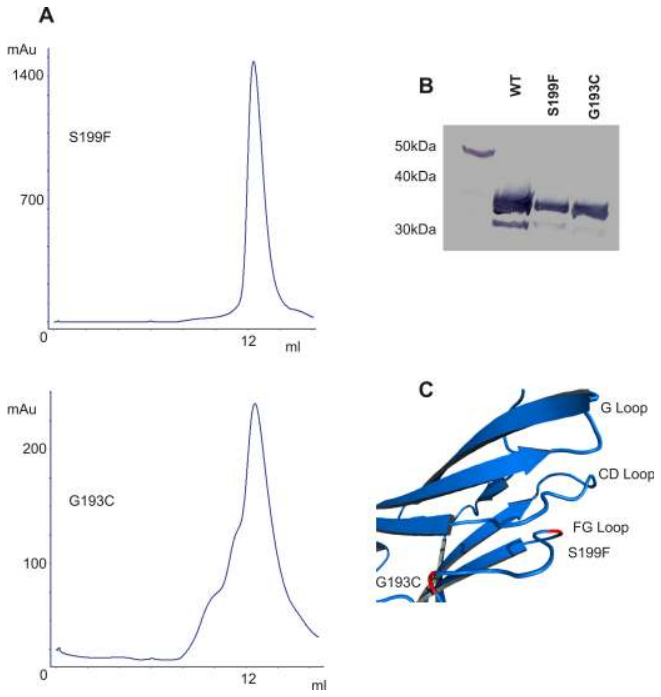

Figure 2.12: *Expression and purification of activating mutants S199F and G193C.* ***A*** *Western blot comparing the expression of the wild-type KirBac9.2 to mutants S199F and G193C.* ***B*** *Size exclusion chromatography of S199F and G193C. Both mutants eluted predominantly in their tetrameric forms.* ***C*** *The location of the mutations is shown on a homology model of KirBac9.2.*

The expression of the mutant channels was tested and was found not to be significantly different from that of the wild-type (Figure 2.12A). The stability of these proteins was also comparable to that of the wild-type KirBac9.2, as shown in Figure 2.12B. For these reasons, both activatory mutants were put through the crystallisation trial. Crystals grew readily of both mutants in conditions similar to those supporting growth of the wild-type protein crystals. However, the diffraction was very poor (not shown) and the crystallisation attempts were abandoned.

2.4 Summary

We were able to produce significant quantities of KirBac9.2 in a monodisperse and seemingly stable form, which we also used in functional assays described in the next chapter. Despite this, well diffracting crystals could not be obtained. What little diffraction could be recorded showed that the channel crystallised with a very large unit cell, which could be indicative of some flexibility and inherent disorder within the protein. The best crystals were obtained in the presence of a detergent belonging to the FosCholine family, suggesting that this disorder might be alleviated to some extent by the presence of lipid-like molecules. Attempts to express chimeras of KirBac9.2 and the previously crystallised KirBac1.1 and KirBac3.1 failed to produce any protein.

It was therefore decided to focus on the methods developed here for the successful expression and purification of KirBac9.2 and to use the highly pure protein for functional characterisation.

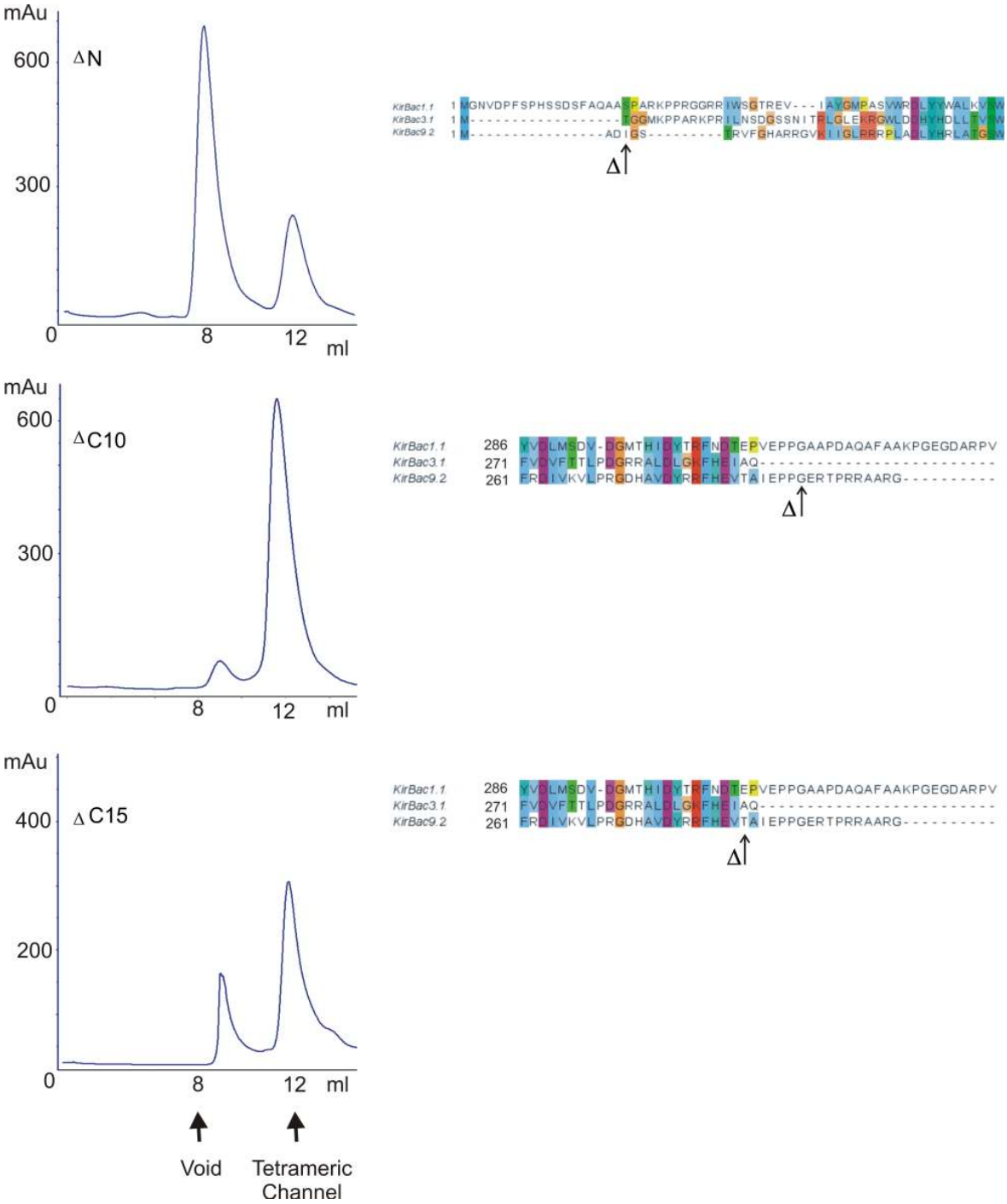

Figure 2.13: *Truncations of KirBac9.2. The gel-filtration profiles of ΔN and ΔC15 indicate that these proteins have some tendency to aggregate. However, no visible precipitation was observed.*

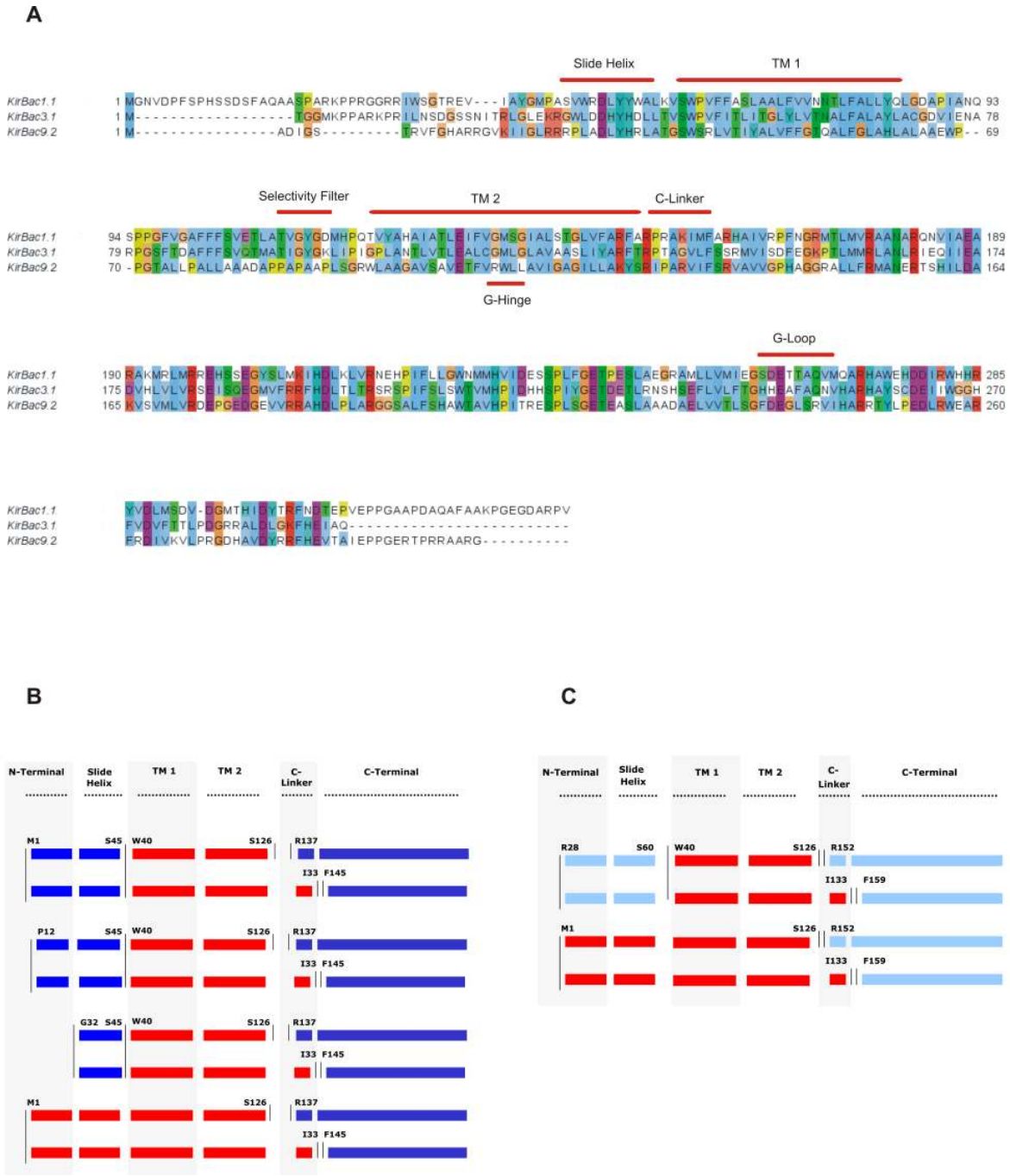

Figure 2.14: ***A*** *An alignment of KirBac9.2, KirBac1.1 and KirBac3.1.* ***B*** *The composition of KirBac9.2 and KirBac3.1 chimeras. KirBac9.2 domains are shown in red and KirBac3.1 domains are shown in dark blue. The annotations correspond to residues where the two channels have been fused to create the chimera.* ***C*** *Construction of KirBac9.2 (red) and KirBac1.1(light blue) chimeras.*

Chapter 3

Functional Characterisation of KirBac9.2

3.1 Introduction

This chapter describes a variety of functional assays used to investigate the function of KirBac9.2.

Normally, ion channel activity is measured by electrophysiological recordings of channels recombinantly expressed in cultured cells or oocytes. However, this is difficult for many prokaryotic channels. But because these channels can be expressed and purified it is possible to use techniques which involve reconstitution into lipid vesicles and bilayers to assay their function.

Firstly, we measured the channel activity of KirBac9.2 directly using a liposomal flux assay [135, 136]. This method provides a good platform for macroscopic studies of ion channels and was chosen for two reasons: firstly, because we were able to purify the channel in a stable form for incorporation into liposomes; and secondly because the experimental setup of this technique allows for easy manipulation of the lipid, pH and ionic environment of the protein. In this part of the study, the permeation and block of monovalent as well as divalent cations is tested. All flux assays were performed in the laboratory of Professor Colin Nichols (Washington University in St. Louis, MO, USA) with the help and advice of Drs. Shizhen Wang and Nazz D'Avanzo.

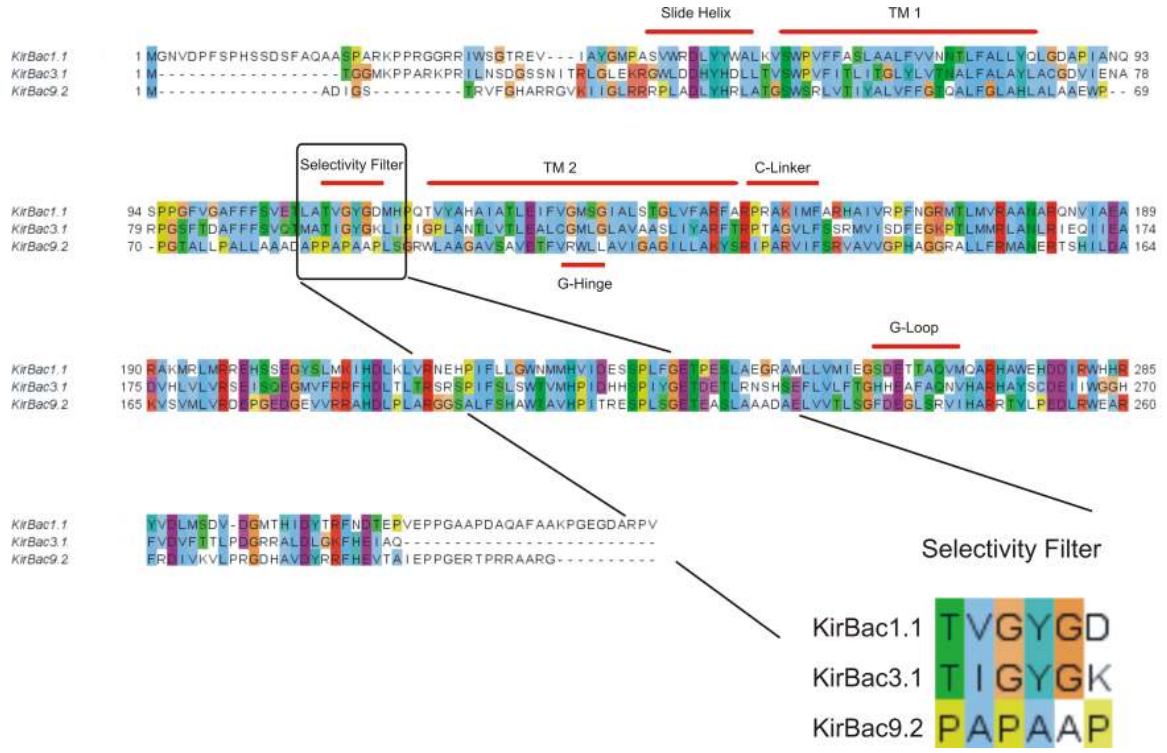

Figure 3.1: *Alignment of KirBac9.2, KirBac3.1 and KirBac1.1. The selectivity filter region is magnified.*

Secondly, we used a random mutagenesis approach to identify activatory mutations in the channel. A strain of K^+-auxotrophic *E.coli* cells are used as a main tool. These cells do not contain any of their native K^+ transporters, and, at low K^+ concentrations, rely entirely on the function of the introduced channel for their survival [137]. By screening a random mutant library of KirBac9.2 in these cells, mutants which increase the activity of the channel are identified. This approach is valuable as it has the potential to identify gating-sensitive regions of the channel. Similar studies of Kir as well as KirBac channels have predicted, quite accurately, gating "hotspots" [138], which were subsequently confirmed by structural data [139].

Finally, the attempts to record single channel currents of KirBac9.2 using a lipid bilayer system are reported.

3.2 Materials and Methods

3.2.1 Liposomal Flux Assays

3.2.1.1 Preparation of KirBac9.2

The KirBac9.2 channel was expressed and purified as described in Chapter 2.

3.2.1.2 $^{22}Na^{+}$ Uptake Assay Solutions Buffers

Buffer B: 10 mM Hepes, 450 mM KCl (KCl substituted with CsCl, RbCl, NaCl, LiCl or 225mM CaCl2, $BaCl_2$, $MgCl_2$, MnCl2 where appropriate), 4 mM NMDG (N-methyl-D-glucamine). Buffer pH was adjusted to 7.4 with NMDG

Buffer C: 10 mM Hepes , 400 mM Sorbitol , 4 mM NMDG. Buffer pH was adjusted to 7.4 with NMDG.

BSA blocking solution: 5 mg/ml of BSA dissolved in 400 mM Sorbitol.

POPG blocking solution: 10 mg/ml of POPG dissolved in 400 mM Sorbitol.

All solutions were filtered through a 0.22μm membrane prior to use.

Preparation of radioactive solutions: Buffer C was complemented with 0.5μCi $^{22}Na^{+}$. For each sample 420μl radioactive solution was made.

A detailed protocol for the flux assays is given in Chapter 5,5.2.2.

3.2.2 *E.coli* Assays

TK2299 *E.coli* cells were engineered to lack all 3 potassium transporter genes (Δkdp, Δtrk, Δkup). The genome of these cells also has a mutation in the recombinase gene endA, meaning that they produce DNA of relatively high quality. The strain was kindely donated to Dr. Stephen Tucker by Professor Wolf Epstein (University of Chicago). A stock of the strain was stored in 30% glycerol at –80 $^{\circ}$C and used to make chemically competent cells.

3.2.2.1 Media for Complementation Assays and Growth Curves

LBK130 (130mM $[K^{+}]$) Medium: 10g Tryptone (Sigma Aldrich), 5g Yeast Extract (Sigma Aldrich), 9.7g KCl.

LB0K (0mM $[K^{+}]$) Medium: 10g Tryptone, 5g Yeast Extract, 7.6g NaCl.

LBK0 medium was used for low potassium screens, and where indicated, supplemented with 1mM, 2mM, 5mM or 7.5mM KCl. To induce expression of the plasmid gene, 0.5mM Isopropyl-β-D-galactopyranoside (IPTG) was added.

3.2.2.2 Complementation Drop Tests

TK2299 cells were transformed and plated on LBK130 medium. From this plate, a colony was used to inoculate a 4ml LBK130 culture. This culture was grown overnight at 37 $^\circ$C in a shaking incubator (220rpm). The cultures were centrifuged at 7,000 RCF for 5 minutes and the supernatant discarded. The bacterial pellet was washed two times in 5ml LBK0 medium, by gentle resuspension followed by centrifugation. The washed pellet was resuspended in 1ml LBK0 medium. The 10^2 dilution was made by transferring $10\mu l$ of this resuspension to $900\mu l$ LBK0 medium. LBK0 plates containing 0.5mM IPTG were made at appropriate potassium concentrations. The prepared cell dilutions were pipetted onto the plates in $5\mu l$ drops and allowed to dry before being incubated at 30 $^\circ$C/37 $^\circ$C for 18-24 hours.

3.2.2.3 *E.coli* Growth Curves

Cells were transformed, grown and washed as described above. LBK0 media was complemented with the specified concentrations of KCl and 0.5mM IPTG. The washed cells were added to final OD600 of 0.05 in a 16ml culture. Cultures were grown at 37 $^\circ$C in a shaking incubator, and their growth monitored by OD600 measurements every 2 hours. All growth curves were done in triplicate.

3.2.3 Creating a Random Mutant Library

Random mutagenesis of wild-type plasmids was done using the manufacturers' protocol form the GeneMorph II Random Mutagenesis kit (Stratagene). A PCR reaction was set up, where the wild-type plasmid was amplified in a PCR reaction using the enzyme Mutazyme II DNA polymerase. Mutazyme II is a blend of two low fidelity polymerases, which produce an unbiased range of mutations with equal mutations to adenines and thymines versus cytosines and guanines. Firstly, primers were designed to amplify the gene to be mutated. Primers contained restriction sites, so that the mutated fragments could be put into an expression vector (pQE60Lac). 100ng wild-type plasmid was used in the PCR reaction, as recommended by the protocols in order to get 1-2 mutations per clone. Following PCR, the input DNA

was digested with the enzyme DpnI, and cleaned up using the PCR purification kit (Qiagen). The cleaned PCR product was eluted in 30μl H2O. To insert the library into the expression vector, restriction digests of both the cleaned PCR product and the target vector were set up. The fragments were gel purified using the QIAEX II Gel Extraction protocol (Qiagen). Concentrations of gel purified material were measured, and the ligation reaction was set up using 3:1 molar ratio of insert to vector. Before adding the T4 ligase (Promega), the ligation mix was heated for 5 minutes at 65 $^\circ$C to reduce vector self-ligation before being incubated for 3 hours at room temperature. The ligation was cleaned by phenol chloroform extraction. The final resuspension was done in 20μl H2O. The cleaned ligated library solution was transformed into Library Efficiency DH5α cells (Invitrogen) according to manufacturer's instructions. After heat shock, the cells were supplemented with 1.8ml SOC media, and incubated in a shaking incubator at 37 $^\circ$C for 30 minutes. 2.5% of the recovered transformed cells were plated onto a LB plate, containing the appropriate antibiotic and left overnight at 37 $^\circ$C. The remainder of the transformed cells were grown in a shaking incubator at 37 $^\circ$C overnight in a 16ml culture. Plasmid purification of the overnight culture was performed the next day, to make the final DNA library. The 2.5% plate was used to estimate the number of clones in the library.

3.2.3.1 Performing the Library Screen

The DNA library was transformed into the TK2299 cells, plated onto LBK0 plates supplemented with 2mM KCl and left to incubate overnight at 37 $^\circ$C. Colonies were picked and grown in liquid culture overnight. Plasmid DNA was isolated, and sequenced. The mutations were identified, and in cases where more than one mutation was present in the open reading frame, single mutants were created in order to test their ability to complement growth individually.

3.2.4 Electrophysiology

3.2.4.1 Preparation of Giant Unilamellar Vesicles (GUVs)

1,2-diphytanoyl-sn-glycero-3-phosphocholine (DPhPC) lipid in powder form (Avanti Polar Lipids) were dissolved in choloform, to a stock concentration of 10mM and stored at –20 $^\circ$C. Cholesterol (Sigma Aldrich) was dissolved in chloroform to a stock concentration of 10mM. In preparation, the lipids and cholesterol were equilibrated to room temperature, and a mixture

was made consisting of $90\mu l$ lipid and $10\mu l$ cholesterol stock in a small glass vial. $20\mu l$ of the mixture was pipetted onto the conductive side of an ITO slide (Nanion), and quickly spread into an even layer using a glass rod. An O-ring was greased lightly and placed around the lipid/chloroform layer. Once the choloform evaporated, $250\mu l$ filtered 1M sorbitol solution was placed inside the O-ring. The ITO slide was placed into the Vesicle PrepPro chamber, and the second ITO slide was placed carefully on top, making sure that no bubbles are introduced. Assembly was completed by carefully placing the top conductive pad on the chamber, and tightening the screws. Following program completion, the size of the vesicles was checked under a microscope, and their ability to form bilayers tested using the Port-a-Patch set-up. The empty bilayers' response to voltage and buffer application was examined.

3.2.4.2 Protein Reconstitution

Purified KirBac9.2 protein was diluted in 50mM HEPES pH 8, 150mM NaCl to 0.1mg/ml. $10\mu l$ protein mixture was added to $90\mu l$ vesicles, mixed gently by pipetting and left at room temperature for 20 minutes. Detergent was removed by addition of Biobeads (BioRad). A small amount of beads was added and the tube gently tapped to mix the contents. The mixture was left at room temperature for another 20 minutes, before being placed at 4 $^\circ$ C for overnight incubation. The next day, the tubes were briefly centrifuged to pellet the beads, and the vesicles removed carefully by pipetting. The vesicles were stored at 4 $^\circ$ C for up to a week.

3.2.4.3 Recordings

5μl vesicles was pipetted onto a glass chip (Nanion), and a 8-16 GΩ seal was formed. Internal and external buffers were kept symmetrical, consisting of 10mM Hepes pH 7, 100mM KCl. Recordings were sampled at 100kHz and filtered at 5kHz (Axon Digidata 1440, Molecular Devices). Data was analysed using pCLAMP 10.2 software (Axon Instruments).

3.3 Results and Discussion

3.3.1 Selectivity and Permeability of KirBac9.2

3.3.1.1 KirBac9.2 in a Liposomal Flux Assay

KirBac9.2, expressed and purified as described in Chapter 2, was reconstituted into POPE:POPG (3:1) liposomes for use in the liposomal flux assays. In these experiments the intraliposomal concentration of a permeant ion is high, while the extraliposomal solution contains a radioactive tracer ion. As the permeant ion leaves the liposome via the reconstituted channel, the radioactive tracer is taken up into the liposomes to make up for the charge lost in the efflux. The principle of this is shown in Figure 3.2. At the end of the experiment, the radioactivity of the liposomes is measured and it is this reading that can be related to channel activity.

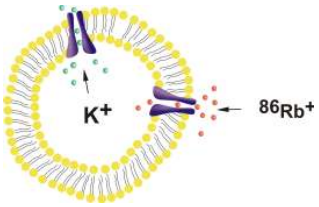

Figure 3.2: *The flux assays depend on a large electrochemical gradient across the liposome membrane to drive efflux of ions through the reconstituted ion channel. This leads to uptake of the radioactive tracer into the liposomes. Channel activity is reflected in the accumulation of radioactive tracer inside the liposomes.*

The initial experiments were performed with $^{86}Rb^{+}$ as the radioactive tracer. Rubidium is used in potassium channel assays because rubidium ions can easily permeate the potassium channel selectivity filter. In addition, the $^{86}Rb^{+}$isotope is relatively easy to handle, as it has a short half-life and only emits β-radiation. However, in the case of KirBac9.2, the use of $^{86}Rb^{+}$gave a poor signal-to-noise ratio (data not shown) and eventually the tracer was substituted with $^{22}Na^{+}$. This isotope of sodium has a very long half life and emits the highly penetrative γ-radiation.

3.3.1.2 Permeation of Monovalent Cations in KirBac9.2

All known Kir and KirBac channels, due to their highly conserved selectivity filter region, show a high preference for K^{+} ions, but can, to some extent, also conduct ions similar in

ionic radius, such as Rb^+. They do not conduct Li^+ and Na^+. As shown in the alignment in Figure 3.1, the selectivity filter region of KirBac9.2 is very different to that of the classical Kir channels, and could have evolved to select for an ion other than K^+. We therefore performed a series of flux assays where the $^{22}Na^+$ uptake was driven by either Li^+, Na^+, K^+, Rb^+ or Cs^+.

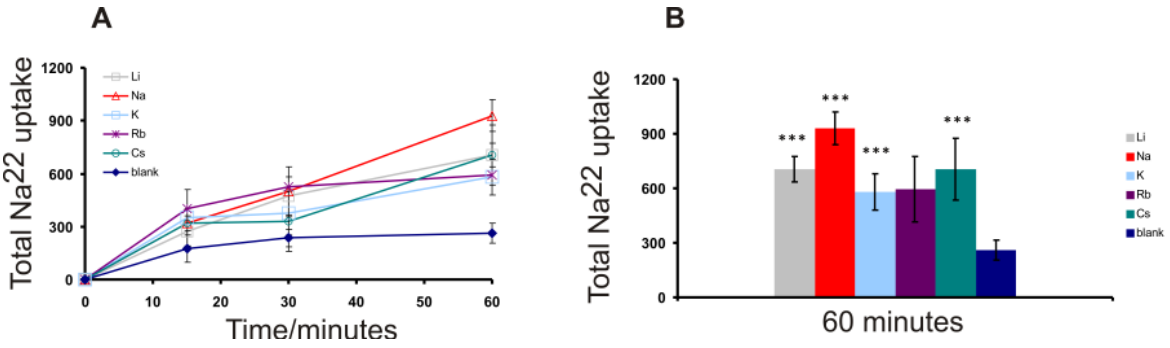

Figure 3.3: *KirBac9.2 permeability to monovalent cations. Intraliposomal buffer consisted of 10mM Hepes pH7.4, 4mM NMDG, 1mM EDTA, 1mM EGTA and 450mM permeant ion. The extraliposomal buffer contained 10mM Hepes pH7.4, 400mM sorbitol, 4mM NMDG, 1mM EDTA, 1mM EGTA and 0.5μCi $^{22}Na^+$* ***A*** *Time course of $^{22}Na^+$uptake drivent by Na^+, K^+, $Li^+$$Rb^+$ and Cs^+.* ***B*** *$^{22}Na^+$uptake at t=60 minutes. Error bars represent S.E.M., n=3. Statistical significance of ionic permeability (compared to blank liposomes) was calculated by t-test at t=60minutes: p_{Li^+}=0.0002, p_{Na^+}=0.003, p_{K^+}=0.006, p_{Rb^+}=0.05, p_{Cs^+}=0.03.*

The activity of the channel was found to be quite low, but significantly above the negative control. The $^{22}Na^+$uptake assay suggested that KirBac9.2 has almost no selectivity, as uptake was driven almost equally by all tested ions (Figure 3.3). A small preference could be seen for Li^+ and Na^+ ions, but considering the signal levels it can be argued that the differences are within the margins of error.

3.3.1.3 Permeability of Divalent Cations in KirBac9.2

KirBac9.2 does not appear to show any significant preference for any of the ions tested, which could be because it is non-selective for monovalent cations. However, the low channel activity that we observe is an important point to consider, especially when studying an unknown channel. In the $^{22}Na^+$ flux experiments, only permeation of monovalent cations is monitored. If the channel is selective for anions, or indeed divalent cations, we would not observe any flux since our radioactive tracer would not be taken up into the liposomes.

In the light of the considerations mentioned above, we wanted to investigate whether KirBac9.2 is capable of conducting divalent cations. Uptake of $^{22}Na^{+}$was assayed in the presence of 225mM $MgCl_2$, $BaCl_2$, $CaCl_2$ and $MnCl_2$. The total charge inside the liposomes, and therefore the gradient over the liposome membranes, was the same as in the experiments performed in the presence of monovalent cations.

The results clearly suggest that divalent ions do not permeate the KirBac9.2 pore in preference to monovalent cations (Figure 3.4A and B).

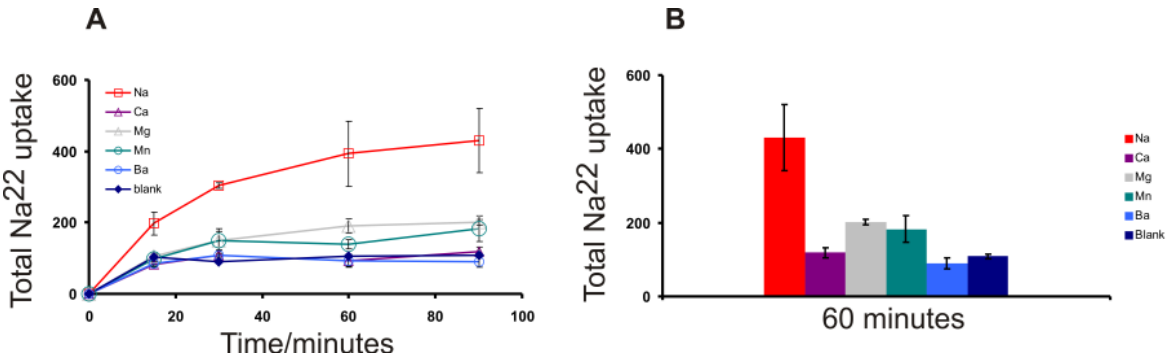

Figure 3.4: *Permeability of divalent ions in KirBac9.2. The intraliposomal buffer consisted of 10mM Hepes pH7.4, 4mM NMDG and 225mM divalent ion. The extraliposomal buffer contained 10mM Hepes pH7.4, 400mM sorbitol, 4mM NMDG and 0.5µCi $^{22}Na^{+}$.* ***A*** *timecourse of $^{22}Na^{+}$uptake driven by Na^{+}compared to Mg^{2+}, Mn^{2+}, $Ca^{2+}$and Ba^{2+}.* ***B*** *Comparison of $^{22}Na^{+}$ uptake driven by Na^{+}, Mg^{2+}, Mn^{2+}, $Ca^{2+}$and Ba^{2+}at t=60 minutes.*

3.3.1.4 Tetrameric Stability Under Varying Ionic Conditions

Studies of KirBac1.1 and KcsA have shown that ions that coordinate tightly in the filter sequence, such as K^{+} and Ba^{2+}, have a positive effect on the tetramer stability of channels, while those which are not permeant tend to disturb the tetrameric assembly [140, 141, 142]. We therefore wanted to determine the stability of the KirBac9.2 tetramer in the presence of Li^{+}, Na^{+}, K^{+} and Cs^{+}.

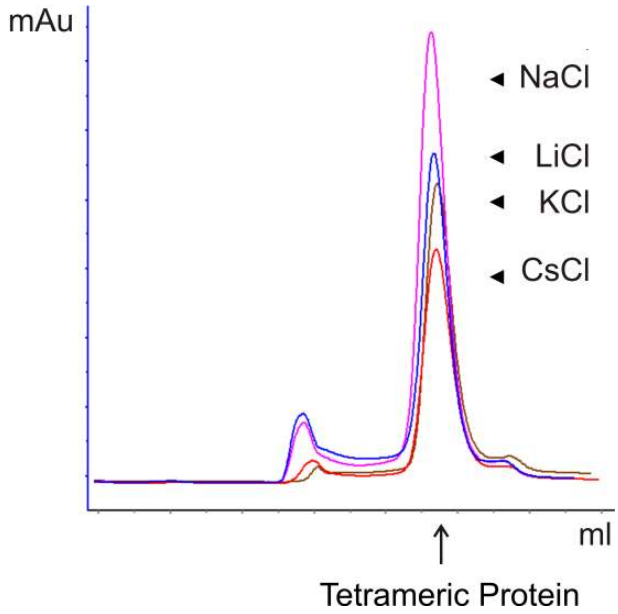

Figure 3.5: *Gel filtration profile of KirBac9.2 purified in 150mM NaCl, LiCl, KCl and CsCl. The protein elutes as a tetramer in the presence of all four salts.*

The protein was expressed, and the purification performed according to the protocol described in Chapter 2. The purification buffers were made with LiCl, NaCl, KCl and CsCl respectively. Following purification, the protein was loaded onto a size exclusion column, previously equilibrated with the appropriate salt buffer. The gel filtration profiles, shown in Figure 3.5, did not change upon varying the salts, which suggests that the channel is stable with any of the tested ions present in its pore.

3.3.1.5 Preliminary conclusions on the Selectivity of KirBac9.2

These initial results suggest that KirBac9.2 is capable of conducting Li^+, Na^+, K^+, Rb^+ and Cs^+ ions, but not the divalent Ca^{2+}, Ba^{2+}, Mg^{2+}, or $Mn^{2+}$and it is therefore likely to be a non-specific monovalent cation channel. The low activity observed in these assays could be due to suboptimal conditions of the assay, such as inappropriate lipid composition of the liposomes, buffer pH or the absence of an agonist. It is also clear that KirBac9.2 is not an anion channel because otherwise we would not have been likely to see any difference in flux between the monovalent and divalent cations, since the chloride ion concentration was intentionally kept at a constant level.

3.3.2 Modulation by PIP_2

PIP_2 is an anionic phospholipid, found at the cytoplasmic leaflet of the plasma membrane of eukaryotic cells. Because the molecule is not found in the membranes of prokaryotic organisms, KirBac channels have not evolved in a way which necessitates activation by PIP_2 . However, PIP_2 has been found to directly interact with the prokaryotic KirBac1.1 and inhibit its function in a dose dependent manner [85].

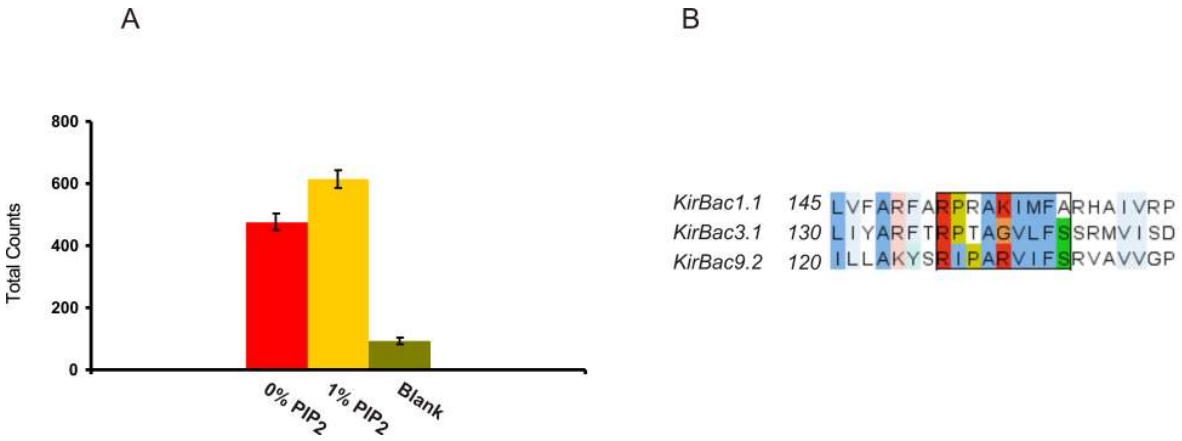

Figure 3.6: *The effect of PIP_2on KirBac9.2 mediated sodium driven $^{22}Na^+$uptake. 1% PIP_2 was included in the POPE:POPG liposome mixture. KirBac9.2 was reconstituted as described previously.* ***A*** *$^{22}Na^+$uptake was measured for 60 minutes. Error bars represent S.E.M, n=3.* ***B*** *An alignment of the C-linker regions of KirBac9.2, KirBac3.1 and KirBac1.1.*

The positively charged residues in the C-linker region of Kir channels have been identified as critical for binding of PIP_2 [143, 85, 48]. To investigate whether inhibition by PIP_2 also occurs in KirBac9.2, the activity of the channel was assayed in liposomes containing 1% $PI(4,5)P_2$, a concentration which inhibits KirBac1.1 activity by >90% [85].

The results, shown in Figure 3.6A, suggest that PIP_2 has no inhibitory effect on KirBac9.2, despite the sequence similarity of the KirBac9.2 C-linker to that of other KirBac channels (Figure 3.6B).

3.3.3 KirBac9.2 Complementation Assay

KirBac9.2 was functionally characterised using a genetic complementation approach in *E.coli*.

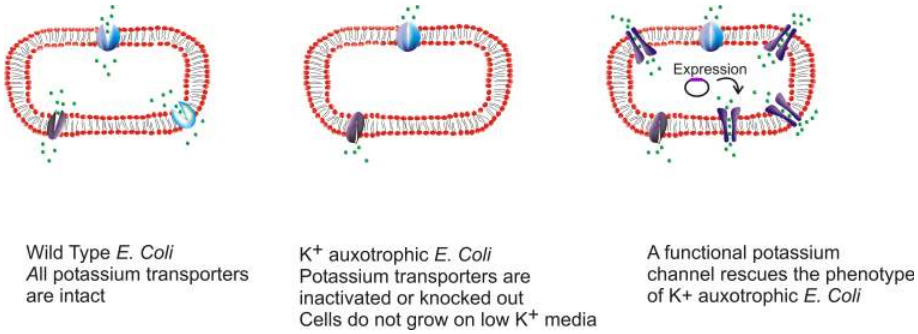

Figure 3.7: *Principle of the genetic complementation assays.*

Here, the ability of the channel to rescue growth of potassium transport deficient *E.coli* was tested in a range of concentrations of potassium. It was found that KirBac9.2 can complement growth of the K^+ auxotrophic *E.coli*, albeit weakly, at 7.5mM KCl (Figure 3.8).

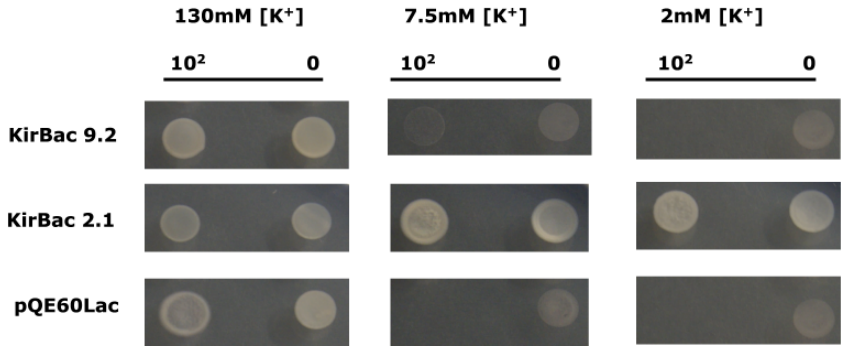

Figure 3.8: *A representative image of the ability of KirBac9.2 to complement growth of TK2299 E.coli. The experiment was repeated >10 times. KirBac9.2 is able to weakly complement growth of K^+ auxotrophic E.coli at 7.5mM KCl. KirBac2.1, which has been found to be highly active in E.coli [80], serves as a positive, and the empty vector pQE60Lac as a negtive control. The transformed E.coli were plated undiluted (0) and diluted 1:100 in LBK0 medium (10^2).*

3.3.3.1 Identification of Activatory Mutations

Although some low intrinsic KirBac9.2 activity could be observed, the channel can still be screened for activatory mutations in *E.coli*. The full open reading frame was randomly mutated, and the library was screened using potassium transport deficient cells (TK2299). The screens were preformed in the presence of a very low KCl concentration (2mM). After screening the full library, 30 clones were isolated. A second round of screening was performed to separate the false positives, and 16 clones were isolated which could successfully rescue the phenotype.

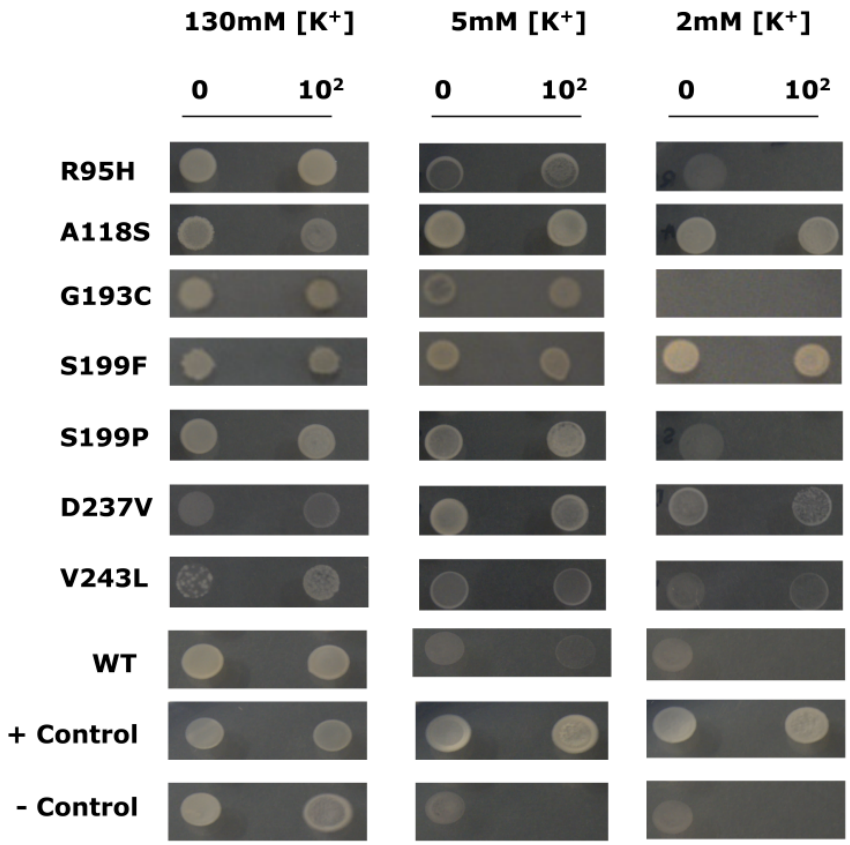

Figure 3.9: *Complementation of K^+ auxotrophic E.coli expressing the activatory KirBac9.2 mutants. KirBac2.1 was used as a positive control and the empty pQE60Lac vector as a negative control. The transformed E.coli were plated undiluted (0) and diluted 1:100 in LBK0 medium (10^2).*

These clones were sequenced, and most were shown to have 1-2 mutations per open reading frame. The mutations were first separated using standard cloning techniques and then tested for their ability to complement growth. Seven unique mutations were found to complement growth, and their complementation is shown in Figure 3.9.

The location of all mutants is shown on a homology model of KirBac9.2 in Figure 3.10. Interestingly, only one of the isolated mutants was found to be close to the selectivity filter region (R95H). The rest, with the exception of A118S, which is located in the lower half of TM2, are concentrated in the cytoplasmic part of the channel. The A118S mutation is similar to the KcsA A108S, which was found to increase the open probability of the channel through destabilising the closed state [144, 145].

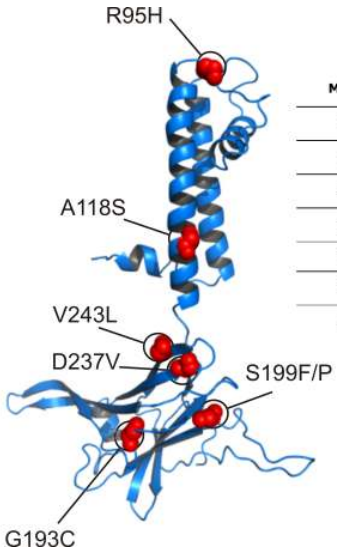

Mutation	Number of times identified in E.Coli screen mutants
R95H	2
A118S	2
G193C	1
S199F	7
S199P	2
D237V	4
V243L	2

Figure 3.10: *List of mutants isolated from the random mutagenesis screen. The location of the mutations is indicated on a homology model of KirBac9.2.*

Two independent mutants of the S199 residue were isolated, with slightly different complementation profiles. S199F complements very strongly, down to 2mM K^+, whereas cells expressing S199P only grow on a minimum 5mM K^+. Based on a homology model of KirBac9.2 this residue is likely to lie on the cytoplasmic interface between subunits.

Residue D237 is found in the region that corresponds to the G-loop. In this complementation assay, changing the aspartate to a valine dramatically improves the channel's ability to complement growth. A mutation of a valine to a leucine in position 243 resulted in powerful complementation of growth, and the only observed case of toxicity in presence of high extracellular potassium. Like D237, V243 is also found in the region which in KirBac channels corresponds to the G-loop. The G-loop region in Kir channels has been shown to be important for channel gating; in K_{ATP} channels mutations in this region can have a large impact on channel activity [146]. Mutations in the cytoplasmic domains might also affect the stability or the role of the cytoplasmic assembly in controlling channel activity [57, 59].

3.3.3.2 Potential Restrictions in the Pore of KirBac9.2

KirBac9.2 contains two potential pore restricting residues in TM2: R110 and W111. These residues are located midway down the inner helix, and align to the glycine hinge region which is conserved in Kir and KirBac channels. A similar restriction was found in the wild-type NaK channel, which has been shown to have very low activity in liposomal flux assays. The

crystal structure of the open NaK showed that the F92 residue introduces a restriction in the pore and the authors concluded that it was the probable cause of the low conductivity of the wild-type channel. Indeed, when a F92A mutation is introduced, its activity in the flux assays increases >10 fold [15] (Figure 3.11)

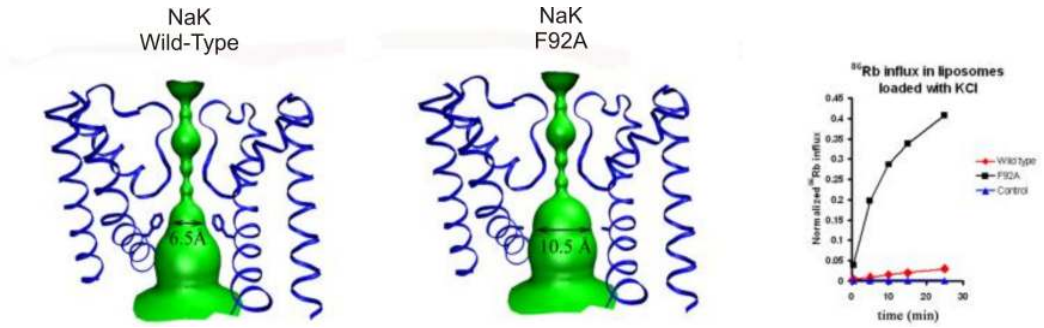

Figure 3.11: *Restriction in the pore of the NaK channel. Mutation F92A increases the activity of the channel in a liposomal flux assay. Figure adapted from [15]*

Similarly, a mutation in Kir6.2, G156R, renders the channel inactive [147]. Full activity of the channel could be restored by introducing a negative charge in position 160 (N160D), possibly through formation of the salt bridge with the arginine in position 156 which would either remove the arginine from the conduction path, or act to neutralise the positive charge and thereby stabilise cations within the pore.

To investigate whether R110 and W111 are restricting the ionic flux, we mutated these residues. Mutations R110A, R110D, R110K and W111A were introduced into the wild-type KirBac9.2 gene and tested for their ability to support growth of K^+ auxotrophic *E.coli*. However, the complementation profiles of all tested mutants were similar to that of the wild-type channel (data not shown), which suggests that residues R110 and W111 do not act to restrict the transmembrane pore.

3.3.3.3 Sensitivity of KirBac9.2 to Block by Barium and Caesium

Caesium and barium ions are classical blockers of potassium channels. It is widely accepted that they bind tightly in the selectivity filter region, thereby preventing passage of K^+ ions. The $^{22}Na^+$ uptake assays suggested that KirBac9.2 is not blocked by either of these ions in a

liposomal environment. However, we wanted to confirm whether the functional properties of the channel were the same in the *E.coli* complementation assay.

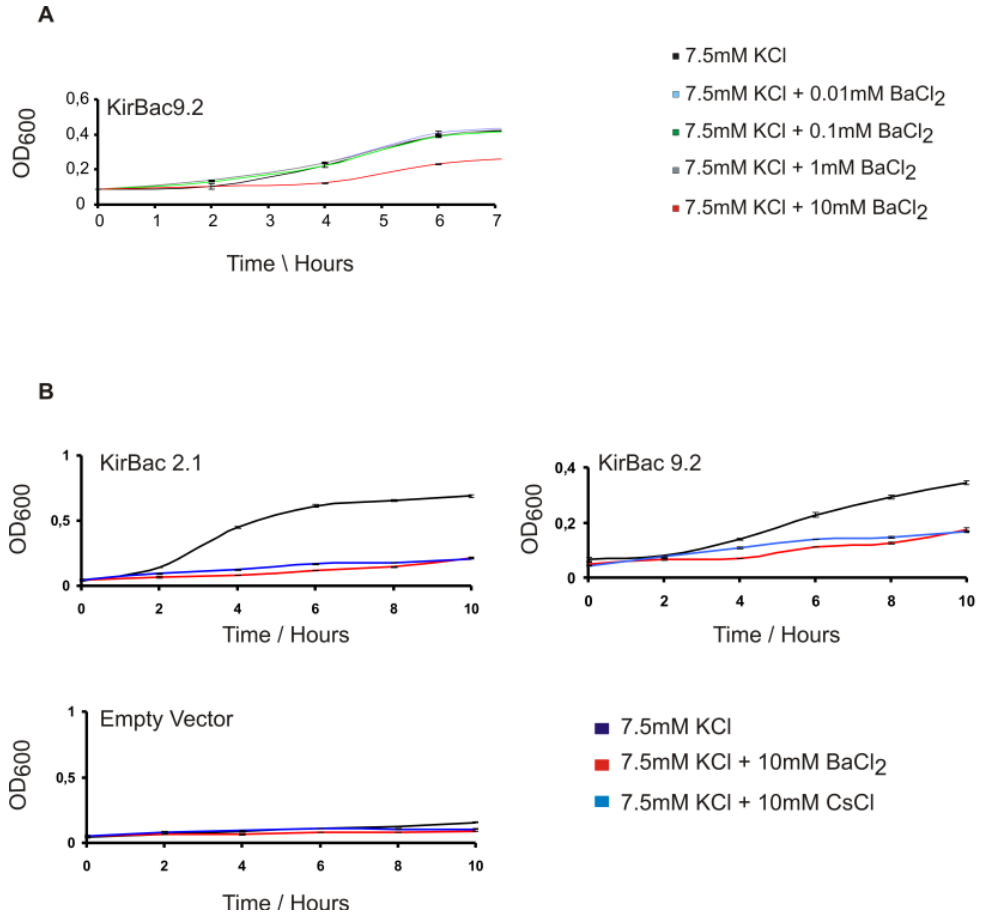

Figure 3.12: ***A*** *Growth of TK2299 cells expressing KirBac9.2 in the presence of 7.5mM KCl and $BaCl_2$. The experiment showed that at least 10mM $BaCl_2$ was required to inhibit growth of the E.coli.* ***B*** *Growth of TK2299 cells expressing KirBac9.2, KirBac2.1 (positive control) and pQE60Lac (negative control) in the presence of 7.5mM KCl (black), 7.5mM KCl and 10mM $BaCl_2$ (red) and 7.5mM KCl and 10mM CsCl (blue). Error bars (at some points smaller than the symbol) represent S.E.M., n=3. Barium and caesium inhibit growth of cells expressing both KirBac2.1 and KirBac9.2.*

TK2299 cells expressing wild-type KirBac9.2 were grown in the presence of 7.5mM K^+, where the channel was found to complement growth, and 10mM Ba^{2+} and Cs^+ respectively. It emerged that both of these ions, when applied to the growth medium, inhibited growth of TK2299 cells (Figure 3.12B).

The $^{22}Na^+$ uptake assays indicated that KirBac9.2 is capable of conducting Cs^+ ions. Studies have shown that caesium is the most toxic alkali metal to microorganisms [148], so the lack of growth in the presence of caesium is not surprising.

The dose response curve of barium (Figure 3.12A) shows that at least 10mM Ba^{2+} is needed to obtain any inhibition of *E.coli* growth.

Complementation of activatory mutants was also measured in the presence of 10mM Ba^{2+} and Cs^{+}, shown in Figure 3.13. Responses to these ions varied slightly amongst the mutants, but the overall picture revealed a reduced sensitivity to barium while the response to caesium remained largely unchanged.

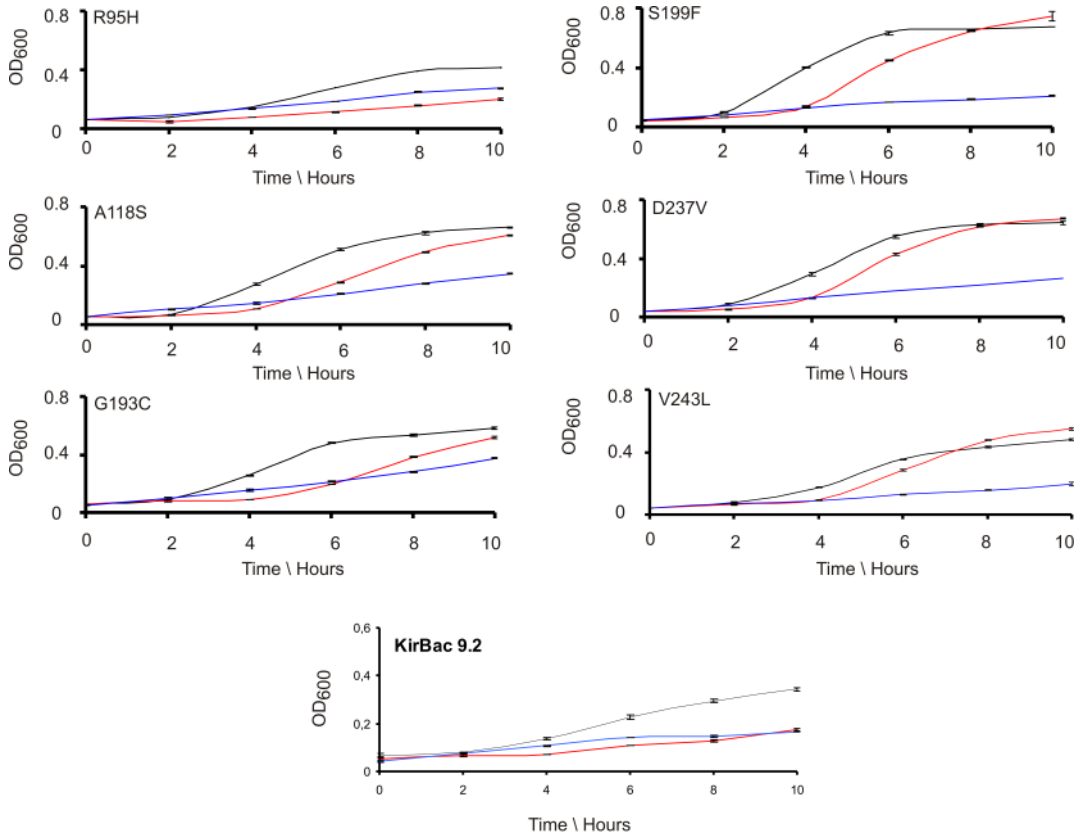

Figure 3.13: *Growth curves of TK2299 cells expressing the KirBac9.2 activatory mutants. Cells were grown in 7.5mM KCl (black), 7.5mM KCl and 10mM $BaCl_2$ (red) and 7.5mM KCl and 10mM CsCl (blue). Bars represent S.E.M.; n=3 for all data points.*

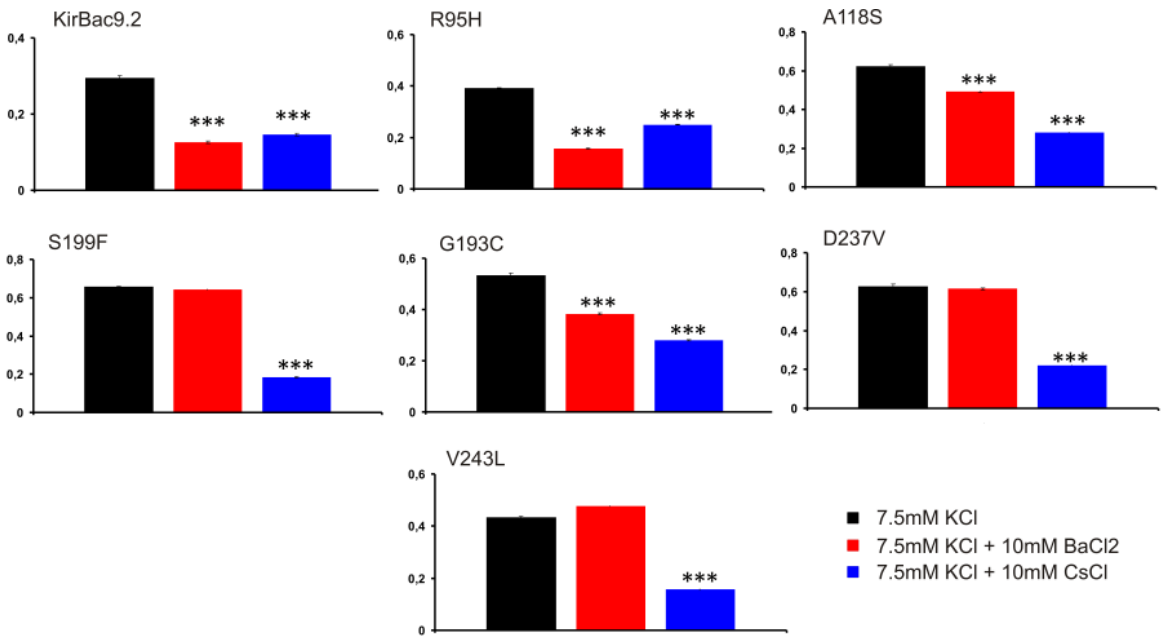

Figure 3.14: *Growth of TK2299 cells expressing the WT and mutant channels at t=8 hours in the presence of 7.5mM KCl (black bars), 7.5mM KCl and 10mM $BaCl_2$ (red bars) and 7.5mM KCl and 10mM CsCl (blue bars). Error bars represent S.E.M., n=3. Asterisks represent statistically significant inhibition of growth (OD600), where p<0.05.*

3.3.4 Towards an Electrophysiological Study of KirBac9.2

Reconstitution of purified channels into planar lipid bilayers or giant liposomes has so far been the most promising approach to study prokaryotic channels. In some ways reconstitution methods are preferable to heterologous expression in cultured cell lines and oocytes because they allow full control of the membrane composition, as well as the intra- and extracellular environments.

Due to time constraints a full electrophysiological characterisation of KirBac9.2 could not be undertaken. However, we do report successfully recorded KirBac9.2 currents using a method which relies on reconstitution of purified proteins into Giant Unilammelar Vesicles (GUVs) [149, 150], shown in Figure 3.15.

We observed putative K^+ currents from KirBac9.2 reconstituted into GUVs, which is an encouraging start for a full characterisation of this channel. These initial results, are shown in Figure 3.16.

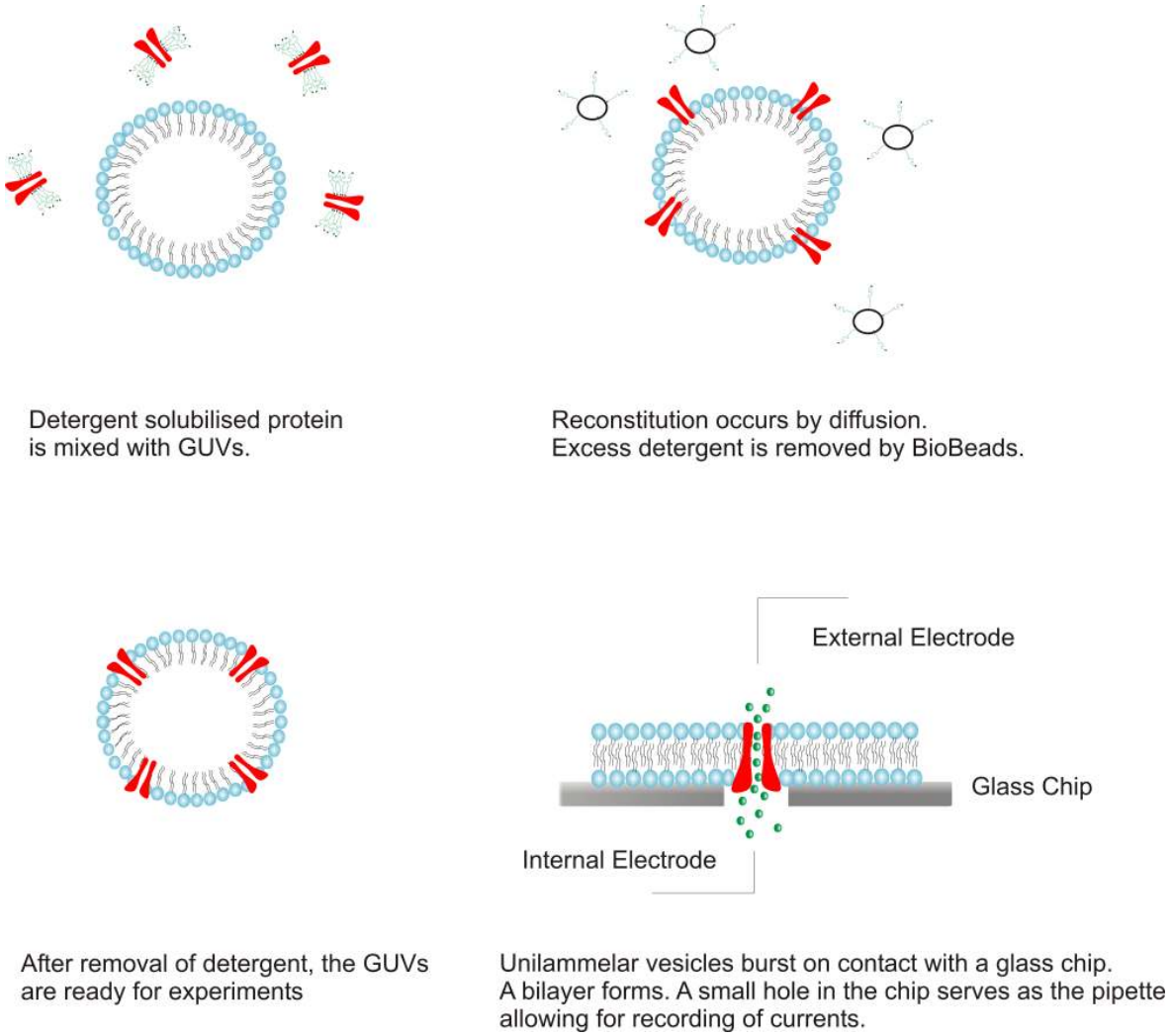

Figure 3.15: *Giant unilamellar vesicles (GUVs) are mixed with detergent-solubilised protein and incubated for 20 minutes at room temperature, before addition of BioBeads. The mixture was incubated at 4 ° C overnight in order to remove excess detergent. The channels diffuse into the vesicles and the excess detergent is adsorbed by the beads. The GUVs with reconstituted channels are placed on a glass chip, which prompts them to burst and leads to bilayer formation. A small aperture in the glass chip acts as a pipette.*

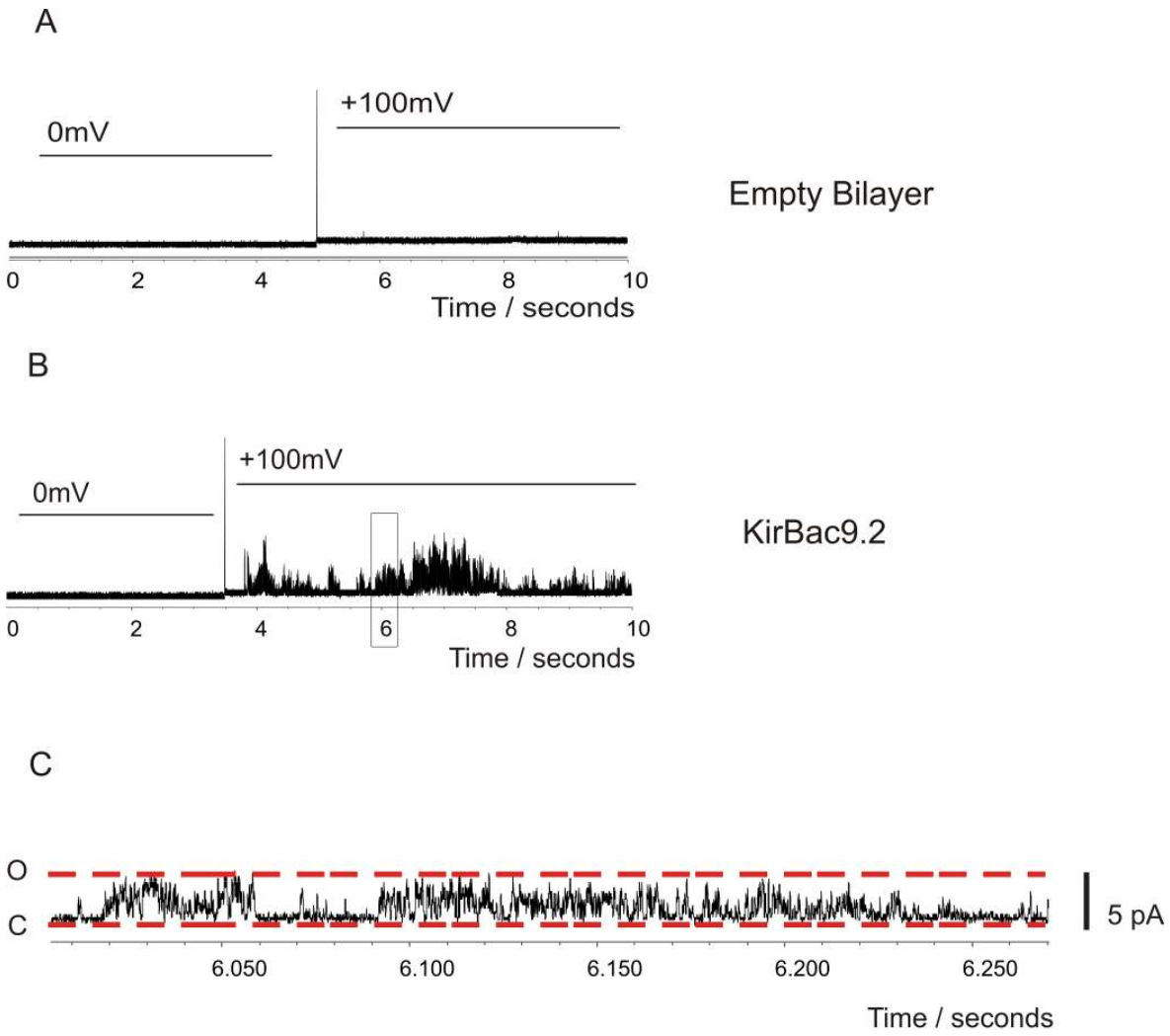

Figure 3.16: ***A*** *Recording of empty bilayers at +100mV, 100mM KCl, 10mM HEPES, pH 7.* ***B*** *Currents recorded from KirBac9.2 reconstituted into GUVs. Activity can be observed at +100mV in symmetrical K^+ solutions consisting of 100mM KCl, 10mM HEPES at pH 7.* ***C*** *A magnification of the recording in panel* ***B****.*

3.4 Summary

This chapter describes the approaches taken towards a functional characterisation of KirBac9.2. The channel appears to be non-selective for monovalent cations. Despite the low channel activity observed in the flux assays, the wild-type channel was able to complement growth of potassium transport deficient *E.coli* at moderate potassium concentrations.

Reconstitution of purified KirBac9.2 into GUVs could prove to be a good approach for an electrophysiological characterisation of KirBac9.2. However, before a detailed electrophysiological characterisation, further macroscopic studies should be performed in order to identify the correct selectivity as well as blockers and activators of the channel.

The activatory mutants identified in this study will be useful tools in any future functional studies of KirBac9.2. It will be interesting to investigate the activity and characteristics of the mutants that have already been purified (as described in 2.3.7.3) in both liposomal flux assays as well as in lipid bilayers in order to compare with the properties of the wild type channel.

Chapter 4

Structural Studies of KirBac3.1 Gating Mutants

4.1 Introduction

The atomic structure of KirBac3.1 was first solved in 2004 (PDB ID 1XL4) [79]. Since then, the conformational landscape of this channel has been expanded by reports of a number of intermediate states, most notably in 2010 by Clarke et al [151] who revealed seven conformations of the closed KirBac3.1 channel. The study made two main points: firstly, it noted that the cytoplasmic domains undergo a rotational movement around the vertical axis of the channel, a conformation that has been termed the "twist" state (Figure 4.1A). Secondly, it was reported that the twist conformation was linked to loss of ionic occupancy in the selectivity filter (Figure 4.1B). This was interpreted as inactivation of the channel at the selectivity filter elicited by rotation of the cytoplasmic domains, i.e. the twist conformation.

Gating at the selectivity filter has been studied in KcsA, where conformational changes in the selectivity filter region are directly coupled to movement of the helix bundle crossing[152, 153, 154] (Figure 4.2). However, all structures published by Clarke et al were in a closed conformation. Also, the selectivity filters in all the reported structures, conductive and "non-conductive", were conformationally identical. The study did not make it clear how the gating at the selectivity filter can occur without structural rearrangements in the selectivity filter, or indeed how the twist conformation might be coupled to the loss of ionic occupancy in the filter.

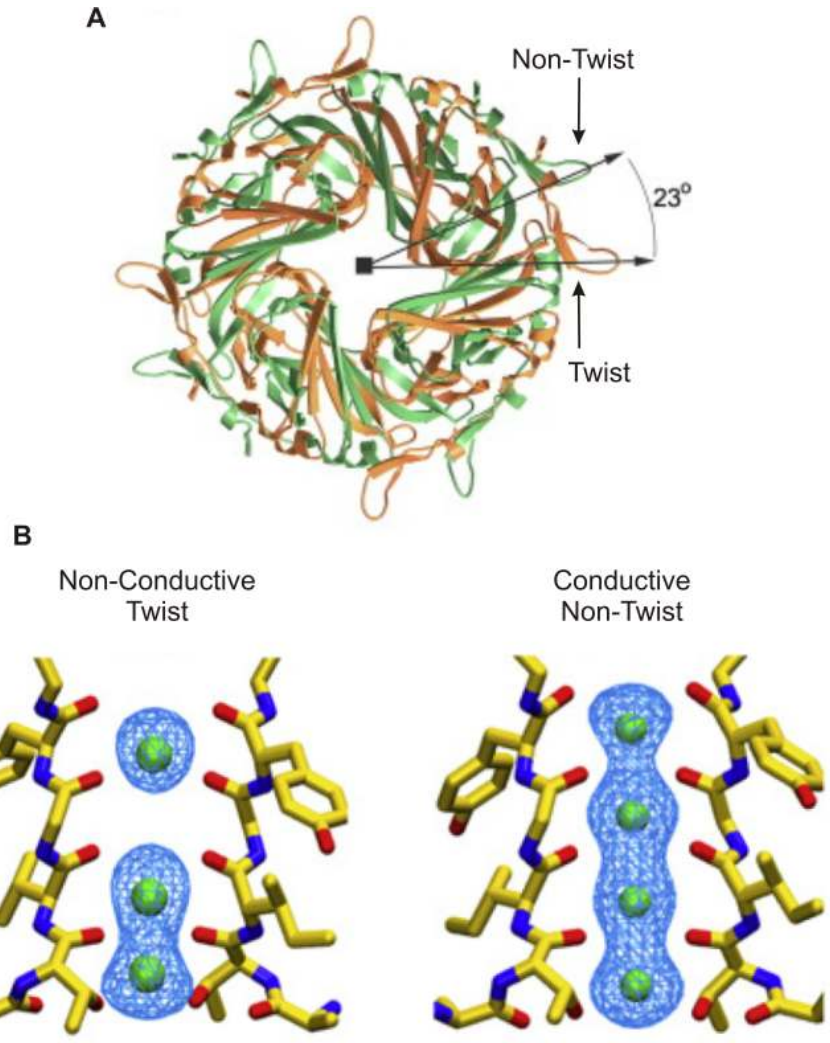

Figure 4.1: ***A*** *The "twist" conformation of the cytoplasmic domains. Top view the cytoplasmic domains of a channel in a non-twist conformation (green) have been superimposed to those of a channel in a twist state (gold). The cytoplasmic assembly undergoes a rotational movement around the vertical axis of the channel.* ***B*** *Loss of density in the selectivity filter observed when the channel is in a twist conformation. Adapted from [151].*

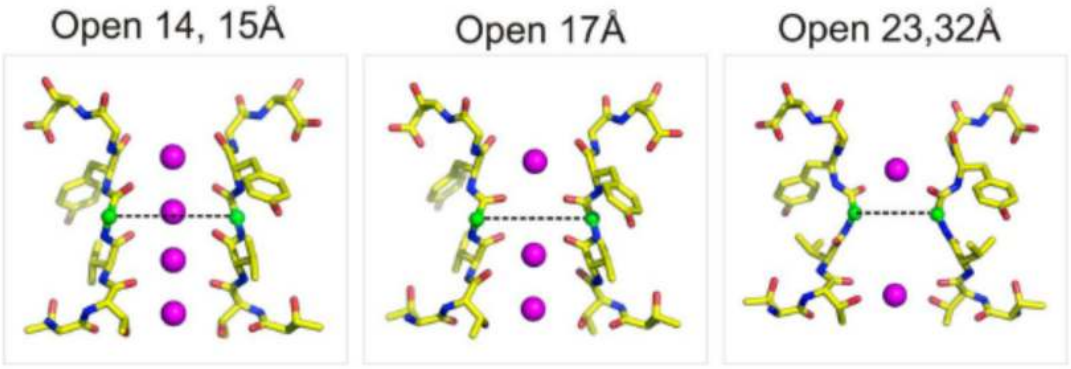

Figure 4.2: *Gating at the selectivity filter (C-type inactivation) in KcsA. The loss of potassium binding sites at the selectivity filter is related to the extent of opening at the helix bundle crossing. The G77 Cα-Cα distances are highlighted by the dotted line. This distance decreases as a function of the helix bundle crossing diameter. Adapted from [153].*

An already ongoing project in the Tucker laboratory to solve the structure of KirBac3.1 in an open conformation resulted in a crystal structure of an activatory mutant of KirBac3.1, S129R [139]. The S129R mutant was identified in a random mutagenesis screen of KirBac3.1 [138]; this mutation occurs in the lower half of the inner helix. The arginines in position 129 point in towards the central pore, and are presumed to push the helices apart thereby forcing the channel into an open conformation. Indeed, the mutant crystallised in an open conformation, i.e. with the diameter of the helix bundle crossing increasing from 12-13Å in the closed state to 17Å in the S129R mutant. In this open conformation the cytoplasmic domains are in the twist state. However, in direct contrast to the report by Clarke et al, no inactivation of the selectivity filter was associated with the twist conformation: the selectivity filter was fully occupied and must therefore be conductive.

In addition to clarifying the relation between the twist conformation and filter gating, the structure of the S129R mutant provided important insight into the mechanism of gating in KirBac3.1. Firstly, an important consequence of twist is the downward movement of the slide helix, which brings it closer to the cytoplasmic domains. Secondly, a rotation of the TM2 helices was observed, as well as a kinking of the TM2 at the conserved glycine hinge. The "kink" originating at the glycine hinge (G120) pushes the helices outward and thereby opens the helix bundle crossing. Finally, the twist in the cytoplasmic domains and the kinks and rotations observed in the TM2 are coupled by interactions between the C-linker, the slide helix

and the intracellular G- and CD-loops (Figure 4.3). Rearrangements of the intracellular and transmembrane domains bring these regions into contact via a displacement of the C-linker, where R137 plays an important role. This, along with the downward movement of the slide helix brought about by the twist, results in a tight network of interactions forming on the interface between the transmembrane and cytoplasmic domains of the channel (Figure 4.5A).

It is not known whether this structure represents the KirBac3.1 channel in its fully open form. Considering the fact that S129R is a gain-of-function mutation, and that the arginine in the structure introduces a restriction in the pore cavity of the channel (Figure 4.4), we are led to believe that the channel must be able to open further in order to overcome the restriction imposed by the mutation.

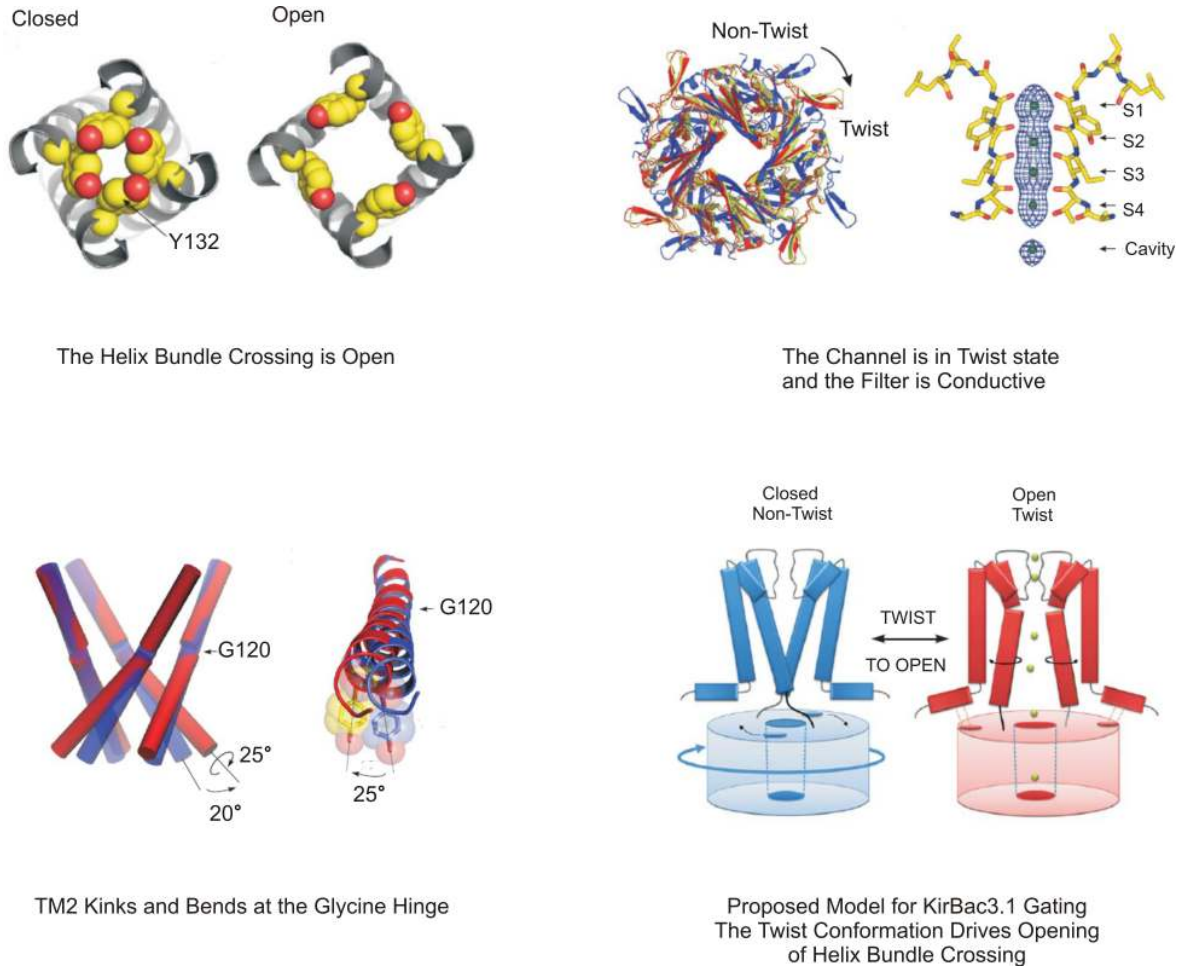

Figure 4.3: *The helix bundle crossing of the S129R mutant is open. The cytoplasmic domains are in twist state, and the selectivity filter is fully occupied. The coupling of the twist conformation to the opening of the helix bundle crossing is thought to depend on the formation of a network of interactions that form at the interface between the cytoplasmic and transmembrane domains. Figures adapted from [139].*

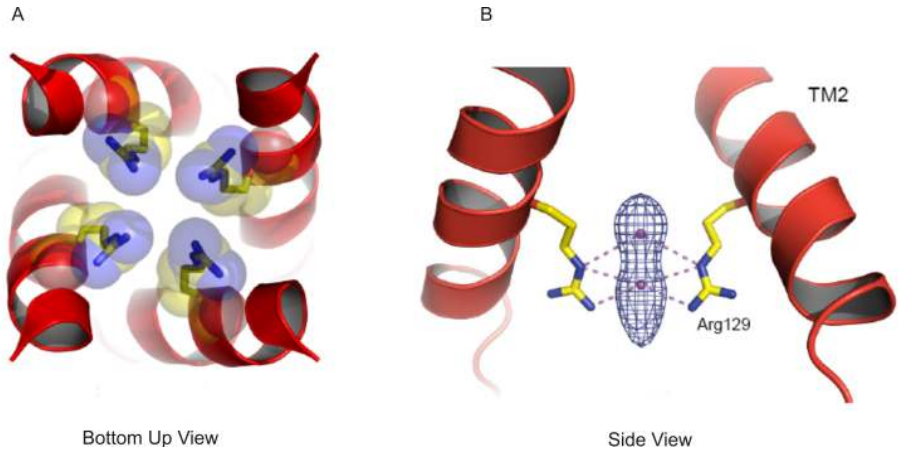

Figure 4.4: *The S129R mutation imposes a restriction in the transmembrane pore of the channel. In the structure of KirBac3.1 S129R (PDB ID 3ZRS) the R129 residues coordinate two chloride ions.* ***A*** *Bottom-up view of the transmembrane pore with the R129 residues shown as sticks and transparent spheres.* ***B*** *Side view of the transmembrane pore, with R129 shown as sticks and the chloride ions shown as purple spheres. Figure adapted from [139].*

Structures of truncated KcsA are available with helix bundle crossing diameters of up to 32Å. However, the presence of the intracellular domains seems to restrict this opening to about 21Å in the structure of the full length KcsA. Whether or not the intracellular apparatus of KirBac3.1 puts a similar restriction on the opening of the helix bundle crossing is not known.

The study described here set out to investigate whether the helix bundle crossing of KirBac3.1 could be opened further. Attempts were made to express and purify other mutants of S129 that showed higher channel activity in genetic complementation screens. However, due to toxicity, these initial attempts failed. Consequently, a double mutant was created carrying the S129R mutation along with an additional activatory mutation at the cytoplasmic interdomain interface, S205L. This chapter reports five new structures of this double gating mutant of KirBac3.1 solved by X-ray crystallography.

4.2 Materials and Methods

4.2.1 *E.coli* Assays

A gene optimised version of the KirBac3.1 was used as background for all mutations. For a detailed description of the complementation assays, please refer to Chapter 3.

4.2.2 Expression of the S129R/S205L Mutant

BL 21 Codon Plus (RP) cells were transformed with KirBac3.1 S129R/S205L cloned into the pET28a vector. An overnight starting culture was used to inoculate 0.5L cultures, which were grown to OD_{600}=1 before expression was induced with 0.5mM IPTG (Apollo Scientific). After induction, the temperature was lowered to 19 $^\circ$ C and growth was continued overnight. Cells were harvested by centrifugation at 12,000 RCF (Beckman Coultier) for 15 minutes at 4 $^\circ$ C.

4.2.3 Purification of the S129R/S205L Mutant

The cells were resuspended in 50mM Tris and 150mM KCl, pH 7.5. The suspension was complemented with 2μg/ml DNAseI (Sigma Aldrich), 0.5mg/ml lysozyme (Fisher Scientific) and a protease inhibitor cocktail tablet (Roche). Following a 20 minute incubation on ice, the suspension was passed through a cell homogeniser (Stansted Fluid Power) 6 times at 12000 psi. The unbroken cells and large debris were removed by centrifugation at 7,000 RCF for 10 minutes.

30mM Decyl Maltoside (Anatrace) was added to the lysed cells, and the solubilisation was performed for 3 hours at 4 $^\circ$ C on a rotating platform. The solubilised material was centrifuged at 70,000 RCF for 30 minutes at 4 $^\circ$ C to remove any unsolubilised cells.

The C-terminally His-tagged protein was isolated by binding to TALON cobalt resin (Clontech) for 1 hour at 4 $^\circ$ C. Following binding, the resin was washed with the lysis buffer complemented with 1. 2mM Tridecyl Maltoside (TriDM) 2. 10mM Imidazole, 500mM KCl, 2mM TriDM 3. 20mM Imidazole, 2mM TriDM. Finally, the protein was eluted in 50mM Tris, 150mM KCl, 400mM Imidazole and 0.5mM TriDM, pH 7.5. Before the gelfiltration step, the protein was concentrated on a filtration device with a 50kDa cutoff membrane (Amicon). Gelfiltration was done on a Superdex200 column (GE Healthcare). The sample was run with a buffer of 50mM Tris, 150mM KCl and 0.5mM TriDM, pH 7.5. Detergent exchange was

performed by washing the sample with 3x15 ml gelfiltration buffer where TriDm has been replaced with 14mM HEGA-10. The protein was concentrated to 0.5ml in a 15ml filtration device (50kDa cutoff membrane), and then diluted with the HEGA-10 buffer. The protein concentration was adjusted to 8mg/ml and the sample filtered through a 0.22μm filter to remove any large impurities.

4.2.4 Crystallisation

A grid screen was designed around the original conditions for KirBac3.1 crystallisation [151]

Crystallisation was set up on a 96-well MRC crystallisation plate (Hampton Research). The upper drop: 150nl protein, 150nl reservoir solution The lower drop: 100nl protein, 200nl reservoir solution Drops were set up using the Mosquito robot (TTP LabTech)

The finished crystallisation plates were incubated at 22 $^\circ$ C. Crystals appeared after 3-4 days.

4.2.4.1 Crystal Harvesting

Crystals were harvested using LithoLoops (Molecular Dimensions). Cryoprotection was achieved by washing the crystals with a variation of their mother liquor with an increased precipitant concentration, and following this they were flash frozen in liquid N_2.

4.2.5 Data Collection

Data was collected at 100 K using a Pilatus 6M detector at the I-24 beamline at the Diamond Light Source to a resolution of between 2.80Å and 2.46Å at a wave length of λ=0.978 Å. Following the initial space group estimation by iMOSflm, a strategy for data collection was calculated using the "strategy" function of iMOSflm [104]. 140 degrees of images were collected for each of the data sets, with 5 images for each degree.

4.2.6 Molecular Replacement and Model Building

Data was indexed and integrated with iMOSflm, and the spacegroup confirmed by Pointless [155]. Scala [155] was used to scale and merge the integrated data in the space group. Five percent of the reflections were set aside in the free R set. Molecular replacement was carried out with Phaser [156] using a search model derived from PDB 3ZRS, which allowed for instant interpretation of the maps. These were iteratively rebuilt using Coot [157, 158].

4.2.7 Refinement

Refinement of the structures was performed by Dr. Vassilly Bavro and Dr. Joao Muniz.

The model was refined in real space using Coot, and refined using BUSTER-TNT [159], which included a final round of translation, libration and screw-rotation (TLS) anisotropic refinement, as implemented in BUSTER-TNT. The F0-Fc map maxima were assessed for possible presence of ligands, which allowed determination of the presence of lipid/detergent/spermidine moieties. The refinement of ligands was performed using the Phenix Elbow [160, 161, 162] software. All data refinement statistics are given in tables 1-5.

4.3 Results and Discussion

4.3.1 Testing the Proposed Model of Gating in KirBac3.1

The structure of the KirBac3.1 S129R mutant revealed a tight network of interactions at the interface of the cytoplasmic domains and the transmembrane domains which were proposed to couple the twist conformation of the cytoplasmic domains to the opening of the helix bundle crossing. Residue Y38 in the slide helix appeared to be crucial in this coupling, with the hydroxy group of Y38 bonding with the G-loop residue Q252 of the neighbouring subunit. To investigate the importance of this network, we introduced a Y38F mutation into a clone already carrying the activatory S129R mutation and tested the ability of the double mutant to support growth of K^+ auxotrophic *E. coli*.

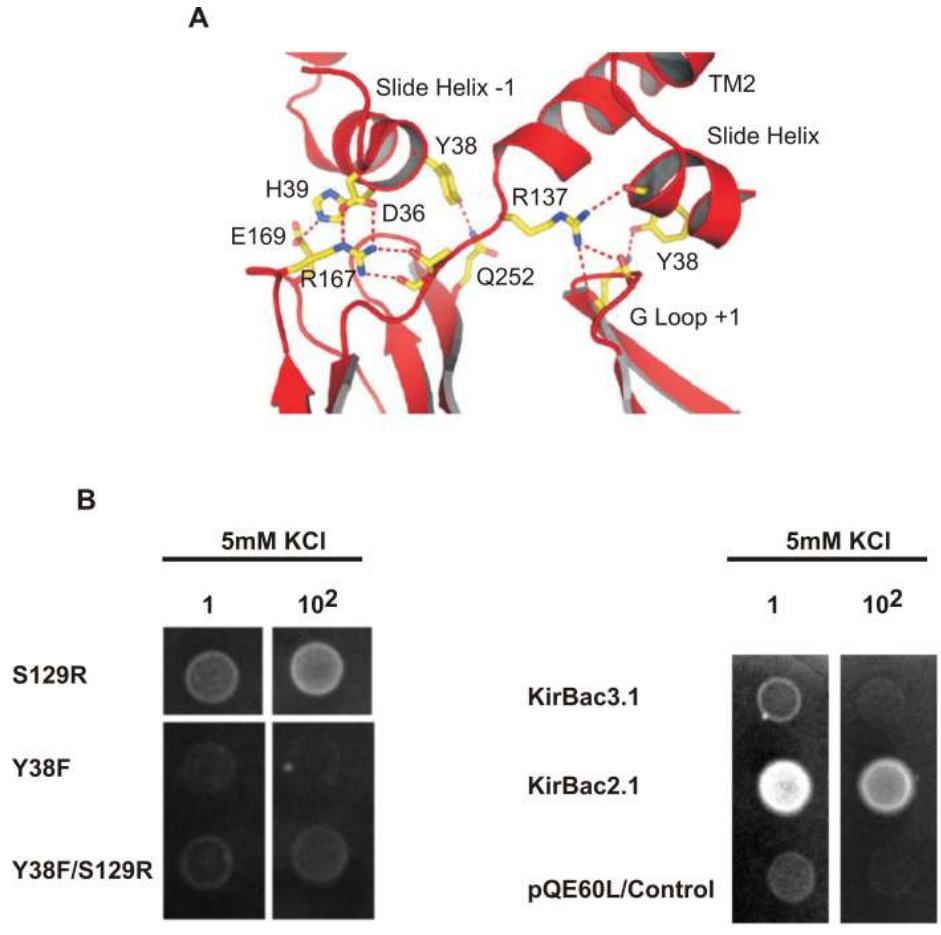

Figure 4.5: ***A*** *The proposed network of interactions at the interface of the transmembrane and cytoplasmic domains.* ***B*** *Breaking the interaction network by mutating the slide helix Y38 residue to an F abolishes the ability of the S129R mutant channel to complement growth of K^+ auxotrophic E. coli. Both* ***A*** *and* ***B*** *were adapted from [139].*

Indeed, the double mutant did not complement growth of *E. coli,* suggesting that the interaction between Y38 and Q252 is crucial for coupling the twist conformation to the opening of the helix bundle crossing and supporting the proposed model for gating of KirBac3.1.

4.3.2 Identification of Additional Gating Mutants at S129

In order to isolate a mutant with a potentially larger opening of the helix bundle crossing, we substituted the serine in position 129 of the wild-type KirBac3.1 with different residues and screened the mutants in K^+ auxotrophic *E. coli.* Introducing any charged (R, K, D, E) or bulky (Q, N) residue in this position resulted in good complementation of growth of the potassium transport deficient E. coli cells. Substitutions with smaller, hydrophobic amino acids, such as alanine and leucine did not complement growth. Of all the S129 mutants, the ones which complemented growth best were substitutions with glutamine and aspartate. Complementation data is shown in Figure 4.6.

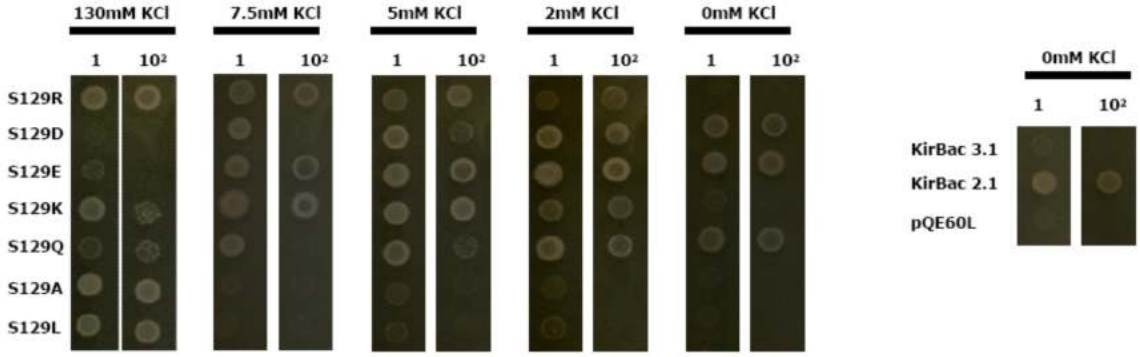

Figure 4.6: *Genetic complementation assay of S129 mutants. Strong complementation is obtained by substituting the serine with aspartate, glutamate or glutamine. Aspartate and glutamate substitutions result in toxicity at high potassium concentrations. Good complementation is observed in all channels where the serine has been substituted with charged residues. Substitutions with small, non-polar residues do not result in complementation. KirBac2.1 is used as a positive, and the empty vector pQE60L as a negative control.*

4.3.2.1 Expression of KirBac3.1 S129Q and S129D

The S129Q and S129D mutations were introduced into the wild-type KirBac3.1, and expressed as described in the methods section. However, the mutant channels were expressed at very

low levels and the purified protein proved very unstable (Data not shown). All attempts to improve the yield and stability of the protein, including expression in the presence of barium in order to block channel activity and reduce toxicity as well as purification of S129D and S129Q expressed in TK2299 K^+ auxotrophic *E.coli* cells, were unsuccessful.

Possible Reasons for Low Expression and Instability of S129D and S129Q mutants

Why is purification of S129D and S129Q mutant channels so difficult? The complementation assays show that these channels are expressed and functional. However, we cannot know how well the proteins express, even in the K^+ auxotrophic *E. coli*. Complementation assays are extremely sensitive to small changes in channel activity, and it is possible that the expression becomes down regulated in the case of highly active channels. So, even if complementation is observed, it is unknown how many channels are expressed in each cell to obtain the phenotype. Considering that in our large scale expression experiments the cell pellet per litre bacterial culture was typically between 10-15% of that normally obtained for the cells expressing the S129R mutant, it is likely that toxicity plays a part in the difficulties we faced when trying to express these channels. This problem is likely to be amplified in strains which are optimised for protein over expression, as the larger number of channels in the cell membrane will lead to increased toxicity.

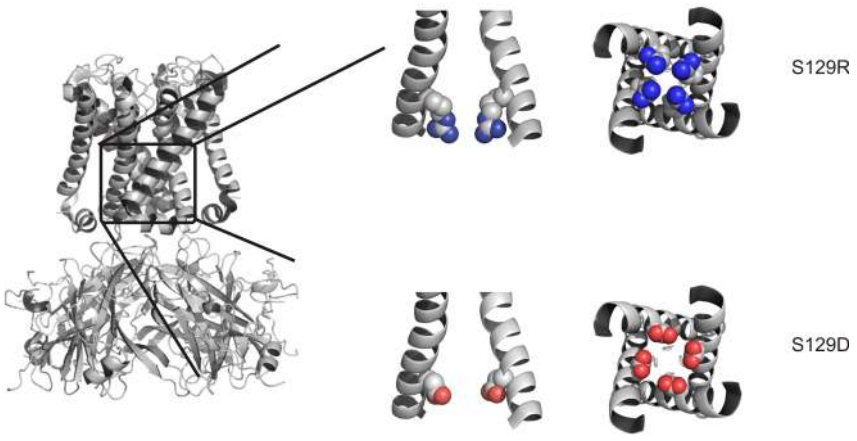

Figure 4.7: *The transmembrane pore of the S129R mutant compared to a modelled pore of a S129D mutant. The region of interest is boxed and magnified in the panels on the right. For ease of viewing, the sideview only shows two TM2 helices. The bottom-up view shows all four TM2 helices. The S129R and S129D residues are shown as spheres.*

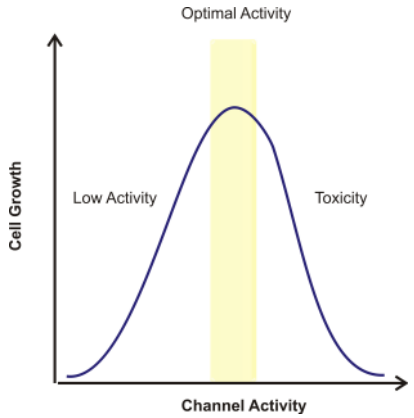

$$I_K = N\, P_o\, i$$

Figure 4.8: *The relationship between cell growth and channel activity in K^+auxotrophic E. coli. The channel current is dependent on the nuber of channels, their open probability and their conductance. Channels which are overly active may cause toxicity in K^+auxotrophic E. coli by allowing too much potassium to enter the cells.*

4.3.3 Double Mutant

Since the attempts to express and purify an S129 mutant with a higher degree of activity than S129R failed, an alternative approach was used to obtain a mutant with a larger opening of the helix bundle crossing. The expression and purification of the S129R mutant was very stable, and the channel had already proved a good candidate for crystallisation. So, to obtain a more active channel that can be expressed and purified, an additional activatory mutation was introduced into the KirBac3.1 gene already carrying the S129R mutation. The random mutagenesis screen of KirBac3.1 [138] identified a number of activatory mutations in this protein. They can be divided into two large clusters: the first one concentrated at the bottom of the TM2 (residues 120-129), all typified by substitutions of small polar with charged bulky side chains, and the second one spread around the cytoplasmic domains, and a lot more varied (Figure shown in Chapter 5, 5.2). One of the mutations in the cytoplasmic part which had a very good complementation profile was S205L. The mechanism by which this substitution increases the activity was not immediately obvious. However, its position close to the interface between the subunits could mean that it plays a role in stabilising the twist conformation. By combining the S129R mutation in the TM2, which, as described earlier, stabilises the coupling between the transmembrane and cytoplasmic domains, with the S205L mutation in the cytoplasmic part, which might be involved in facilitating the twist conformation, it might be possible to observe a different open conformation of the channel.

4.3.3.1 Expression and Purification of the S129R/S205L Double Mutant

The S205L was introduced into the KirBac3.1 gene cloned into pET28a, already carrying the S129R mutation. The expression and purification were performed as described in the methods section. The results of the expression and purification of the protein were similar to those of S129R, indicating a similar level of stability in spite of the presence of the S205L mutation. The protein, purified in TriDM, ran as a tetramer on the size exclusion column (Figure 4.9) .

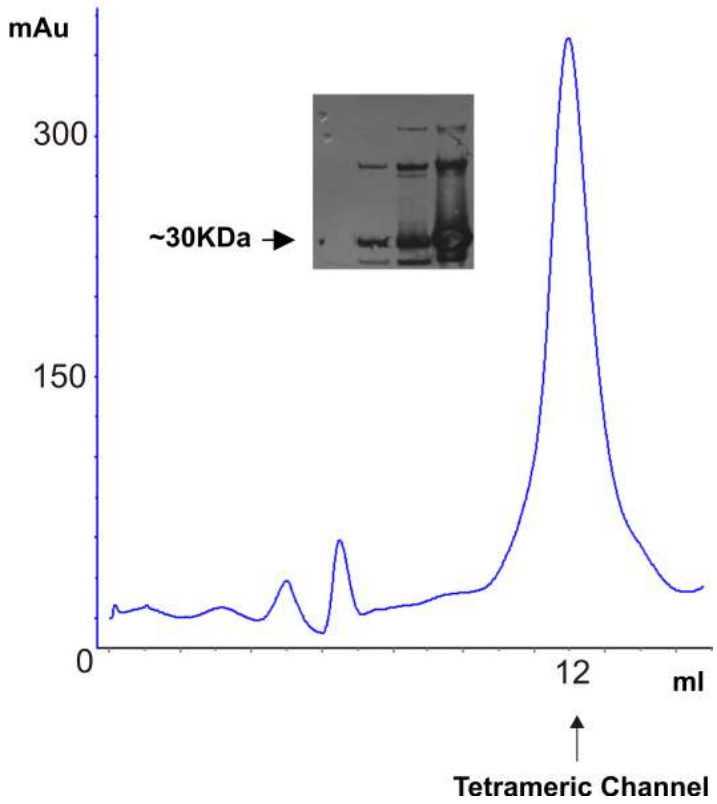

Figure 4.9: *Purification of the S129R/S205L mutant channel. The protein eluted as a tetramer from the size exclusion column. The column buffer consisted of 150mM KCl, 50mM Tris, 0.5mM TriDM at pH7.5.*

4.3.3.2 Crystallisation of the S129R/S205L Double Mutant

Following the methods for crystallisation of the S129R mutant [139], the TriDM detergent was replaced with HEGA-10 after gel filtration. Crystallisation was set up as described in the methods section. The plate was incubated at 22 $^{\circ}$C for 3 days before crystals appeared. Their appearance was orthorhombic, with dimensions of ~ 100 x 100 x 50μm.

4.3.4 Structure of KirBac3.1 S129R/S205L

The structure of the double mutant was solved at 2.80Å resolution. Refinement of all structures in this chapter was done by Dr. Vassiliy Bavro and Dr. Joao Muniz. All data collection and refinement statistics are shown in Figures 4.29-4.33. The channel crystallised in space group $P2_12\ 2_1$, with two molecules in the asymmetric unit. An alignment with the S129R structure shows that the two conformations are strikingly similar. No further opening at the helix bundle crossing was observed, and the Y132 Cα-Cα distance is ~17Å in both cases. As in the case of S129R structure, the selectivity filter was found to be fully occupied leading to the conclusion that the channel is conductive (Figure 4.10) .

From examination of this structure, it was not immediately obvious how, or if, the S205L mutation might contribute to the opening of the channel. At first glance, the pocket around the residue is virtually unchanged between the two structures. However, upon closer examination it became evident that subtle rearrangements enabled a salt bridge to form between residues D197 and R202 of neighbouring subunits (Figure 4.11)

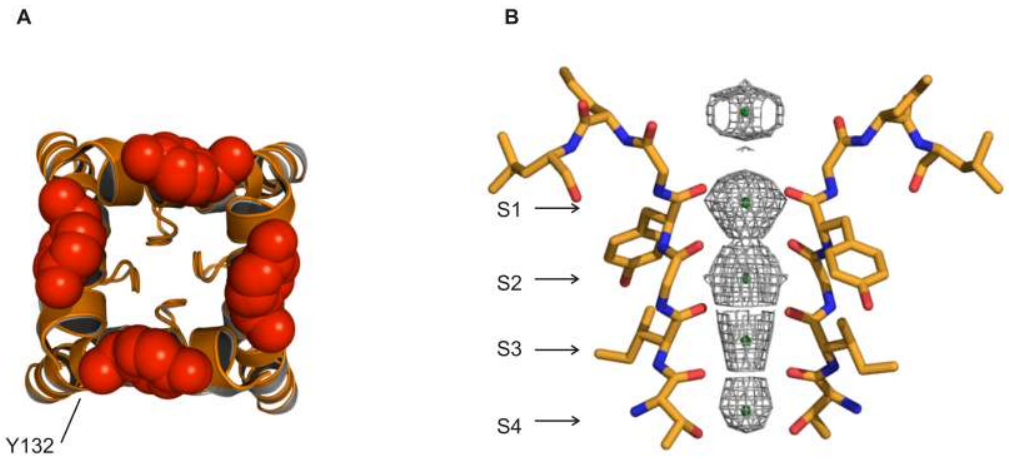

Figure 4.10: ***A*** *Alignment of the S129R (grey) and the S129R/S205L (orange) helix bundle crossing viewed from the cytoplasmic cavity. Y132 is shown in red spheres. No further opening of the helix bundle crossing was observed.* ***B*** *The filter of the double mutant is fully occupied. The potassium ions are shown as green spheres. The $2F_o$-$F_c$map is contoured at $\sigma 4$.*

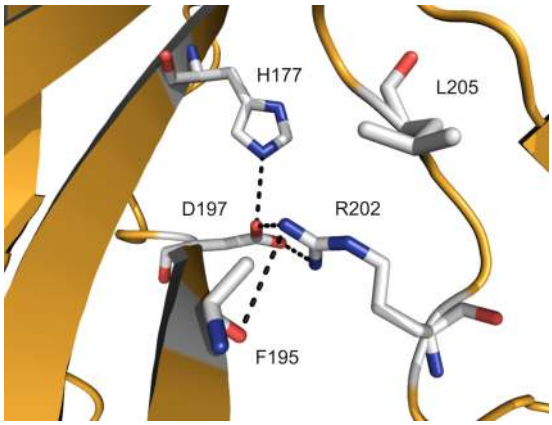

Figure 4.11: *Intersubunit interactions at the cytoplasmic interface of the S129R/S205L mutant. A novel salt bridge is observed between R202 and D197. Residue L205 is also shown in sticks.*

The quality, and indeed the resolution of the crystal data, is improved compared to that of the single mutant S129R suggesting that the S205L mutation acts to stabilise the tetramer, and indirectly also the crystal lattice.

4.3.5 Crystallisation in the Presence of Ligands

Since well diffracting crystals of the S129R/S205 mutant grew readily, we attempted to crystallise the S129R/S205L channel in the presence of barium, magnesium, spermine and spermidine. Previous study by Clarke et al suggested binding sites for barium, magnesium and polyamines in the KirBac3.1 channel [151].

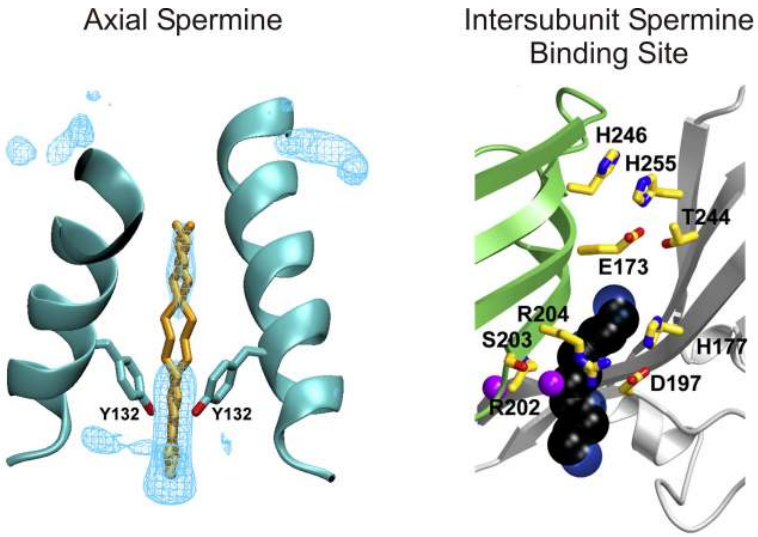

Figure 4.12: *Polyamine binding sites in KirBac3.1observed by Clarke et al . The axial sperime is seen in the transmembrane pore of the channel. A sperimne molecule is also observed at the cytoplasmic interface between subunits. Adapted from [151].*

However, despite the high profile nature of this study, we could not reproduce the published figures based on the density maps deposited in the PDB. Here we aim to reproduce the results published by Clarke et al and provide a better picture of binding of ions and polyamines in KirBac3.1. We present four structures of the KirBac3.1 double gating mutant S129R/S205L obtained in the presence of $MgCl_2$, $BaCl_2$, spermine and spermidine.

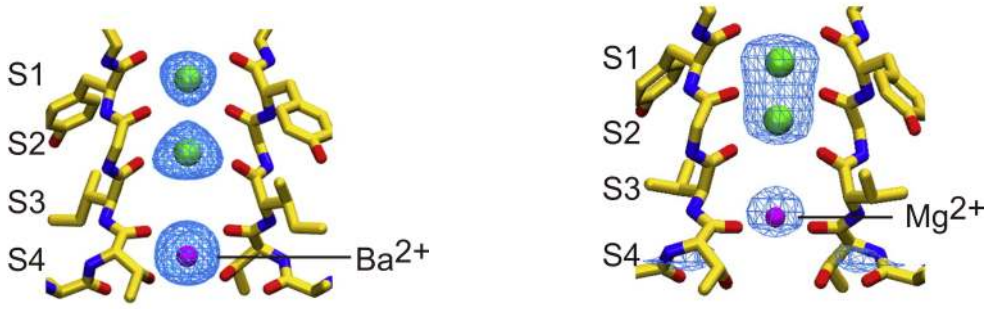

Figure 4.13: *Barium and magnesium binding in the selectivity filter of KirBac3.1. The figure was adapted from [151]*

4.3.5.1 Barium

In the presence of barium, crystals of the double mutant diffracted to 2.65Å. The protein crystallised in space group P4 2_1 2. However, in contrast to what was observed by Clarke et al, no barium ions were detected in the density maps (Figure 4.14) .

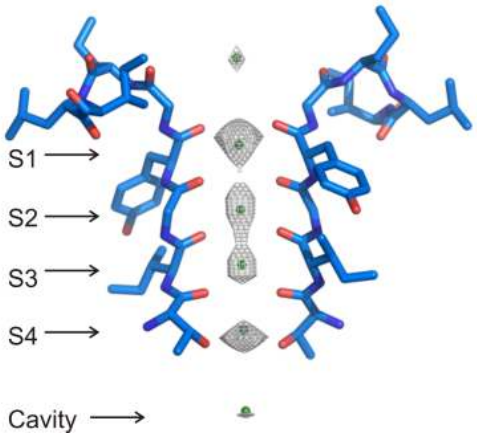

Figure 4.14: *The selectivity filter of the S129R/S205L mutant crystallised in the presence of barium. No densities were observed in the filter that could be assigned to barium ions. The potassium ions are shown as green spheres, and the $2F_o$-$F_c$map is contoured at $\sigma 4$.*

Nevertheless, inclusion of barium in the crystallisation did improve the resolution and quality of the data. In this higher resolution structure, a density located in the space between TM1 and TM2 was observed and assigned to a PEG molecule (Figure 4.15B). A lipid molecule was modelled into a density in the intra-vestibular groove created by T244 and N253 (Figure 4.15A).

Occurrence of small molecules and traces of lipids carried over from the purification process is not uncommon, especially in high resolution structures. Often, the binding observed is non-specific and merely serves to support the protein crystallisation.

The overall structure is very similar to the previously described, native S129R/S205L structure. There are a few subtle differences in the vicinity of the leucine 205. Interestingly, we observe two conformations of R202 – one forming a salt bridge with D197, and one interacting with the backbone of F195, shown in Figure 4.16.

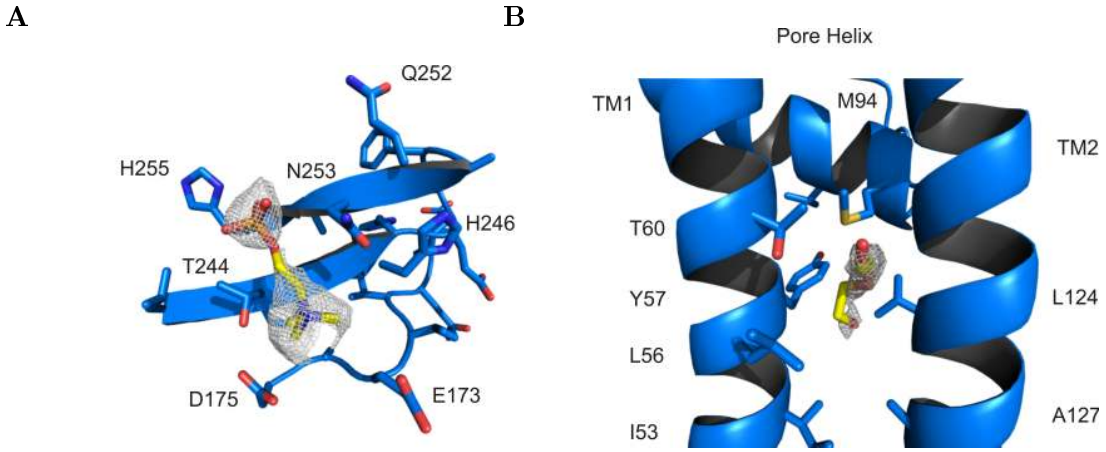

Figure 4.15: *Small molecules observed in the structure.* ***A*** *A phosphocholine moiety is observed on the internal face of the cytoplasmic cavity, between residues T244 and N253.* ***B*** *A PEG molecule was modelled into a density observed between the transmembrane helix residues Y57 and L124. $2F_o$-$F_c$maps are shown for both molecules, contoured at σ1.5.*

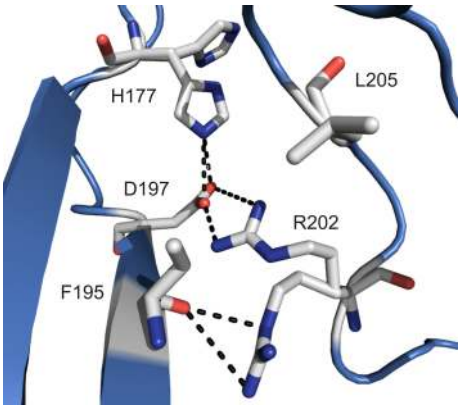

Figure 4.16: *The intersubunit connections. R202 is observed in two conformations. One conformation establishes a salt bridge with D197, while the other bonds with the backbone of F195.*

4.3.5.2 Magnesium

Addition of magnesium to the crystallisation conditions resulted in crystals diffracting to 2.58Å. The channel crystallised in the space group $P2_1\ 2_1\ 2$. Despite the different space group, the overall structure of the channel was almost identical to that of the previous two structures described. However, no magnesium ions were detected in the density maps. Two channel subunits form the assymetric unit in this structure. The asymmetry arises from differences at the subunit interfaces. In chain A of the asymmetric unit R202 is observed

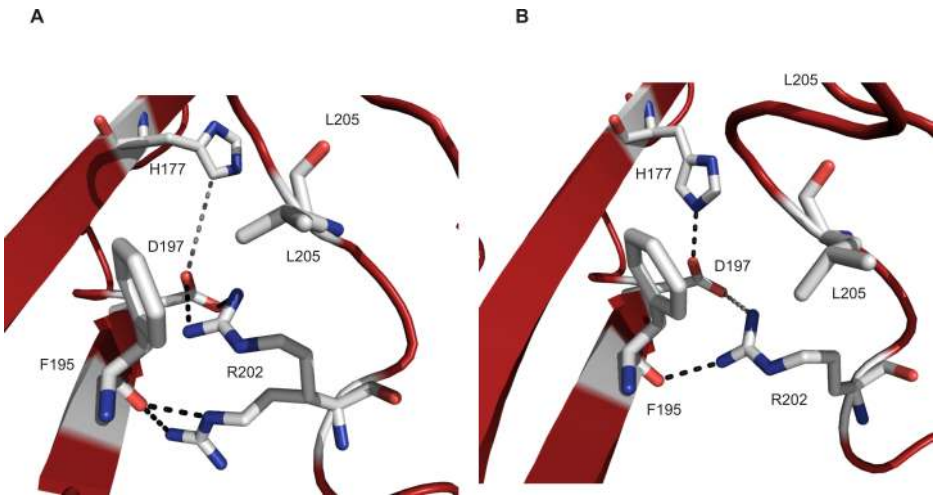

Figure 4.17: *The two subunit interfaces in the double mutant structure crystallised in the presence of magnesium.* ***A*** *In chain A, the R202 bonds with both D197 and F195.* ***B*** *In chain B, the distance between R202 and D197 is >5Å (grey dashes), but the connection to the backbone carbonyl of F195 is maintained.*

in two conformations: one forming a salt bridge with D197 and the other bonding with the backbone carbonyl of F195 (Figure 4.17A). However, in chain B, the distance between D197 and R202 is increased to ~5Å, suggesting that formation of the saltbridge has not occurred. The bond with the backbone of F195 is still present (Figure 4.17B).

4.3.5.3 Spermine

KirBac3.1 S129R/S205L crystallised in the presence of spermine in space group $P2_1\ 2_1\ 2$. The crystals diffracted to 2.77Å. The study by Clarke et al showed the spermine molecule coordinated by residues H177, D197, S203 and R204, in a vertical orientation at the internal side of the intersubunit interface. In this new structure, the spermine molecule is also found at this interface (Figure 4.18A). However, the novel intersubunit connections have shifted the binding site away from the cytoplasmic pore. A comparison of the spermine binding sites is shown in Figure 4.18B.

Polyamines are long, flexible molecules and when they are observed in crystal structures it is difficult to know if their binding in grooves is physiological and specific, or acting merely to stabilise lattices. In contrast to the structures previously reported by Clarke et al, we observe no axial spermine.

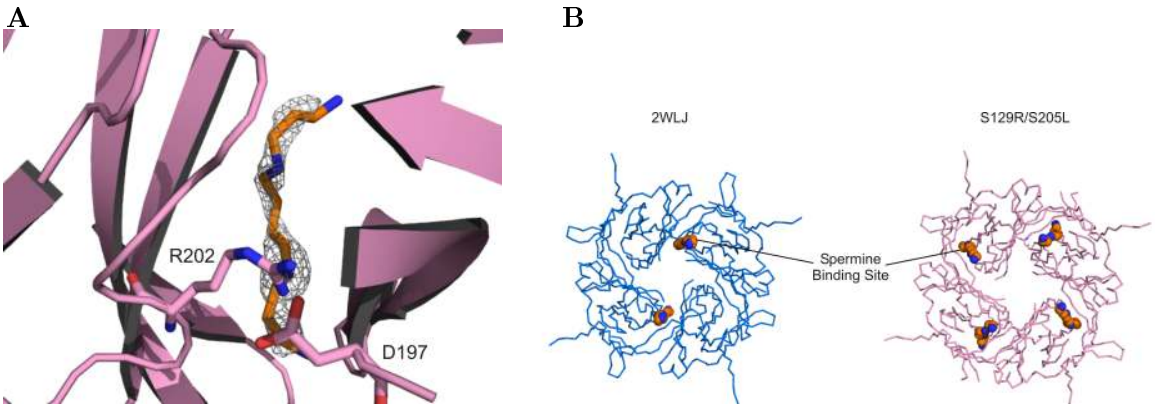

Figure 4.18: ***A*** *The observed location of the spermine molecule in the S129R/S205L structure, with the $2F_o$-F_c map contoured at $\sigma 1$. The molecule is viewed form inside the cytoplasmic cavity.* ***B*** *Compared to the previously observed binding site, the molecule is placed further away from the cytoplasmic cavity, probably due to the change in intersubunit interactions.*

4.3.5.4 Spermidine

In the presence of spermidine, the channel crystallised in the space group P4 2_1 2 and the crystals diffracted to 2.46Å. This was our highest resolution structure, as well as the highest resolution KirBac structure available. However, no densities were present that could be assigned to a spermidine molecule.

In the structure of the S129R mutant, residue R137 was found to play a critical role in the displacement of the C-linker (Figure 4.5A). In this S129R/S205L structure, R137 is observed in three conformations: firstly, bonding with the backbone carbonyls of R134 and A133 at the bottom of TM2, secondly, tightening the bond with the backbone L42 in the slide helix and finally interacting with the backbones of E248 and A249 in the G-loop. The interactions are shown in Figure 4.19. These interactions emphasise its importance for coupling between the transmembrane and cytosolic domains.

Perhaps the most interesting observation in this structure is the presence of two densities in the cytoplasmic cavity of the channel that have been modelled as potassium ions. The first one, shown in Figures 4.20 and 4.22, is coordinated by D175 and E173, a residue that in the mammalian strong rectifier Kir2.2 corresponds to E225. This glutamate in Kir2.2 has been shown to play a role in inward rectification, as well as concentration of cations in the cytoplasmic cavity. The distances between the potassium ion and the carboxyl groups of E173 and D175 are 7-8.5Å. This suggests that the ion is coordinated in a fully, or almost fully, hydrated state. However, despite the presence of densities that could be interpreted as water molecules, the signal of these is weak, which is why the potassium ion has been modelled without any surrounding water molecules. The second potassium ion is located approximately midway down the cytoplasmic pore, shown in Figures 4.21 and in 4.22. The diameter of the pore at this location is ~20Å, which means that the ion would have to be coordinated in a hydrated form. Also in this case, the water molecules surrounding the ion are poorly resolved.

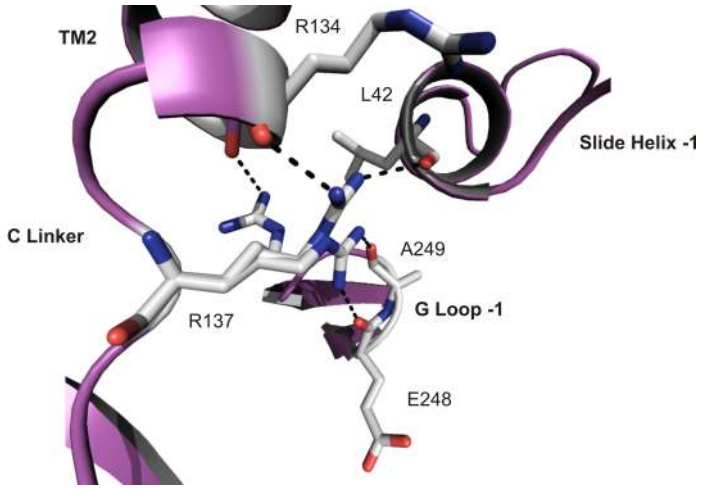

Figure 4.19: *The three conformations of R137. In this structure, R137 interacts with the slide helix and the G Loop of the neighbouring , as well as with the TM2 of the same subunit.*

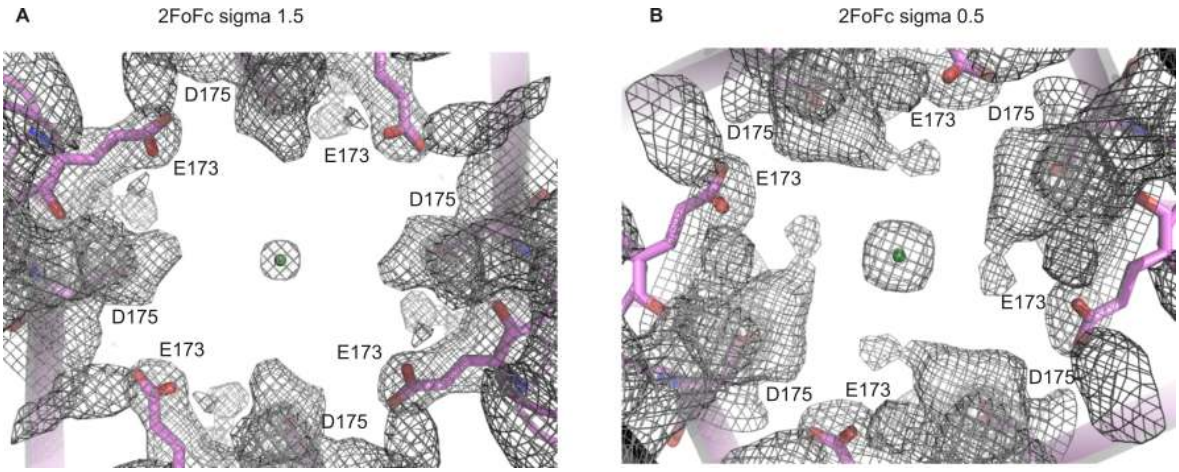

Figure 4.20: *Top-down view of the cytoplasmic cavity. The cross section of the $2F_o$-F_c map showing the potassium ion (green spheres) coordinated by E173 and D175. The ion is thought to be hydrated, although densities that can correspond to water molecules were not resolved at $>\sigma 0.5$.*

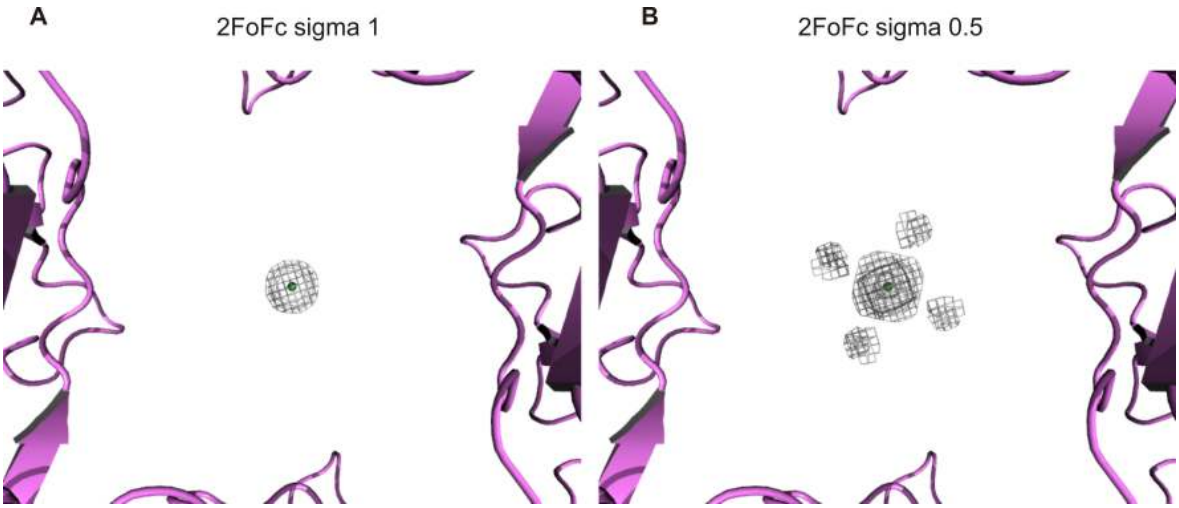

Figure 4.21: *Top-down view of the cytoplasmic cavity. The second potassium ion observed in the cytoplasmic cavity. The $2F_o$-F_c map contoured at $\sigma 1$ does not indicate the presence of surrounding water molecules. However, at lower σ values, densities can be observed that may correspond to a hydration shell.*

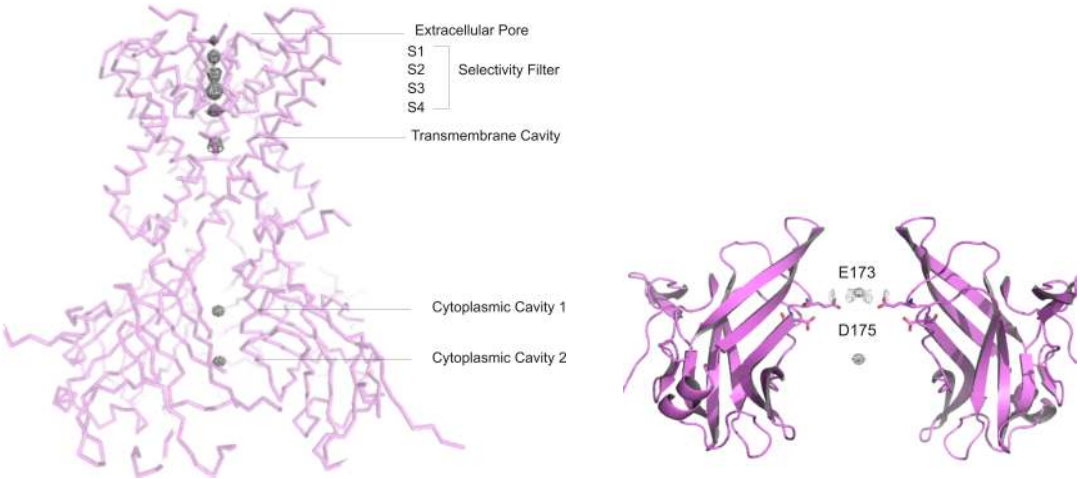

Figure 4.22: *All potassium ions modelled in the structure. Ions in the transmembrane pore and the selectivity filter are contoured at $2F_o$-F_c σ 4, while the ions in the cytoplasmic cavity are contoured at $\sigma 1.5$. The figure on the right is a side view of the cytoplasmic domains alone. For clarity, only two subunits are shown. The $2F_o$-$F_c$map is contoured at $\sigma 1.5$ showing the two modelled potassium ions in the cytoplasmic cavity.*

4.3.6 Analysis and Comparison

4.3.6.1 Twist

The wild-type KirBac3.1 has been crystallised with its cytoplasmic domains in a number of rotational states, i.e. the non-twist and twist states. It is likely that the energy barrier between the twist and non-twist states is low and that some extent of rotational movement of the cytoplasmic domains can occur without resulting in the opening of the helix bundle gate. However, the structures of the KirBac3.1 S129R and S129R/S205L channels have all been crystallised in the twist state, which suggests that the S129R mutation locks the channel in the twist conformation.

4.3.6.2 Intersubunit interactions

The structures of the S129R/S205L possess a novel intersubunit interaction between D197 and R202 when compared to the structure of S129R. But, how do intersubunit interactions compare across the available structures of different conformational states?

Here we will consider four different structures- a closed non-twist structure (PDB ID 2WLJ), a closed twist structure (PDB ID 2X6C), an open twist structure of the KirBac3.1 S129R mutant (PDB ID 3ZRS) and the structure of the double mutant S129R/S205L.

From examination of the four structures in Figure 4.23 it is evident that there are two prinicpal interaction points responsible for maintaining the cytoplasmic intersubunit connections in KirBac3.1. Here we will address them as the upper and lower "clasp". The upper clasp, defined by the connection between R257 and E248 remains constant in all the available structures. The lower clasp in both closed structures, as well as in the open S129R structure, is made up of the E173, D175 and H177 triad. However, in the S129R/S205L mutant the lower clasp consists of the saltbridge between D197 and R202, an interaction unique to this double mutant structure. The location of the lower clasp in the S129R/S205L mutant shifts down-and-out with respect to the upper clasp. (Figure 4.23 for a top view of the interactions, and Figure 4.23 for a side view). The increased spacing between the two principal intersubunit connections may act to stabilise the tetramer in the twist conformation.

Residues D197 and R202 are highly conserved in KirBac channels, which indicates that the interaction we observe in this structure is potentially important in all members of the KirBac family. It is, however, interesting to note that in KirBac6.1, the mutation of the R202

equivalent, R210, to a cysteine results in activation of the KirBac6.1 channel. Also, a mutation of the residue equivalent to R257, which in KirBac3.1 is a part of the upper clasp, results in activation [138]. Since the atomic structure of KirBac6.1 is not available, it is difficult to predict how these mutations may act to activate the channel. It is possible that these residues serve a different purpose in KirBac6.1 than that observed in KirBac3.1.

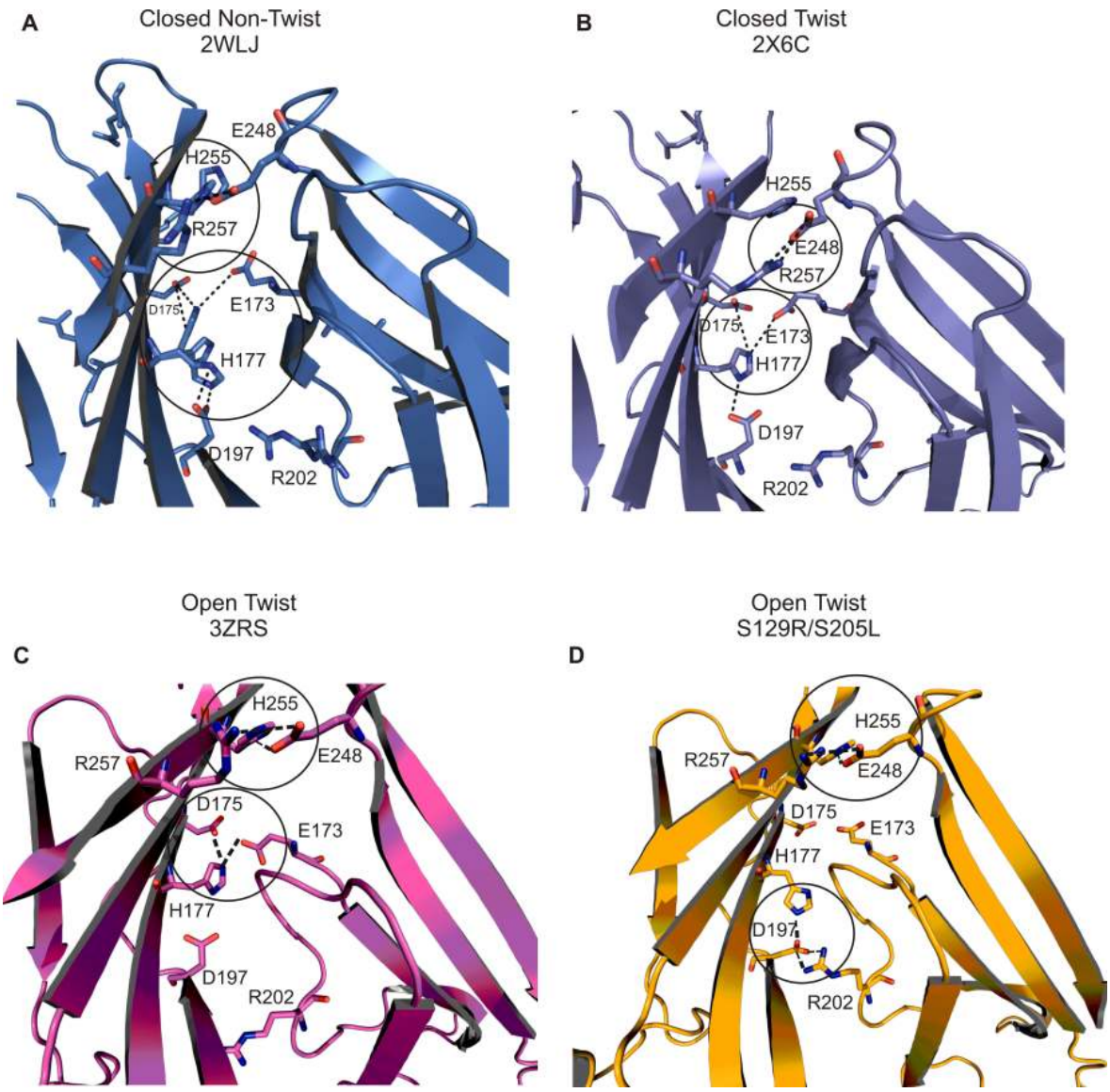

Figure 4.23: *The cytoplasmic intersubunit space in four different KirBac3.1 structures. The upper and lower clasps are circled. In* ***A*** *the upper clasp is made up of H255, R257 and E248, while the lower one consists of H177, E173 and D175. In the closed twist state shown in panel* ***B****, the connections are similar, with the exception of the absence of H255 from the upper clasp. In the open twist state,* ***C****, H255 R257 and E248 form the upper clasp and H177, E173 and D175 the lower one. The upper clasp of the double mutant structure,* ***D****, is the same, but the connections that make up the lower clasp are novel, formed by D197 and R202.*

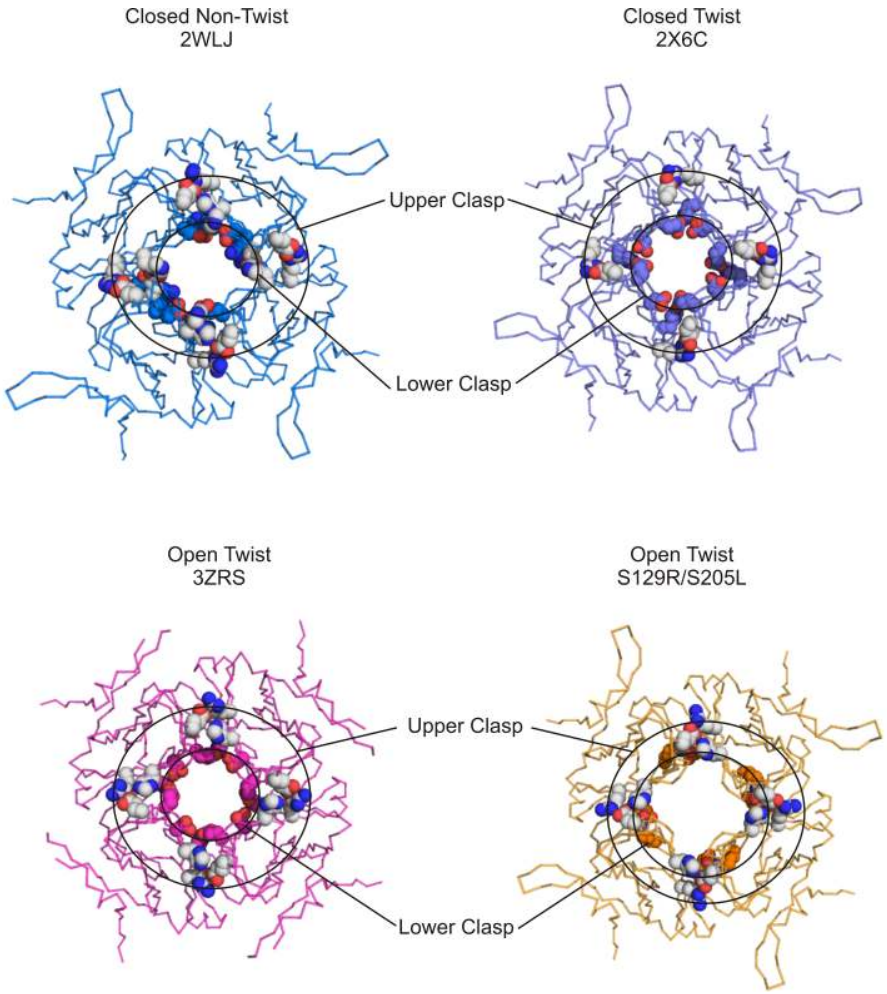

Figure 4.24: *The location of cytoplasmic intersubunit connections in different structures of KirBac3.1. The upper clasp is marked in grey, and the lower one in coloured spheres. Note the location of the lower clasp in the S129R/S205L mutant, where the subunit connections have moved away from the cytoplasmic pore.*

4.3.6.3 Changes in the Cytoplasmic Pore Environment

As discussed in the previous section, the structures of the S129R/S205L mutant have helped us identify a novel intersubunit connection between D197 and R202 that in this mutant replaces the connections formed by the triad of E173, D175 and H177 which are observed in the other structures of KirBac3.1. Here we will focus on the changes to the cytoplasmic pore that are a direct consequence of this shift.

In all KirBac3.1 structures to date, negatively charged residues E173 and D175 engage with H177 at the cytoplasmic subunit interface to stabilise the tetrameric channel. However, when

their role in maintaining the oligomeric structure of the channel is taken over by D197 and R202, these charged residues are released from their interaction with H177 and change their rotamer conformation to point away from the intersubunit pocket and into the cytoplasmic pore (Figure 4.25). Therefore, as a direct consequence of the D197-R202 interaction, the cytoplasmic pore of the S129R/S205L mutant is lined with the negatively charged sidechains of E173 and D175 which may act to change the electrostatic properties of the cytoplasmic cavity (Figure 4.26).

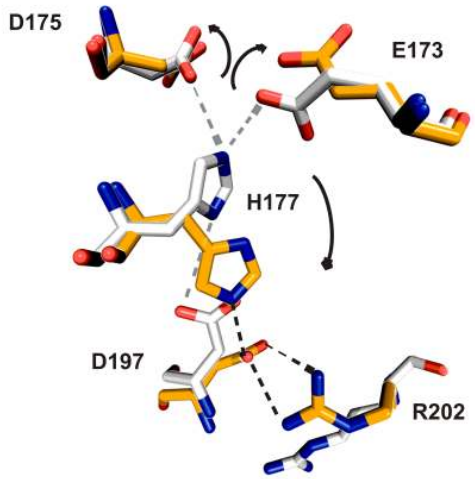

Figure 4.25: *Alignment of the subunit interface residues of the closed KirBac3.1, with the cytoplasmic domains in the twist state (grey) and the open S129R/S205L structure (gold). Formation of the salt bridge between D197 and R202 pulls down residue H177, and thereby releases E173 and D175 from their engagement with H177. The negatively charged residues are free to face in towards the cytoplasmic pore.*

It is interesting to note that E173 and D175 in our highest resolution structure provide the cytoplasmic pore with a binding site for a potassium ion. An alignment with the eukaryotic channels shows that residue E173 is conserved, and in Kir2.2 corresponds to E225 (Figure 4.27). This glutamate is well documented to play an important role in rectification in eukaryotic channels by providing a coordination site for polyamines in the cytoplasmic vestibule [56, 57, 59, 163].

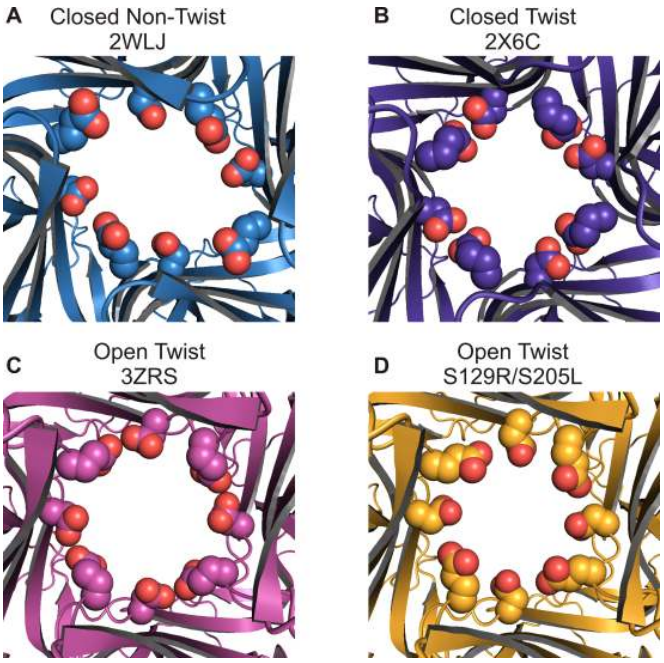

Figure 4.26: *Top-down view of the arrangement of E173 and D175 relative to the cytoplasmic pore in different conformations of KirBac3.1. viewed from the extracellular pore.*

In Kir2.2, the cytoplasmic vestibule has two narrowings where polyamines and cations are thought to bind. One of these binding sites is made up of the four E225 residues, and the other of the "gasket" structure (Figure 4.27). The diameter of the cytoplasmic cavity measured at E225, as well as at the gasket, is ~9.5Å, which allows coordination of hydrated ions and polyamine molecules. These binding sites are quite flexible, and are dependent on the rotamer conformation of the residues. Their main function is to facilitate movement of the polyamines to their binding site proper, which is found in the transmembrane pore. Indeed, ablating E225 in the cytoplasmic vestibule of Kir2.1 and Kir2.2 slows down the kinetics of polyamine block, but does not abolish it [57, 163]. Another interesting effect of charge neutralisation in the cytoplasmic vestibule of Kir2.1 is that it lowers the overall conductance of the channel [52]. It has therefore been postulated that the negative charges in the cytoplasmic pore also act to increase the local concentration of potassium, and thereby ensure a sufficient supply of ions to the transmembrane region.

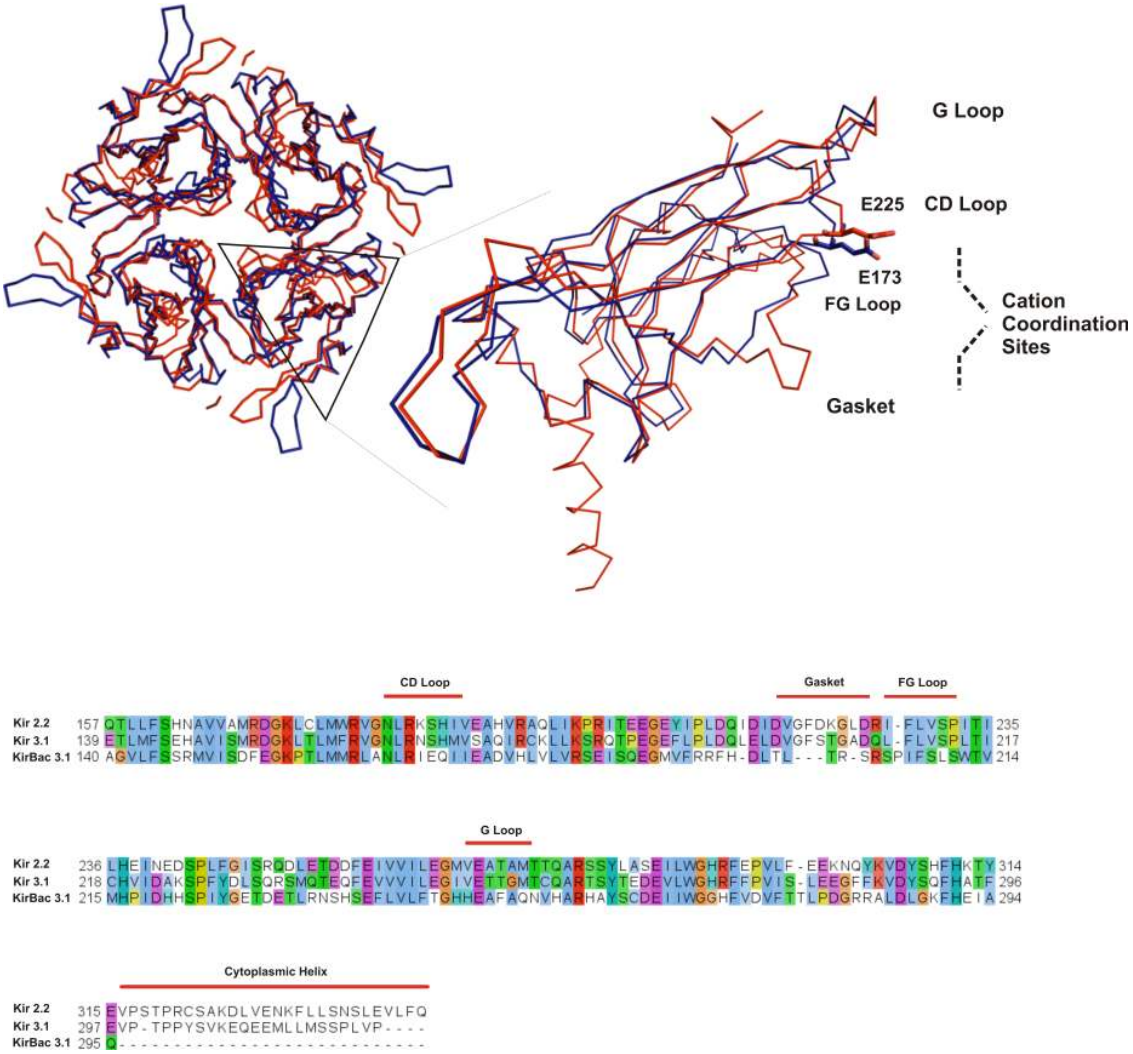

Figure 4.27: *A structural alignment of the cytoplasmic domains of KirBac3.1 S129R/S205L mutant (blue) and Kir2.2 (3SPI) (red). Residue E225 in the strong rectifier Kir2.2 corresponds to E173 in KirBac3.1. In Kir2.2, E225 along with the "gasket" loop provides the cytoplasmic pore with cation coordination sites. They play an important role in facilitating polyamine block, as well as in maintaining normal channel conductance. The gasket loop is not found in prokaryotic channels.*

The structure described here presents us with the idea that the twist of the cytoplasmic domains of KirBac3.1 not only acts to position the individual parts of the channel to engage in interactions that lead to opening of the helix bundle gate, but may also, through subtle rearrangements of the intersubunit connections, result in changes in the electrostatic environment of the cytoplasmic cavity in order to increase the local concentration of cations.

Eukaryotic Kir channels are tightly regulated by a number of factors in order to ensure that the fine electrochemical balance required for normal functioning of cells is maintained. Our knowledge of the function and regulation of the prokaryotic Kir channels is unfortunately still limited, but we know that two of the most prominent regulating mechanisms of eukaryotic Kir

channels do not apply in KirBacs: regulation by PIP_2 (since prokaryotic cell membranes do not contain this molecule) and polyamines (since KirBac channels do not possess the "rectification control site" in TM2). The observation made here, that the twisting of the intracellular domains is associated with a change in the electrostatic environment of the cytoplasmic cavity could be a reflection of a regulating mechanism unique to KirBac channels, rendered obsolete in eukaryotic Kir channels by evolution of other, more appropriate regulatory machinery.

4.4 Summary

The overall architecture of structures of the double mutant S129R/S205L and the single mutant S129R were strikingly similar. Contrary to the expectations at the start of this study, no further widening of the helix bundle crossing was observed.

Our ligand binding experiments did not yield any conclusive results. However, in all cases, the presence of ligands improved the quality and the resolution of the data. The only ligand observed in the structures is spermine. Its location in the channel was similar to that observed by Clarke et al. However, considering the fact that its "binding site" is a large, solvent accessible interdomain region, it is likely that the binding is not physiologically significant, but merely serves to stabilise the tetramer. In spite of the absence of any large conformational changes, a detailed analysis of the double mutant structures has revealed two novel features.

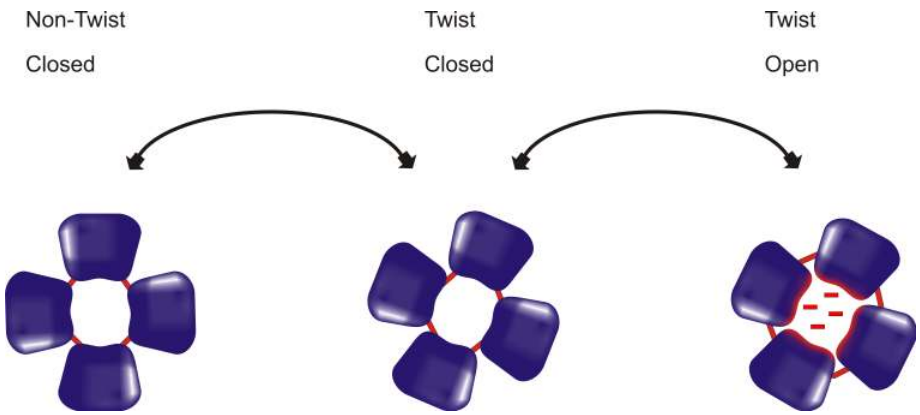

Figure 4.28: *Model for KirBac3.1 activation. The channel can cycle between the non-twist and twist states without resulting in opening of the helix bundle crossing gate. When the appropriate stabilising interactions have formed, twist can be translated into opening of the channel. This leads to release of the negatively charged residues E173 and D175, previously engaged in stabilising the tetramer, and allows them to point in towards the cytoplasmic pore. The resulting change in the electrostatic environment facilitates concentration of cations in the cytoplasmic cavity.*

The first was a tight intersubunit interaction between D197 and R202 at the cytoplasmic interface of the S129R/S205L double mutant. This salt bridge may act to stabilise the tetramer in the twist state, and consequently also the open state of the helix bundle crossing.

The second, a direct consequence of the formation of the D197-R202 salt bridge, was the release of E173 and D175 from their role as stabilisers of the tetramer, and the change in their rotamer conformation. In the structures of the S129R/S205L double mutant, these residues were found to be pointing in towards the central cavity of the cytoplasmic pore, and could be acting to increase the conductance of the channel by concentrating cations in the region. This hypothesis was supported by the observation of a potassium ion coordinated by E173 and D175 in our highest resolution structure. This presents us with the idea that the shift in subunit interactions following the twist movement of the cytoplasmic domains changes the electrostatic environment of the KirBac3.1 cytoplasmic pore, thereby priming the channel to enter its fully conductive, open state.

S129R/S205L	
Data Collection	
Space group	$P\ 2_1\ 2\ 2_1$
Cell Dimensions, Å	80.140 90.000 125.090
Cell Angles, Degrees	90.00 90.00 90.00
Resolution (Highest Shell)	30.95 -2.80 (2.94 -2.80)
Completenes for Range (Highest Shell), %	99.26 (99.26)
Refinement	
Resolution (Highest Shell)	67.47-2.65 (2.86-2.65)
Number of Reflections	14540
R_{Work}/R_{free} %	22.72/22.35
Number of Protein Atoms	3952
Number of Ligand/Ion Atoms	31
Number of Water Atoms	22
Mean B Value	99.30
R.M.S. Bond Lengths, Å	0.010
R.M.S. Angles, Degrees	1.09

Figure 4.29: *Collection and refinement data for the KirBac3.1 S129R/S205L mutant.*

S129R/S205L	
Magnesium	
Data Collection	
Space group	P 2_1 2_1 2
Cell Dimensions, Å	103.270 114.407 89.792
Cell Angles, Degrees	90.00 90.00 90.00
Resolution (Highest Shell)	34.83 –2.58 (2.66 - 2.58)
Completenes for Range (Highest Shell), %	99.73 (99.73)
Refinement	
Resolution (Highest Shell)	24.82-2.46 (2.66 - 2.58)
Number of Reflections	34061
R_{Work}/R_{free} %	18.96/22.34
Number of Protein Atoms	4394
Number of Ligand/Ion Atoms	162
Number of Water Atoms	131
Mean B Value	64.77
R.M.S. Bond Lengths, Å	0.010
R.M.S. Angles, Degrees	1.19

Figure 4.30: *Collection and refinement data for the KirBac3.1 S129R/S205L mutant in the presence of magnesium.*

S129R/S205L	
Barium	
Data Collection	
Space group	P 4 2_1 2
Cell Dimensions, Å	103.190 103.190 89.180
Cell Angles, Degrees	90.00 90.00 90.00
Resolution (Highest Shell)	67.47-2.65 (2.86-2.65)
Completenes for Range (Highest Shell), %	99.95 (99.95)
Refinement	
Resolution (Highest Shell)	67.47-2.65 (2.86-2.65)
Number of Reflections	14540
R_{Work}/R_{free} %	19.96/24.84
Number of Protein Atoms	2177
Number of Ligand/Ion Atoms	55
Number of Water Atoms	29
Mean B Value	60.57
R.M.S. Bond Lengths, Å	0.010
R.M.S. Angles, Degrees	1.195

Figure 4.31: *Collection and refinement data for the KirBac3.1 S129R/S205L mutant in the presence of barium.*

S129R/S205L	
Spermine	
Data Collection	
Space group	P 2_1 2_1 2
Cell Dimensions, Å	105.363 109.889 90.005
Cell Angles, Degrees	90.00 90.00 90.00
Resolution (Highest Shell)	58.09 –2.77 (2.87 - 2.77)
Completenes for Range (Highest Shell), %	99.74 (99.99)
Refinement	
Resolution (Highest Shell)	24.82-2.46 (2.59 - 2.46)
Number of Reflections	27153
R_{Work}/R_{free} %	18.22 / 22.72
Number of Protein Atoms	4394
Number of Ligand/Ion Atoms	268
Number of Water Atoms	214
Mean B Value	66.17
R.M.S. Bond Lengths, Å	0.010
R.M.S. Angles, Degrees	1.19

Figure 4.32: *Collection and refinement data for the KirBac3.1 S129R/S205L mutant in the presence of spermine.*

S129R/S205L	
Spermidine	
Data Collection	
Space group	P 4 2_1 2
Cell Dimensions, Å	105.650 105.650 89.900
Cell Angles, Degrees	90.00 90.00 90.00
Resolution (Highest Shell)	24.82-2.46 (2.59 - 2.46)
Completenes for Range (Highest Shell), %	99.99 (99.99)
Refinement	
Resolution (Highest Shell)	24.82-2.46 (2.59 - 2.46)
Number of Reflections	19036
R_{Work}/R_{free} %	17.97 / 24.82
Number of Protein Atoms	2244
Number of Ligand/Ion Atoms	205
Number of Water Atoms	187
Mean B Value	50.43
R.M.S. Bond Lengths, Å	0.010
R.M.S. Angles, Degrees	1.10

Figure 4.33: *Collection and refinement data for the KirBac3.1 S129R/S205L mutant in the presence of spermidine.*

Chapter 5

Functional Studies of a Bacterial Kir Channel, KirBac3.1

5.1 Introduction

KirBac3.1 is one of the structurally best characterised ion channels, with 13 unique structures deposited in the Protein Database. Despite the wealth of structural data on this protein, its function remains poorly understood. In this study we employ the liposomal $^{86}Rb^{+}$ uptake assay, to functionally characterise the wild-type as well as some of the gating mutants of KirBac3.1 which were previously identified in the Tucker laboratory .

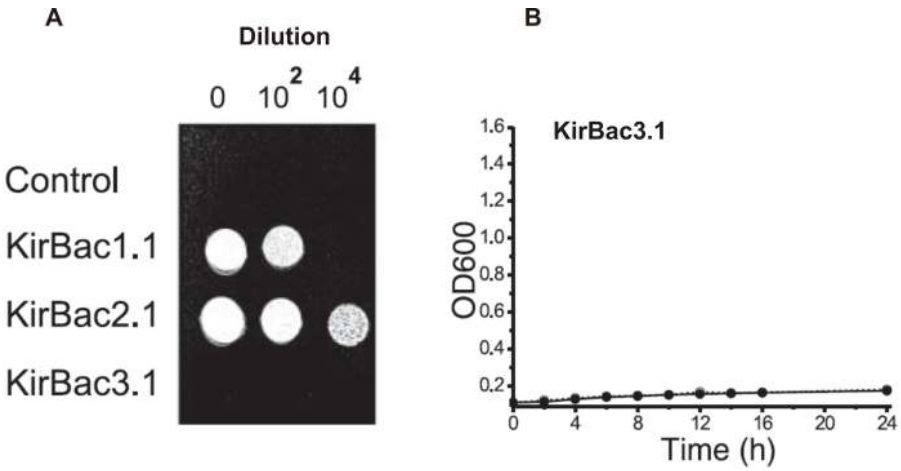

Figure 5.1: *The wild-type KirBac3.1 does not complement growth of K^{+} auxotrophic E. coli. Adapted from [80].*

Firstly, we investigated the sensitivity of the KirBac3.1 channel to $[H^+]$. Secondly, we examined the effect of PIP_2 and divalent cations on the activity of KirBac3.1. The final section of this chapter describes the preliminary attempts to express functional KirBac3.1 channels in *Xenopus Laevis* oocytes.

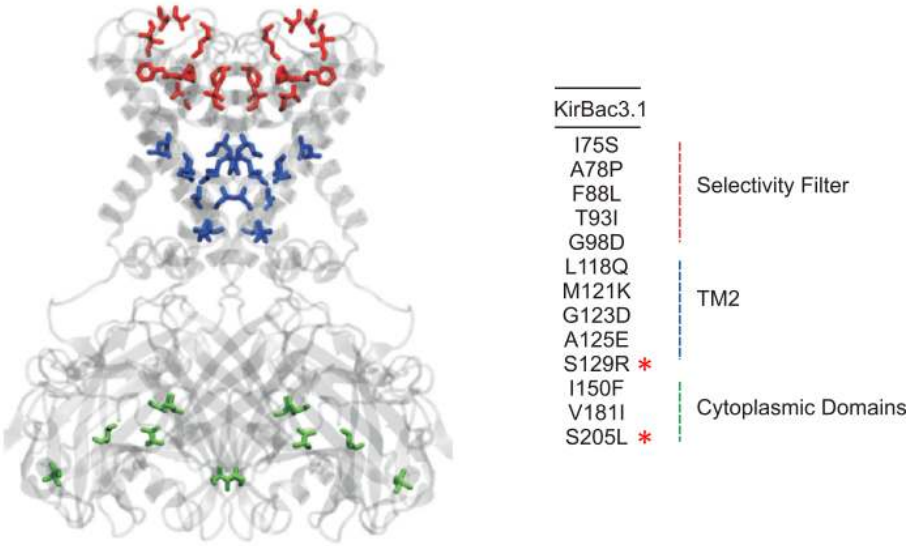

Figure 5.2: *List of activatory mutations identified through a random mutagenesis screen. Mutations in the selectivity filter are coloured in red, mutations in the TM2 are marked in blue and finally, the mutations in the cytoplasmic domains are coloured green. The mutants studied in this chapter are marked with an asterix. The figure is adapted from [138]*

5.2 Materials and Methods

5.2.1 Preparation of KirBac3.1

KirBac3.1 and its mutants were prepared as described in Chapter 4. The storage buffer for all proteins consisted of 50mM Tris pH 7.8, 150mM KCl and 0.5mM TriDM. Flux assays were performed within 24 hours of the final purification steps.

5.2.2 Liposomal $^{86}Rb^{+}$ Uptake Assay

All lipid stocks were prepared and used as described in the Materials and Methods section of Chapter 3.

5.2.2.1 Solutions

Buffer B: 10 mM Hepes (substituted with MES, Tris or CAPSO where appropriate), 450 mM KCl, 4 mM NMDG, 1 mM EDTA ,1 mM EGTA . The buffer pH was adjusted with NMDG.
Buffer C: 10 mM Hepes (substituted with MES, Tris or CAPSO where appropriate), 400 mM Sorbitol, 4 mM NMDG, 1 mM EDTA, 1 mM EGTA. The buffer pH was adjusted with NMDG.
BSA blocking solution: 5 mg/ml of BSA dissolved in 400 mM Sorbitol.
POPG blocking solution: 10 mg/ml of POPG dissolved in 400 mM Sorbitol.
All solutions were filtered through a 0.22μm membrane prior to use.

5.2.2.2 Preparation of Columns

Sephadex G-50 gelfiltration resin was soaked in dH_20 and left to swell overnight at 4°C. Columns were prepared by pipetting 1.5ml resin into a 5ml plastic single use plastic column (Pierce). The resin was allowed to settle, taking care that the no air pockets form witin the column. Two sets of columns were prepared for each experiment. One set was washed 5 times with 5ml of Buffer B (the ion rich buffer), while the other was equilibrated with Buffer C.

Dowex ion-exchange resin was first washed 5 times with 95% ethanol, and rinsed 5 times with water. 1 M NMDG was added to the resin suspended in water and it was allowed to incubate for 1–2 h. The charged resin was washed extensively with water until the pH dropped below 9 and stored at 4°C.

Dowex columns were prepared by pipetting 1ml of resin onto a plastic column and allowed to settle. The colum was washed 5 times with 400mM sorbitol.

5.2.2.3 Preparation of Proteoliposomes

POPE and POPG were mixed in a 3:1 ratio in a glass tube and diluted with an equal volume of 0.9M KCl, making the final total concentration of lipid 1mg/ml, and the final concentration of KCl 450mM. The mixture was incubated for 2 hours at room temperature. 5μl protein at a concentration of 2mg/ml (10μg total) was placed at the bottom of an eppendorf tube, and 95μl of the lipid mixture was added. The protein was incubated with the lipids for 20-30 minutes.

Sephadex G50 columns equilibrated with buffer B were partially dehydrated by centrifugation for 10 seconds at 1000 RCF. The mixture of lipids and protein was pipetted carefully in the centre of the column and the column was centrifuged at 700 RCF for 10 seconds to remove the CHAPS detergent. The flowthrough, containing the newly formed proteoliposomes, was collected. To remove external potassium ions, the liposomes were filtered through a partially dehydrated Sephadex column equilibrated in buffer C.

Proteoliposomes, containing 450mM KCl in the internal solution and no potassium in the external buffer were collected in a glass tube.

5.2.2.4 Preparation of Radioactive Solutions

0.5μCi $^{86}Rb^{+}$ was added to Buffer C. For each sample 420μl radioactive solution was made.

5.2.2.5 $^{86}Rb^{+}$ Uptake Assay

To each proteoliposome sample 420μl buffer C containing $^{86}Rb^{+}$was added, allowing 10 second intervals between each sample. 60μl samples were taken out at the stated time points.

To remove extraliposomal ions, samples were placed on the Dowex column and the proteoliposomes eluted with 2ml 400mM sorbitol.

16ml scintillation liquid was added to each eluted proteoliposome sample and the radioactive content of the proteoliposomes was measured in a scintillation counter.

At the end of the timecourse, the liposomes were treated with 1 μg/ml valinomycin to establish the maximal $^{86}Rb^{+}$ uptake. Following treatment, the liposomes were filtered through the Dowex column and eluted as above.

5.2.3 Expression of KirBac3.1 in *Xenopus laevis* Oocytes

5.2.3.1 Codon Optimisation

A wildtype KirBac3.1 gene optimised for mammalian expression was synthesised by Genscript, and cloned into the pBF vector.

5.2.3.2 Preparation of mRNA

The pBF vector containing the codon optimised KirBac3.1 gene was linearised with MluI, and the linearised DNA cleaned using the Qiagen PCR clean-up protocol. Linearisation was confirmed by running a sample on an agarose gel.

The in vitro transcription was carried out using the mMESSAGE mMACHINE sp6 kit, according to manufacturer's protocol. The reaction was incubated at 42°C for 2 hours, before adding 1μl DNAse to break down the input DNA. After a 15 minute DNAse treatment at 37°C, the RNA was purified using the RNeasy kit (Qiagen). Cleaned RNA was run on an agarose gel to verify the quality of the product, and the concentration was measured using the Nanodrop spectophotometer. mRNA was diluted to appropriate concentrations for injection into oocytes.

5.2.3.3 Expression

Xenopus laevis oocytes were injected with 50nl of either 10ng/μl or 100ng/μl mRNA solution. The injected cells were incubated at 18°C for 1-4 days.

5.2.3.4 Confirmation of KirBac3.1 Expression

40 oocytes injected with 10ng/μl KirBac3.1 mRNA were resuspended in 50μl 50mM HEPES pH 7.5, 150mM KCl, 10% sucrose, protease inhibitor cocktail and DNAseI. The cells were broken by passage through a 25G needle 5-10 times and flash frozen in liquid nitrogen. This was repeated on day1-day4 from injection of the cells. A batch of uninjected cells was also prepared.

The broken cells were centrifuged at 200,000 RCF for 30 minutes at 4°C. The supernatant was discarded and the membrane fraction resuspended using a 25G needle in 200μl 50mM HEPES pH 7.5, 150mM KCl, 10% sucrose and protease inhibitor cocktail. The suspension

was complemented with 1% TRITON-X and 0.5% CHAPS. Membranes were solubilised at room temperature for 3 hours on a rotating wheel.

The solubilised membranes were centrifuged at 70,000 RCF for 15 minutes to remove unsolubilised material. The supernatant was loaded onto 50μl pre-equilibrated TALON Cobalt resin. The binding step was performed on a rotating wheel overnight at 4°C.

The resin was washed twice with the resuspension buffer complemented with 10 and 20mM imidazole, before the protein was eluted in 100μl buffer containing 400mM imidazole.

5.2.3.5 Western Blotting

35μl protein was loaded onto a 14-16% Bis-Tris gel (Invitrogen) and run for 45 minutes at 200V.

The protein was transferred to a PVDF membrane using the iBlot (Invitrogen). The membrane was blocked by incubation in TBS-Tween buffer containing 2.5% dried, skimmed milk for 1 hour. After two 10 minute washes in TBS-Tween, the anti-His antibody conjugated to Alkaline Phosphatase (Invitrogen) was added. The antibody incubation time was two hours at room temperature. The membrane was again washed two times in TBS-Tween buffer. The membrane was incubated with 5ml chromogenic substrate (Invitrogen) until bands started to appear. The reaction was stopped by addition of water.

5.2.3.6 Electrophysiological Recordings

Current recordings were obtained from excised giant patches in an inside-out configuration. Pipette solution consisted of 120mM KCl, 10mM HEPES, 1.8mM $CaCl_2$at pH7.2, and the bath solution contained 120mM KC, 10mM MES, 2mM EDTA, 1mM sodium pyrophosphate (pH5), 120mM KCl, 10mM HEPES, 2mM EDTA, 1mM sodium pyrophosphate (pH7.2 and pH8). Recordings were sampled at 10kHz and filtered at 5kHz (Axopatch 200B, Molecular Devices). Data was analysed using pCLAMP 10.2 software (Axon Instruments). All solutions were applied to the cytoplasmic/intracellular side of the excised patch. Currents were recorded using a voltage ramp protocol which ran from -100mV to +100mV.

5.3 Results and Discussion

KirBac3.1 was expressed and purified as described in Chapter 3, and reconstituted into POPE:POPG (Ratio 3:1) liposomes. The intraliposomal K^+ concentration was kept at 450mM, while the extraliposomal solution contained a 0.5μCi of the radioactive $^{86}Rb^+$ isotope.

Unless otherwise indicated, the changes in buffer pH were applied to both the intra- and extraliposomal environment. PIP_2 was incorporated into the vesicles by mixing the stated percentage of PIP_2 into the lipids before the protein was added. The readings were normalised to maxium $^{86}Rb^+$ uptake, facilitated by the ionophore valinomycin

The initial flux assay results were obtained according to the protocol previously developed for KirBac1.1 [84], where the pH was kept at 7.4 The flux levels were relatively low, but significantly above the negative control which suggests that the purified KirBac3.1 is functional.

These measurements were similar to previous studies of KirBac3.1, which suggested that the activity of the wild-type channel was low [83].

5.3.1 KirBac3.1 pH dependence

All eukaryotic Kir channels are sensitive to pH in that they are inhibited under acidic conditions. We wanted to investigate whether the function of KirBac3.1 was dependent on pH, and if so, to what extent.

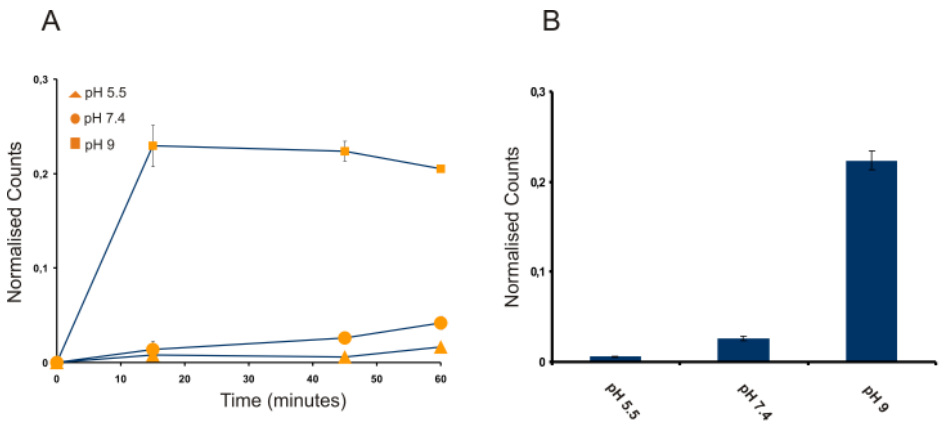

Figure 5.3: *The flux assay showed a large increase in KirBac3.1 activity under alkaline conditions. The bars represent the normalised $^{86}Rb^+$ uptake at 45 minutes. Error bars represent +/- S.E.M., n=3.*

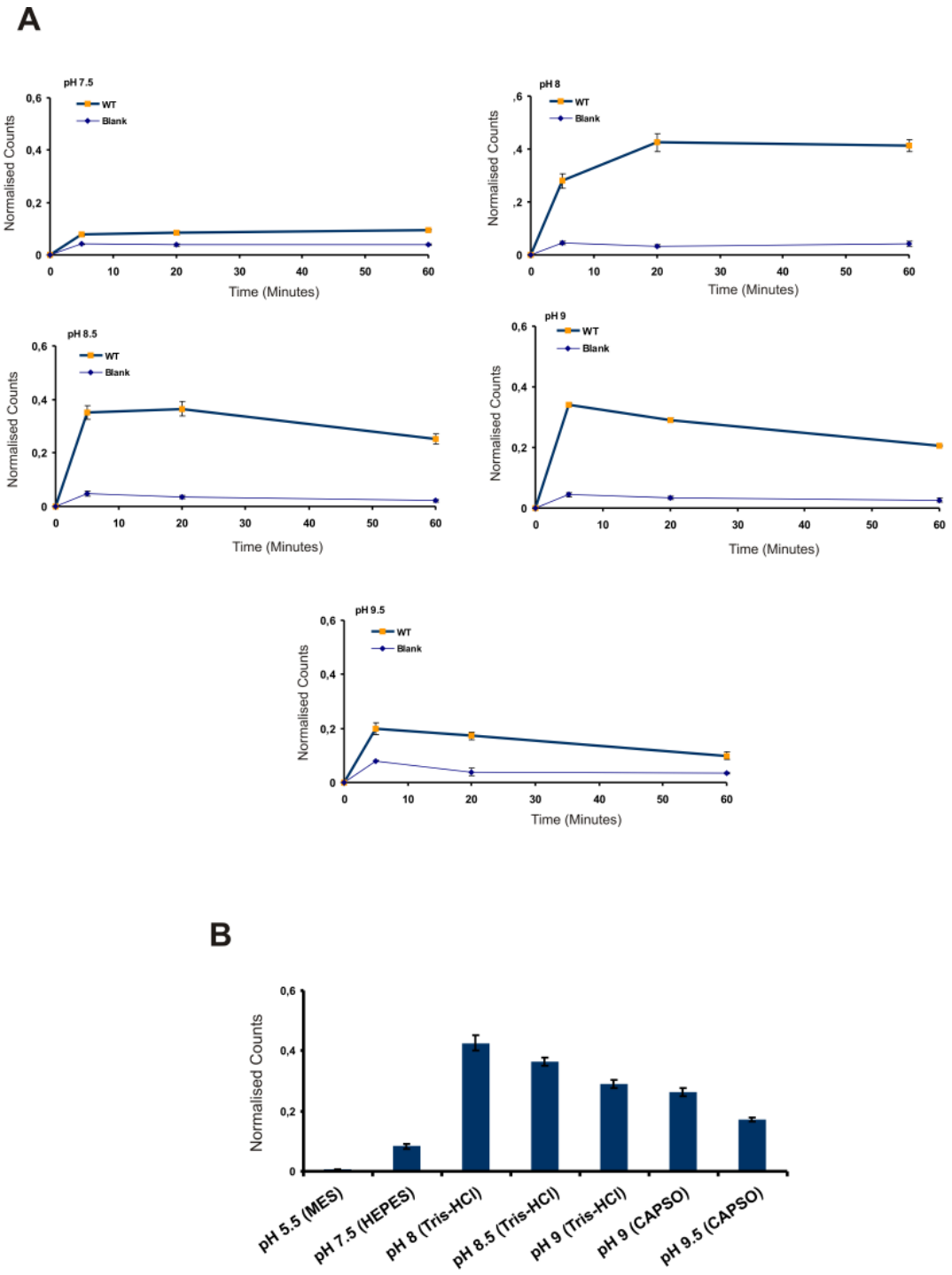

Figure 5.4: ***A*** *60 minute time course of* $^{86}Rb^{+}$ *uptake at pH 7.5-9.5.* ***B*** *Bar graph representing the normalised* $^{86}Rb^{+}$ *uptake at 45 minutes. KirBac3.1 is fully activated at pH 8, with the function steadily decreasing as the pH value increases to 9.5. The error bars represent S.E.M, n=3. The experiments presented in this figure were done by Dr. Shizhen Wang.*

Initially, an experiment was designed to probe the activity of the wild-type channel in acidic and alkaline environments, compared to the activity observed under neutral pH. The flux assay was performed at pH 5.5 (10mM MES), pH 9 (10mM Tris-HCl) and pH 7.4 (10mM HEPES).

KirBac3.1 showed a small decrease in activity at pH 5 when compared to pH 7.4. However, at alkaline pH a >10 fold increase in channel activity was observed (shown in Figure 5.3).

In order to further investigate the pH sensitivity of KirBac3.1, channel activity was measured over a range of pH values from pH 7.5 to pH 9.5, with 0.5 step increments.

The experiments at pH 9 were performed both in a Tris-HCl and a CAPSO buffer in order to minimise the possibility of chemical bias, i.e. to ensure that the activation observed at pH 9 is due to $[H^+]$ and not induced by the chemical composition of the buffer.

The results revealed that the channel appears to be fully activated at pH 8, with the activity decreasing steadily as the pH increases to 9.5 (Figure 5.4).

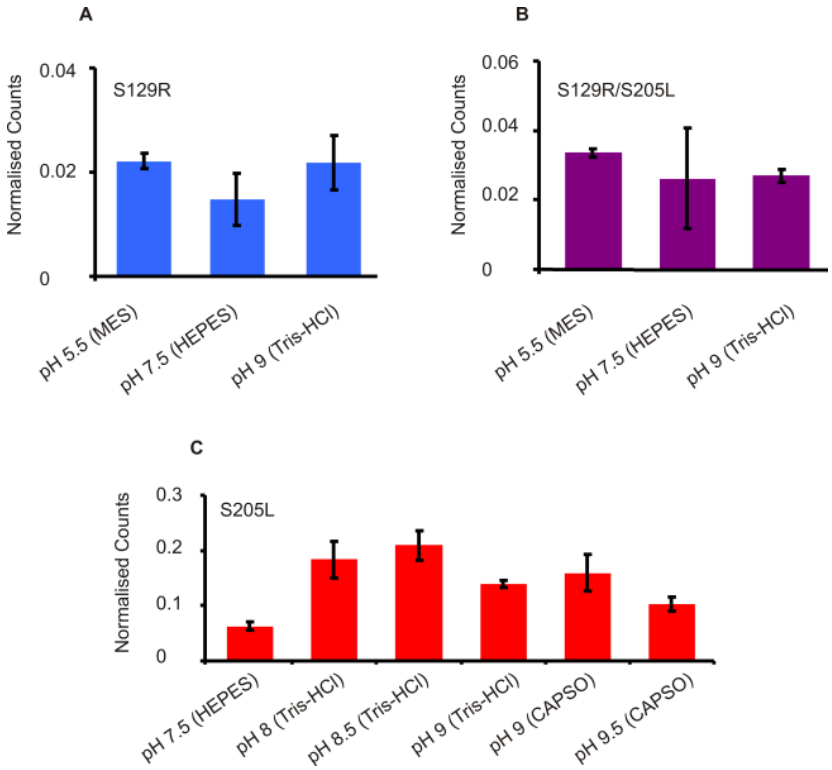

Figure 5.5: *The pH dependency of the KirBac3.1 activatory mutants. Channels carrying the S129R mutation showed low activity in the flux assays, and no increase in activity in response to changes in the pH was observed. The response of the S205L mutant is similar to that of the wild-type. Bars represent normalised* $^{86}Rb^+$ *uptake at 45 minutes.*

5.3.1.1 pH Dependence of KirBac3.1 Activatory Mutants

Given the strong pH dependence of the wild-type channel, we next wanted to examine the effect of pH on some of the activatory mutants of KirBac3.1 isolated from a random mutagenesis screen.

We tested mutations S129R, S205L as well as S129R/S205L. These mutants had previously been expressed and purified in a stable form, and were therefore suitable for $^{86}Rb^{+}$ uptake experiments.

However, mutants S129R and S129R/S205L showed little activity in the flux assays and, as shown in Figure 5.5A and B, they did not exhibit any change in activity across the pH range tested. This result was surprising as previous studies had shown that the S129R mutant was more active than the wild-type channel [138]. One explanation could be that the S129R mutation obstructs the transmembrane pore and thereby lowers the flux, but more experiments are required to explain the low activity of these mutants. (The position of the S129R mutation is shown in Figure 4.4 of Chapter 4)

However, the S205L mutant follows the same trend as the wild-type channel (Figure 5.5C). The activity is low at acidic pH (not shown), as well as pH 7.5, and reaches maximum at pH 8.

A degree of sensitivity to pH is an intrinsic feature of all Kir channels, and it is thought to be facilitated by a number of titratable inter- and intrasubunit interactions. The differences in pH sensitivity amongst channels seem to rely on connections that stabilise either the closed or open state. KirBac3.1 is the only prokaryotic Kir channel known to be affected by changes in the neutral range of pH. However, more work is needed to understand the molecular basis for its pH sensitivity.

5.3.2 The Effect of PIP_2 on KirBac3.1 Activity

In spite of not being native to prokaryotic cells, PIP_2 has been found to directly interact with KirBac1.1 and inhibit its function in a dose dependent manner. In the absence of other regulatory ligands, PIP_2 has proven a useful tool in the functional studies of KirBac1.1 [164]. To investigate whether inhibition by PIP_2 also occurs in KirBac3.1, the activity of the wild-type channel was assayed in liposomes containing 1% PIP_2 , a concentration which decreases KirBac1.1 activity by >90%, as shown in Figure 5.6 [85]. KirBac3.1 was only moderately

inhibited by PIP_2, as shown in 5.7.

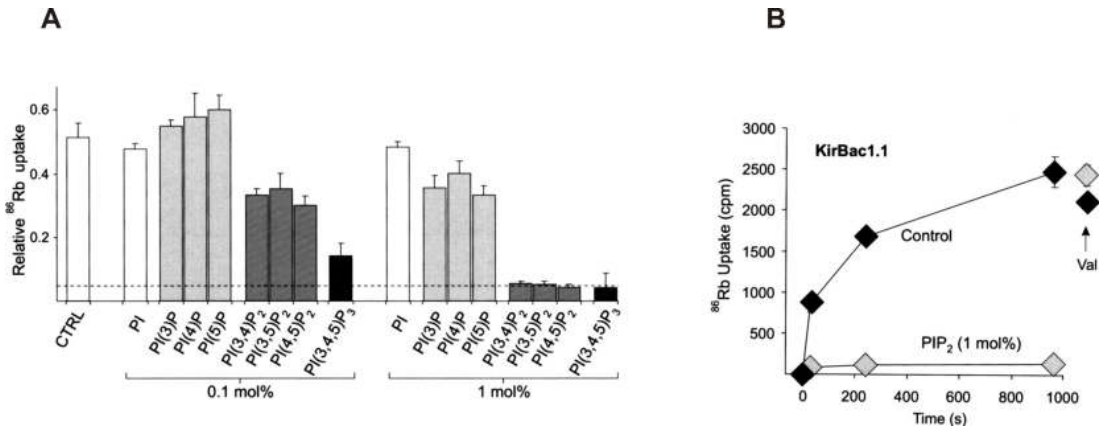

Figure 5.6: *Inhibition of KirBac1.1 by phosphoinositides.* ***A*** *KirBac1.1 is inhibited by PI(3,4)P_2,PI(4,5)P_2 as well as PI(3,5)P_2 and PI(3,4,5)P_3. The degree of inhibition is dose-dependent.* ***B*** *Time course of KirBac1.1 function in the absence (black squares) and presence (grey squares) of 1% PIP_2. Figure adapted from [85].*

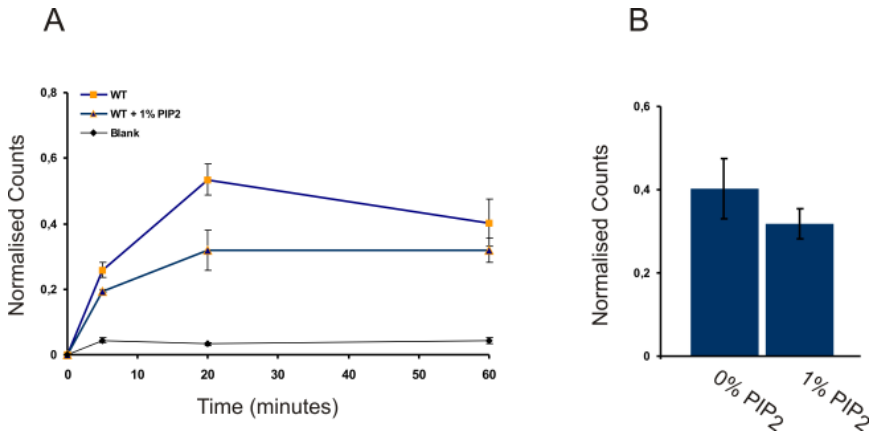

Figure 5.7: *Inhibition of KirBac3.1 flux by 1% PIP_2.* ***A*** *Timecourse for KirBac3.1 $^{86}Rb^+$uptake at pH8 in the presence of 1% PIP_2. Error bars represent S.E.M., n=3.* ***B*** *The bars represent normalised $^{86}Rb^+$ uptake at 60 minutes. The difference between KirBac3.1 $^{86}Rb^+$uptake in the presence of 1%PIP_2 was not found to be significantly lower than the $^{86}Rb^+$uptake in the absence of PIP_2 ($p>0.05$)*

5.3.2.1 KirBac Channels and PIP_2

A possible reason for the differences in response to PIP_2 between the highly homologous KirBac1.1 and KirBac3.1 channels could be in the amino acid sequences of their respective C-linker regions. The positively charged residues in the C-linker region have been found to

be of crucial importance for PIP_2 binding in eukaryotic Kir channels (figure 5.8A). The C-linker region of KirBac1.1 contains more charged residues than that of KirBac3.1 (Figure 5.8D), which suggests that its binding affinity for PIP_2 might be higher and lead to a greater inhibitory effect.

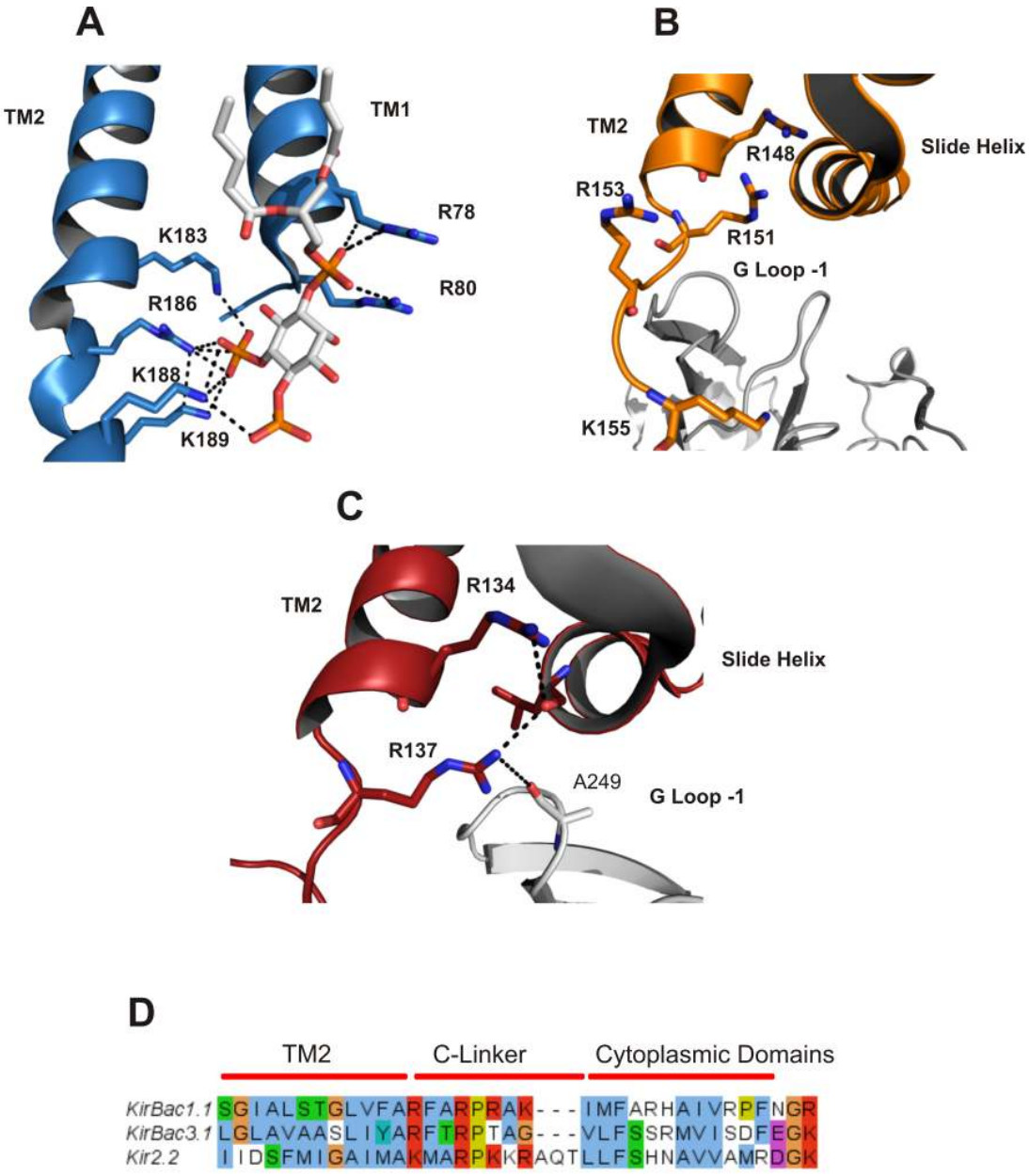

Figure 5.8: ***A*** *PIP_2 binding site in Kir2.2. The molecule is coordinated by the positively charged residues in the C-linker, K183, R186, K188 and K189 [48].* ***B*** *The C-linker region of KirBac1.1 (PDB ID 1P7B). The charged residues are shown as sticks.* ***C*** *C-linker of KirBac3.1 in the open conformation (PDB ID 3ZRS), with R134 and R137 shown as sticks. Dashes represent the interactions with the G-loop and the slide helix.* ***D*** *The alignment of the C-linker regions of Kir2.2, KirBac1.1 and KirBac3.1. The Kir C-linkers are three amino acids longer, and contain a larger number of charged residues. KirBac1.1 has four charged residues in the C-linker region, whereas KirBac3.1 only has two.*

5.3.3 KirBac3.1 Block by Divalent Cations

Magnesium and polyamines underlie inward rectification in Kir channels through intracellular voltage dependent block. KirBac channels do not possess the "rectification controller" residue, and are consequently not blocked by magnesium ions [81].

In recent years there have been some intriguing reports on the effect of Mg^{2+} ions on KirBac3.1. The presence/absence of magnesium has been used to modulate the closed and open states of the channel. An AFM study suggested that magnesium ions induce a conformational change leading to channel closure [111]. Furthermore, a radiolysis study used magnesium to modulate the conformational states of KirBac3.1 [165]. Finally, KirBac3.1 was crystallised with a magnesium ion bound in its selectivity filter, which apparently blocks the channel [151].

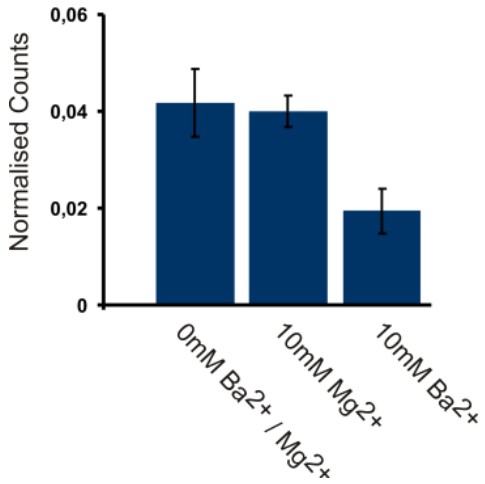

Figure 5.9: *Block of KirBac3.1 flux by divalent cations. At pH 7.4 Mg^{2+}ions do not affect the activity of the channel, while Ba^{2+}ions block the flux.*

To probe the effect of magnesium ions on KirBac3.1, the activity of the channel was assayed in the presence of 10mM $MgCl_2$. As a control, the experiment was also performed in the presence of 10mM $BaCl_2$, since all K^+ selective pores are blocked by barium ions.

KirBac3.1 flux was significantly inhibited by barium, but magnesium failed to produce any effect on the channel at pH 7.4 (Figure 5.9). These results suggest that magnesium does not block the channel and that it has no other direct effect on the function of KirBac3.1. However, these experiments were performed at pH 7.4 where the activity of KirBac3.1 is not

optimal. It is therefore possible that the effects of magnesium are masked by the low activity of the channel.

5.3.4 Expression of KirBac3.1 in *Xenopus laevis* Oocytes

Previous attempts to express KirBac channels in eukaryotic cells have been largely unsuccessful. The reasons for this are manyfold, but one significant reason is thought to be the presence of PIP_2 in eukaryotic plasma membranes. As stated before, PIP_2 is only found in the plasma membranes of eukaryotic cells and it is not present in the cells of prokaryotic organisms. PIP_2 has been found to inhibit the function of KirBac1.1, and this inhibition may have played a role in the difficulties involved in obtaining functional expression of KirBac1.1 in *Xenopus laevis* oocytes.

However, the modest inhibition of KirBac3.1 activity by PIP_2 suggests that functional expression of this channel might be possible in oocytes. We therefore created a wild-type gene of KirBac3.1 codon optimised for expression in mammalian systems.

The first step following mRNA injection into oocytes was to confirm that the protein was in fact expressed in the cell membrane. The membranes of injected cells were isolated by ultracentrifugation, and solubilised before the protein was purified by binding to TALON cobalt resin.

A western blot, shown in Figure 5.10A, confirmed that the channel is indeed expressed in the cell membranes.

The second step was to investigate whether it was possible to record any currents from the channel. Whole-cell two-electrode voltage clamp could only detect very small currents (not shown). However, a better response was seen from inside-out excised macro-patches where the intracellular pH could be modulated. The currents observed, although relatively small, were pH sensitive and perfusion of the inside-out patch resulted in an increase in currents at pH 8 (Figures 5.10B and C). Currents were not observed in excised macro-patch recordings of uninjected oocytes (not shown).

These results may open up interesting possibilities for future functional studies of KirBac3.1. However, at present more experiments are required to confirm that the currents observed indeed are originating from KirBac3.1 channels and not due to alteration in membrane permeability which could result from overexpression of KirBac3.1 mRNA.

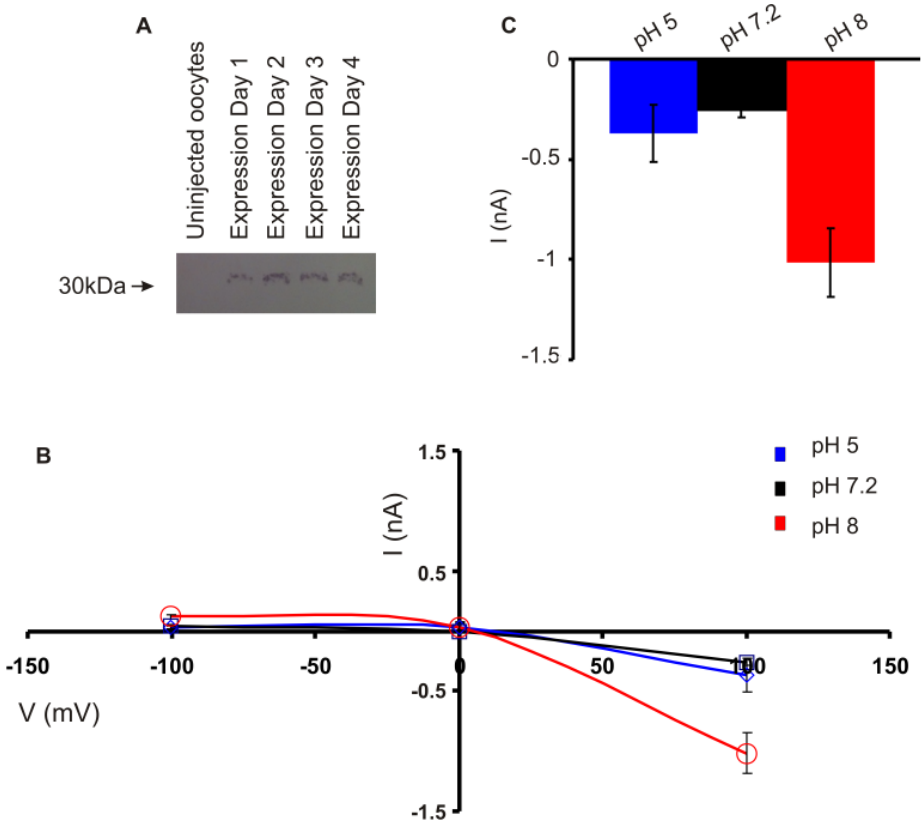

Figure 5.10: ***A*** *KirBac3.1 expression in Xenopus laevis membranes was confirmed by western blot.* ***B*** *Excised inside-out giant patch recordings. The current-voltage relationship in oocytes injected with KirBac3.1 mRNA. Currents were recorded at pH 5, 7.2 and 8. Error bars represent S.E.M, n=2. Pipette solution contained 120mM KCl, 10mM HEPES, 1.8mM $CaCl_2$ at pH7.2. Bath solutions were made as follows: 120mM KCl, 10mM HEPES, 2mM EDTA, 1mM sodium pyrophosphate. The pH was adjusted to 7.2 and 8. For the pH5 solution 10mM MES buffer was used instead of HEPES.* ***C*** *Current magnitudes at +100mV. The error bars represent S.E.M, n=2. The experiments were performed by Dr. Giovanna Bucci.*

5.4 Summary

This initial study of KirBac3.1 function shows that KirBac3.1 is a pH sensitive channel, functioning optimally at pH 8. However, the mutants carrying the S129R mutation did not respond to changes in pH, while the S205L mutant behaved like the wild-type channel.

The effect of the anionic lipid, PIP_2 , was also tested. In contrast to KirBac1.1, KirBac3.1 was only modestly inhibited by the molecule. This may be attributed to the amino acid sequence of its C-linker region, which does not contain as many positively charged residues as that of KirBac1.1 and may consequently result in a lower binding affinity for PIP_2. KirBac3.1 was efficiently blocked by 10mM Ba^{2+}, but was not affected by 10mM Mg^{2+} at pH 7.4.

Chapter 6

Future Directions

The work presented in this thesis contributes to our understanding of ion channels, from both a structural and a functional perspective. The characterisation of a novel ion channel KirBac9.2 presented in the first part of this study sheds light on the modular design of the inward rectifying potassium channels. It demonstrates that despite the high level of homology, modular evolution of parts of the channel can occur to produce a protein of unique properties. The non-selective nature of KirBac9.2 sets it apart from the other known KirBac channels. However, the results reported in this thesis pose many questions: what is the reason for its low apparent conductivity? What is the basis for its apparent insensitivity to PIP_2? Where is the primary gate of this channel? Are there factors, such as pH, that can affect its activity? Further functional studies of KirBac9.2, for which the groundwork has already been laid, would answer these questions and potentially also aid future attempts to obtain the crystal structure of the channel. Indeed, the techniques used to functionally characterise KirBac9.2 can also be employed to study the other novel members of the KirBac family, KirBac9.1 and KirBac11.1. Since both of these channels can be expressed and purified in a stable form, it should be possible to explore their function using methods that rely on reconstitution into liposomes and lipid bilayers.

The structural studies of KirBac3.1 double gating mutant have revealed a new feature in the gating mechanism of this channel. The findings suggest a change in the electrostatic environment of the cytoplasmic cavity associated with the twist conformation. which has not been observed in previous studies. This presents us with the idea that the twist conformation not only serves to bring into contact the cytoplasmic and transmembrane parts of the channel, but may also act to facilitate concentration of cations in the cytoplasmic cavity. Functional

studies of KirBac3.1 presented here demonstrate that the channel is highly sensitive to changes in the pH in the physiological range. This type of pH sensitivity has not been observed in KirBac channels before, and therefore offers a multitude of opportunities for enhancing the understanding of pH gating.

6.1 Functional Studies of KirBac Channels

In this thesis a number of different approaches to study the function of KirBac channels have been described. In particular the methods involving reconstitution of purified protein into lipid vesicles has the potential to yield results. The rubidium uptake assay could be applied to the novel KirBac channels, KirBac9.1, KirBac9.2 and KirBac11.1 to determine their correct selectivity and to identify blockers and activators of these channels. Following these initial studies, a full electrophysiological characterisation can be undertaken using the Port-a-Patch system, described in 3.3.4. Other approaches, such as Droplet-on-Hydrogel bilayers can also be applied [166]. The activatory mutants of KirBac9.2 identified in this thesis will be useful tools for the further functional studies of this channel

6.2 A Future Role for KirBac Channels

The field of ion channel research has been developing at a fast pace over the last decade. At the time of their discovery, prokaryotic channels offered a valid and crucial model for structural studies of eukaryotic Kir channels. However, with emerging technological advances, the challenges involved in handling mammalian, and indeed human proteins are becoming more manageable. Indeed, recent years have seen reports of a number of human membrane protein structures, among others the TWIK-1 [167] and TRAAK [168] K2P channels, the mitochondrial ABC transporter, ABCB10, and the histamine H1 receptor [169]. So, with the focus shifting to more physiologically relevant targets, what is the remaining relevance of channels of prokaryotic origin? Prokaryotic channels still have a number of advantages, since they are typically easier to express and purify, considerably cheaper to produce and easier to handle than their eukaryotic counterparts. These characteristics mean that they can be employed to develop and test new approaches to study of ion channels and so will remain a workhorse until the biochemical approaches for working with eukaryotic channels inevitably improve.

Bibliography

[1] Papazian D.M. Schwarz T.L. Tempel, B.L. Cloning of genomic and complementary DNA from Shaker, a putative potassium channel gene from Drosophila. *Science*, 237(4816):749 753, 1987.

[2] Dworetzky S.I. Trojnacki J.T. Gribkoff, V.K. Cloning and expression of a human large conductance calcium activated potassium channel. *Molecular Brain Research*, 27(1):189 193, 1994.

[3] Boim M.A. Ho K. Shuck M.E. Bienkowski M.J. Block J.H. Slightom J.L. Yang Y. Brenner B.M. Hebert, S.C. ROMK inwardly rectifying ATP sensitive K+ channel. ii. cloning and distribution of alternative forms. *American Journal of Physiology Renal Fluid and Electrolyte Physiology*, 268(6 37 6):F1132 F1140, 1995.

[4] Ho K. Nichols C.G. Lederer W.J. Lytton J. Vassilev P.M. Kanazirska M.V. Hebert, S.C. Cloning and expression of an inwardly rectifying ATP regulated potassium channel. *Nature*, 362(6415):31 38, 1993.

[5] Krapivinsky G. Medina I. Eng L. Krapivinsky L. Yang Y. Clapham, D.E. A novel inward rectifier K+ channel with unique pore properties. *Neuron*, 20(5):995 1005, 1998.

[6] Sakura H. Ammala C. Smith P.A. Gribble F.M. Ashcroft, F.M. Cloning and functional expression of the cDNA encoding a novel ATP sensitive potassium channel subunit expressed in pancreatic beta cells, brain, heart and skeletal muscle. *FEBS Letters*, 377(3):338 344, 1995.

[7] Doyle D.A. Cabral J.M. Pfuetzner R.A. Kuo A. Gulbis J.M. Cohen S.L. Chait B.T. MacKinnon, R. The structure of the potassium channel: Molecular basis of K + conduction and selectivity. *Science*, 280(5360):69 77, 1998.

[8] Capener C.E. Shrivastava I.H. Ranatunga K.M. Forrest L.R. Smith G.R. Sansom, M.S.P. Homology modeling and molecular dynamics simulation studies of an inward rectifier potassium channel. *Biophysical Journal*, 78(6):2929 2942, 2000.

[9] Tieleman D.P. Biggin P.C. Smith G.R. Sansom, M.S.P. Simulation approaches to ion channel structure function relationships. *Quarterly Reviews of Biophysics*, 34(4):473 561, 2001.

[10] Shrivastava I.H. Capener C.E. Forrest L.R. Sansom, M.S.P. Structure and dynamics of K channel pore lining helices: A comparative simulation study. *Biophysical Journal*, 78(1):79 92, 2000.

[11] Zhou Y. Morais-Cabral J.H. Kaufman A. Mackinnon, R. Chemistry of ion coordination and hydration revealed by a K+ channel Fab complex at 2.0 angstrom resolution. *Nature*, 414(6859):43 48, 2001.

[12] Alam A. Jiang, Y. Structural studies of ion selectivity in tetrameric cation channels. *Journal of General Physiology*, 137(5):397 403, 2011.

[13] Bertil Hille. *Ion channels of excitable membranes.* Sinauer, Sunderland, Mass, 2001.

[14] Heginbotham L. Lu-Z. Abramson T. MacKinnon, R. Mutations in the K + channel signature sequence. *Biophysical Journal*, 66(4):1061 1067, 1994.

[15] Alam A. Jiang, Y. High resolution structure of the open NaK channel. *Nature Structural and Molecular Biology*, 16(1):30 34, 2009.

[16] Shi N. Ye-S. Alam A. Chen L. Jiang, Y. Atomic structure of a Na+ and K+ conducting channel. *Nature*, 440(7083):570 574, 2006.

[17] Neyton J. Miller, C. Discrete Ba2+ block as a probe of ion occupancy and pore structure in the high conductance Ca2+ activated K+ channel. *Journal of General Physiology*, 92(5):569 586, 1988.

[18] Morais-Cabral J.H.-Zhou Y. MacKinnon, R. Energetic optimization of ion conduction rate by the K+ selectivity filter. *Nature*, 414(6859):37–40, 2001.

[19] Payandeh-J. Scheuer-T. Zheng N. Catterall, W.A. The crystal structure of a voltage gated sodium channel. *Nature*, 475(7356):353 359, 2011.

[20] Zhang-X. Ren-W. Decaen P. Yan C. Tao X. Tang L. Wang J. Hasegawa K. Kumasaka T. He J. Wang J. Clapham D.E. Yan, N. Crystal structure of an orthologue of the NaChBac voltage gated sodium channel. *Nature*, 486(7401):130 134, 2012.

[21] McCusker-E.C. Bagneris-C. Naylor C.E. Cole A.R. D'Avanzo N. Nichols C.G. Wallace, B.A. Structure of a bacterial voltage gated sodium channel pore reveals mechanisms of opening and closing. *Nat Commun*, 3(1102), 2012.

[22] Lopatin-A.N. Makhina-E.N. Nichols, C.G. Potassium channel block by cytoplasmic polyamines as the mechanism of intrinsic rectification. *Nature*, 372(6504):366 369, 1994.

[23] Mcnicholas-C.M. Macgregor-G.G. Islas L.D. Yang Y. Hebert S.C. Giebisch, G. pH dependent modulation of the cloned renal K+ channel, ROMK. *American Journal of Physiology Renal Physiology*, 275(6 44 6):F972 F981, 1998.

[24] Schulte-U. Hahn-H. Wiesinger H. Peter Ruppersberg J. Fakler, B. pH dependent gating of ROMK (Kir1.1) channels involves conformational changes in both N and C termini. *Journal of Biological Chemistry*, 273(51):34575 34579, 1998.

[25] Schulte-U. Hahn-H. Konrad M. Jeck N. Derst C. Wild K. Weidemann S. Ruppersberg J.P. Fakler B. Ludwig, J. pH gating of ROMK (Kir1.1) channels: Control by an arg lys arg triad disrupted in antenatal bartter syndrome. *Proceedings of the National Academy of Sciences of the United States of America*, 96(26):15298 15303, 1999.

[26] Karolyi-L. Konrad-M. Kockerling A. Ziegler A. Zimmermann D.K. Roth B. Wieg C. Grzeschik K. H. Koch M.C. Seyberth H.W. Vargas R. Forestier L. Jean G. Deschaux M. Rizzoni G.F. Niaudet P. Antignac C. Feldmann D. Lorridon F. Cougoureux E. Laroze F. Alessandri J. L. David L. Saunier P. Deschenes G. Hildebrandt F. Vollmer M. Proesmans W. Brandis M. Van Den Heuvel L.P.W.J. Lemmink H.H. Nillesen W. Monnens L.A.H. Knoers N.V.A.M. Guay Woodford L.M. Wright C.J. Madrigal G. Hebert, S.C. Mutations in the gene encoding the inwardly rectifying renal potassium channel, ROMK, cause the antenatal variant of bartter syndrome: Evidence for genetic heterogeneity. *Human Molecular Genetics*, 6(1):17 26, 1997.

[27] Simon-D.B. Karet-F.E. Rodriguez Soriano J. Hamdan J.H. DiPietro A. Trachtman H. Sanjad S.A. Lifton, R.P. Genetic heterogeneity of Bartter's syndrome revealed by mutations in the K+ channel, ROMK. *Nature Genetics*, 14(2):152 156, 1996.

[28] Plaster-N.M. Tawil-R. Tristani-Firouzi M. Canun S. Bendahhou S. Tsunoda A. Donaldson M.R. Iannaccone S.T. Brunt E. Barohn R. Clark J. Deymeer F. George Jr. A.L. Fish F.A. Hahn A. Nitu A. Ozdemir C. Serdaroglu P. Subramony S.H. Wolfe G. Fu Y. H. Ptacek, L.J. Mutations in Kir2.1 cause the developmental and episodic electrical phenotypes of andersen's syndrome. *Cell*, 105(4):511 519, 2001.

[29] Tristani-Firouzi M.-Jensen J.L.-Donaldson M.R. Sansone V. Meola G. Hahn A. Bendahhou S. Kwiecinski H. Fidzianska A. Plaster N. Fu Y. H. Ptacek L.J. Tawil, R. Functional and clinical characterization of KCNJ2 mutations associated with LQT7 (Andersen syndrome). *Journal of Clinical Investigation*, 110(3):381 388, 2002.

[30] Huang-C. L.-Feng S. Hilgemann, D.W. Direct activation of inward rectifier potassium channels by PIP2 and its stabilization by Gbeta gamma. *Nature*, 391(6669):803 806, 1998.

[31] Ivanina-T. Rishal-I. Varon-D. Mullner C. Frohnwieser Steinecke B. Schreibmayer W. Dessauer C.W. Dascal, N. Mapping the gbeta gamma binding sites in GIRK1 and GIRK2 subunits of the G protein activated K+ channel. *Journal of Biological Chemistry*, 278(31):29174 29183, 2003.

[32] Murthy-M. Azizan-E.A.B. Brown-M.J. O'Shaughnessy, K.M. Characterization of a novel somatic KCNJ5 mutation deli157 in an aldosterone producing adenoma. *Journal of Hypertension*, 2012.

[33] Scholl-U.I. Nelson Williams C.-Yue P. Grekin R. Wyatt R.J. Dillon M.J. Couch R. Hammer L.K. Harley F.L. Farhi A. Wang W. H. Lifton, R.P. Hypertension with or without adrenal hyperplasia due to different inherited mutations in the potassium channel KCNJ5. *Proceedings of the National Academy of Sciences of the United States of America*, 109(7):2533 2538, 2012.

[34] Pessia-M. Imbrici P. Cristina D'Adamo M. Salvatore L. Tucker, S.J. Differential pH sensitivity of Kir4.1 and Kir4.2 potassium channels and their modulation by heteropolymerisation with Kir5.1. *Journal of Physiology*, 532(2):359 367, 2001.

[35] Rapedius-M. Paynter J.J. Fowler P.W. Shang L. Sansom M.S. Tucker S.J. Baukrowitz, T. Control of pH and PIP2 gating in heteromeric Kir4.1/Kir5.1 channels by h bonding at the helix bundle crossing. *Channels (Austin, Tex.)*, 1(5):327 330, 2007.

[36] Reichold-M. Zdebik A.A. Lieberer E. Rapedius M. Schmidt K. Bandulik S. Sterner C. Tegtmeier I. Penton D. Baukrowitz T. Hulton S. A. Witzgall, R. KCNJ10 gene mutations causing EAST syndrome (epilepsy, ataxia, sensorineural deafness, and tubulopathy) disrupt channel function. *Proceedings of the National Academy of Sciences of the United States of America*, 107(32):14490 14495, 2010.

[37] Sala-Rabanal M. Kucheryavykh L.Y. Skatchkov S.N. Eaton M.J. Nichols, C.G. Molecular mechanisms of EAST/SeSAME syndrome mutations in Kir4.1 (KCNJ10). *Journal of Biological Chemistry*, 285(46):36040 36048, 2010.

[38] Williams-D.M. Lopes C.M.B. Rosenhouse-Dantsker A. Connelly H.L. Matavel A. O Uchi J. McBeath E. Gray, D.A. Molecular basis of decreased Kir4.1 function in SeSAME/EAST syndrome. *Journal of the American Society of Nephrology*, 21(12):2117 2129, 2010.

[39] Srivastava-R. Aslam M. Kalluri-S.R. Schirmer L. Buck D. Tackenberg B. Rothhammer V. Chan A. Gold R. Berthele A. Bennett J.L. Korn T. Hemmer, B. Potassium channel Kir4.1 as an immune target in multiple sclerosis. *New England Journal of Medicine*, 367(2):115 123, 2012.

[40] Casamassima-M. D'Adamo M.C. Pessia-M. Tucker, S.J. Identification of a heteromeric interaction that influences the rectification, gating, and pH sensitivity of Kir4.1/Kir5.1 potassium channels. *Journal of Biological Chemistry*, 278(44):43533 43540, 2003.

[41] Tanemoto-M. Kittaka N. Inanobe-A. Kurachi, Y. In vivo formation of a proton sensitive K+ channel by heteromeric subunit assembly of Kir5.1 with Kir4.1. *Journal of Physiology*, 525(3):587 592, 2000.

[42] Tucker-S.J. Imbrici P. Salvatore-L. D'Adamo M.C. Pessia, M. pH dependence of the inwardly rectifying potassium channel, Kir5.1, and localization in renal tubular epithelia. *Journal of Biological Chemistry*, 275(22):16404 16407, 2000.

[43] Paulais-M. Bloch Faure M.-Picard N. Jacques T. Ramakrishnan S.K. Keck M. Sohet F. Eladari D. Houillier P. Lourdel S. Teulon J. Tucker, S.J. Renal phenotype in mice lacking the Kir5.1 (KCNJ16) K + channel subunit contrasts with that observed in SeSAME/EAST syndrome. *Proceedings of the National Academy of Sciences of the United States of America*, 108(25):10361 10366, 2011.

[44] Clark-R.H. McTaggart J.S. Webster-R. Mannikko R. Iberl M. Sim X.L. Rorsman P. Glitsch M. Beeson D. Ashcroft, F.M. Muscle dysfunction caused by a KATP channel mutation in neonatal diabetes is neuronal in origin. *Science*, 329(5990):458 461, 2010.

[45] Gloyn-A.L. Pearson E.R. Antcliff-J.F. Proks P. Bruining G.J. Slingerland A.S. Howard N. Srinivasan S. Silva J.M.C.L. Molnes J. Edghill E.L. Frayling T.M. Temple I.K. Mackay D. Shield J.P.H. Sumnik Z. Van Rhijn A. Wales J.K.H. Clark P. Gorman S. Aisenberg J. Ellard S. Nj(ö)lstad P.R. Ashcroft F.M. Hattersley, A.T. Activating mutations in the gene encoding the ATP sensitive potassium channel subunit Kir6.2 and permanent neonatal diabetes. *New England Journal of Medicine*, 350(18):1838 1849, 2004.

[46] Proks-P. Girard C. Haider-S. Gloyn A.L. Hattersley A.T. Sansom M.S.P. Ashcroft, F.M. A gating mutation at the internal mouth of the Kir6.2 pore is associated with DEND syndrome. *EMBO Reports*, 6(5):470 475, 2005.

[47] Hejtmancik-J.F. Jiao X. Li-A. Sergeev Y.V. Ding X. Sharma A.K. Chan C. C. Medina I. Edwards, A.O. Mutations in KCNJ13 cause autosomal dominant snowflake vitreoretinal degeneration. *American Journal of Human Genetics*, 82(1):174 180, 2008.

[48] Hansen-S.B. Tao X. MacKinnon, R. Structural basis of PIP 2 activation of the classical inward rectifier K + channel Kir2.2. *Nature*, 477(7365):495 498, 2011.

[49] Whorton-M.R. MacKinnon, R. Crystal structure of the mammalian GIRK2 K + channel and gating regulation by G proteins, PIP 2, and sodium. *Cell*, 147(1):199 208, 2011.

[50] Kurata-H.T. Phillips L.R. Rose-T. Loussouarn G. Herlitze S. Fritzenschaft H. Enkvetchakul D. Nichols C.G. Baukrowitz, T. Molecular basis of inward rectification: Polyamine interaction sites located by combined channel and ligand mutagenesis. *Journal of General Physiology*, 124(5):541 554, 2004.

[51] Stanfield-P.R. Davies N.W. Shelton-P.A. Sutcliffe M.J. Khan I.A. Brammar W.J. Conley, E.C. A single aspartate residue is involved in both intrinsic gating and blockage by Mg2+ of the inward rectifier, IRK1. *Journal of Physiology*, 478(1):1 6, 1994.

[52] Yang-J. Jan Y.N. Jan, L.Y. Control of rectification and permeation by residues in two distinct domains in an inward rectifier K+ channel. *Neuron*, 14(5):1047 1054, 1995.

[53] Wible-B.A. Taglialatela M. Ficker-E. Brown, A.M. Gating of inwardly rectifying K+ channels localized to a single negatively charged residue. *Nature*, 371(6494):246 249, 1994.

[54] Bichet-D. Grabe M. Jan-Y.N. Jan, L.Y. Electrostatic interactions in the channel cavity as an important determinant of potassium channel selectivity. *Proceedings of the National Academy of Sciences of the United States of America*, 103(39):14355 14360, 2006.

[55] Chang H. K. Yeh-S. H. Shieh, R. C. Charges in the cytoplasmic pore control intrinsic inward rectification and single channel properties in Kir1.1 and Kir2.1 channels. *Journal of Membrane Biology*, 215(2 3):181 193, 2007.

[56] Inanobe A. Nakagawa A. Kurachi, Y. Interactions of cations with the cytoplasmic pores of inward rectifier K + channels in the closed state. *Journal of Biological Chemistry*, 286(48):41801 41811, 2011.

[57] Kurata H.T. Cheng W.W. Arrabit-C. Slesinger P.A. Nichols, C.G. The role of the cytoplasmic pore in inward rectification of Kir2.1 channels. *Journal of General Physiology*, 130(2):145 155, 2007.

[58] Nishida M. MacKinnon, R. Structural basis of inward rectification: Cytoplasmic pore of the G protein gated inward rectifier GIRK1 at 1.8 angstrom resolution. *Cell*, 111(7):957 965, 2002.

[59] Pegan S. Arrabit C. Zhou-W. Kwiatkowski W. Collins A. Slesinger P.A. Choe, S. Cytoplasmic domain structures of Kir2.1 and Kir3.1 show sites for modulating gating and rectification. *Nature Neuroscience*, 8(3):279 287, 2005.

[60] Jiang Y. Lee A. Chen-J. Cadene M. Chait B.T. MacKinnon, R. Crystal structure and mechanism of a calcium gated potassium channel. *Nature*, 417(6888):515 522, 2002.

[61] Jiang Y. Lee A. Chen-J. Cadene M. Chait B.T. MacKinnon, R. The open pore conformation of potassium channels. *Nature*, 417(6888):523 526, 2002.

[62] Magidovich E. Yifrach, O. Conserved gating hinge in ligand and voltage dependent K+ channels. *Biochemistry*, 43(42):13242 13247, 2004.

[63] Catterall W.A. Cestele S. Yarov Yarovoy V. Yu F.H. Konoki K. Scheuer, T. Voltage gated ion channels and gating modifier toxins. *Toxicon*, 49(2):124 141, 2007.

[64] Dahlmann A. Li M. Gao Z. McGarrigle D. Sackin H. Palmer, L.G. Regulation of Kir channels by intracellular pH and extracellular K+: Mechanisms of coupling. *Journal of General Physiology*, 123(4):441 454, 2004.

[65] Paynter J.J. Shang L. Bollepalli M.K. Baukrowitz T. Tucker, S.J. Random mutagenesis screening indicates the absence of a separate H+ sensor in the pH sensitive Kir channels. *Channels*, 4(5), 2010.

[66] Rapedius M. Haider S. Browne K.F. Shang L. Sansom M.S.P. Baukrowitz T. Tucker, S.J. Structural and functional analysis of the putative pH sensor in the Kir1.1 (ROMK) potassium channel. *EMBO Reports*, 7(6):611 616, 2006.

[67] Thompson A.N. Posson D.J. Parsa P.V. Nimigean, C.M. Molecular mechanism of pH sensing in KcsA potassium channels. *Proceedings of the National Academy of Sciences of the United States of America*, 105(19):6900 6905, 2008.

[68] Xu H. Yang Z. Cui N. Chanchevalap S. Valesky W.W. Jiang, C. A single residue contributes to the difference between Kir4.1 and Kir1.1 channels in pH sensitivity, rectification and single channel conductance. *Journal of Physiology*, 528(2):267 277, 2000.

[69] Suh B. C. Hille, B. PIP2 is a necessary cofactor for ion channel function: How and why? *Annual Review of Biophysics*, 37:175 195, 2008.

[70] Hilgemann D.W. Ball, R. Regulation of cardiac Na+,Ca2+ exchange and K(ATP) potassium channels by PIP2. *Science*, 273(5277):956 959, 1996.

[71] Hilgemann D.W. Feng S. Nasuhoglu, C. The complex and intriguing lives of PIP2 with ion channels and transporters. *Science"s STKE [electronic resource] : signal transduction knowledge environment*, 2001(111):RE19, 2001.

[72] Jardin I. Redondo P.C. Salido G.M. Rosado, J.A. Phosphatidylinositol 4,5 bisphosphate enhances store operated calcium entry through hTRPC6 channel in human platelets. *Biochimica et Biophysica Acta Molecular Cell Research*, 1783(1):84 97, 2008.

[73] Pochynyuk O. Tong Q. Staruschenko A. Ma H. P. Stockand, J.D. Regulation of the epithelial Na+ channel (ENaC) by phosphatidylinositides. *American Journal of Physiology Renal Physiology*, 290(5):F949 F957, 2006.

[74] Rohacs T. Nilius, B. Regulation of transient receptor potential (TRP) channels by phosphoinositides. *Pflugers Archiv European Journal of Physiology*, 455(1):157 168, 2007.

[75] Rohacs T. Thyagarajan B. Lukacs, V. Phospholipase c mediated modulation of trpv1 channels. *Molecular Neurobiology*, 37(2 3):153 163, 2008.

[76] Voets T. Nilius, B. Modulation of TRPs by PIPs. *Journal of Physiology*, 582(3):939 944, 2007.

[77] Durell S.R. Guy, H.R. A family of putative Kir potassium channels in prokaryotes. *BMC Evolutionary Biology*, 1, 2001.

[78] Kuo A. Gulbis J.M. Antcliff J.F. Rahman T. Lowe E.D. Zimmer J. Cuthbertson J. Ashcroft F.M. Ezaki T. Doyle, D.A. Crystal structure of the potassium channel KirBac1.1 in the closed state. *Science*, 300(5627):1922 1926, 2003.

[79] Gulbis J.M. Kuo A. Smith B. Doyle D.A. Edwards A. Arrowsmith C. Sundstrom, M. Intermediate gating structure 2 of the inwardly rectifying K+ channel kirbac3.1. *PDB ID 1XL6*, 2004.

[80] Sun S. Jo H.G. Paynter J.J. Tucker, S.J. Cloning and functional characterization of a superfamily of microbial inwardly rectifying potassium channels. *Physiological Genomics*, 26(1):1 7, 2006.

[81] Cheng W.W.L. Enkvetchakul D. Nichols, C.G. KirBac1.1: It's an inward rectifying potassium channel. *Journal of General Physiology*, 133(3):295 305, 2009.

[82] D'Avanzo N. Cheng W.W.L. Doyle D.A. Nichols, C.G. Direct and specific activation of human inward rectifier K + channels by membrane phosphatidylinositol 4,5 bisphosphate. *Journal of Biological Chemistry*, 285(48):37129 37132, 2010.

[83] D'Avanzo N. Hyrc K. Enkvetchakul D. Covey D.F. Nichols, C.G. Enantioselective protein sterol interactions mediate regulation of both prokaryotic and eukaryotic inward rectifier K + channels by cholesterol. *PLoS ONE*, 6(4), 2011.

[84] Enkvetchakul D. Bhattacharyya J. Jeliazkova I. Groesbeck D.K. Cukras C.A. Nichols, C.G. Functional characterization of a prokaryotic Kir channel. *Journal of Biological Chemistry*, 279(45):47076 47080, 2004.

[85] Enkvetchakul D. Jeliazkova I. Nichols, C.G. Direct modulation of Kir channel gating by membrane phosphatidylinositol 4,5 bisphosphate. *Journal of Biological Chemistry*, 280(43):35785 35788, 2005.

[86] Petrie L. North N.N. Dollhopf S.L. Balkwill D.L. Kostka, J.E. Enumeration and characterization of iron(iii) reducing microbial communities from acidic subsurface sediments contaminated with uranium(vi). *Applied and Environmental Microbiology*, 69(12):7467 7479, 2003.

[87] Zhang H. Sekiguchi Y. Hanada S. Hugenholtz P. Kim H. Kamagata Y. Nakamura, K. Gemmatimonas aurantiaca gen. nov., sp. nov., a gram negative, aerobic, polyphosphate accumulating micro organism, the first cultured representative of the new bacterial phylum gemmatimonadetes phyl. nov. *International Journal of Systematic and Evolutionary Microbiology*, 53(4):1155 1163, 2003.

[88] D Blow. *Outline of crystallography for biologists*. Oxford University Press, Oxford New York, 2002.

[89] F. Baneyx. Recombinant protein expression in E.coli. *Current Opinion in Biotechnology*, 10(5):411 421, 1999.

[90] Z.S. Derewenda. The use of recombinant methods and molecular engineering in protein crystallization. *Methods*, 34(3):354 363, 2004.

[91] C. Miller. Genetic manipulation of ion channels: A new approach to structure and mechanism. *Neuron*, 2(3):1195 1205, 1989.

[92] Kors C.A. Wallace E. Davies D.R. Li L. Laible P.D. Nollert, P. Effects of impurities on membrane protein crystallization in different systems. *Acta Crystallographica Section D: Biological Crystallography*, 65(10):1062 1073, 2009.

[93] C.G. Tate. Practical considerations of membrane protein instability during purification and crystallisation. *Methods in molecular biology (Clifton, N.J.)*, 601:187 203, 2010.

[94] A. McPherson. Introduction to protein crystallization. *Methods*, 34(3):254 265, 2004.

[95] G. Feher. Mechanisms of nucleation and growth of protein crystals. *Journal of Crystal Growth*, 76(3):545 546, 1986.

[96] T. Bergfors. Screening and optimization methods for nonautomated crystallization laboratories. *Methods in Molecular Biology*, 363:131 151, 2007.

[97] Sonoda Y. Newstead S. Hu N. J. Alguel Y. Nji E. Beis K. Yashiro S. Lee C. Leung J. Cameron A.D. Byrne B. Iwata S. Drew, D. Benchmarking membrane protein detergent stability for improving throughput of high resolution X ray structures. *Structure*, 19(1):17 25, 2011.

[98] D.L. Minor Jr. The neurobiologist's guide to structural biology: A primer on why macromolecular structure matters and how to evaluate structural data. *Neuron*, 54(4):511 533, 2007.

[99] M.C. Wiener. A pedestrian guide to membrane protein crystallization. *Methods*, 34(3):364 372, 2004.

[100] E. Sulkowski. Purification of proteins by IMAC. *Trends in Biotechnology*, 3(1):1 7, 1985.

[101] Mueller U. Nyarsik L. Horn M. Rauth H. Przewieslik T. Saenger W. Lehrach H. Eickhoff, H. Development of a technology for automation and miniaturization of protein crystallization. *Journal of Biotechnology*, 85(1):7 14, 2001.

[102] Alexandrov A.I. Mileni M. Chien E.Y.T. Hanson M.A. Stevens, R.C. Microscale fluorescent thermal stability assay for membrane proteins. *Structure*, 16(3):351 359, 2008.

[103] Garman E.F. Doublie, S. [11] Cryocooling of macromolecular crystals: Optimization methods. *Methods in Enzymology*, 368:188 216, 2003.

[104] Battye T.G.G. Kontogiannis L. Johnson O. Powell H.R. Leslie, A.G.W. iMOSFLM: A new graphical interface for diffraction image processing with MOSFLM. *Acta Crystallographica Section D: Biological Crystallography*, 67(4):271 281, 2011.

[105] Horton R.M. Hunt H.D. Ho S.N. Pullen J.K. Pease, L.R. Engineering hybrid genes without the use of restriction enzymes: Gene splicing by overlap extension. *Gene*, 77(1):61 68, 1989.

[106] Horton R.M. Cai Z. Ho S.N. Pease, L.R. Gene splicing by overlap extension: Tailor made genes using the polymerase chain reaction. *BioTechniques*, 8(5):528 535, 1990.

[107] Arnold K. Bordoli L. Kopp J. Schwede, T. The SWISS MODEL workspace: A web based environment for protein structure homology modelling. *Bioinformatics*, 22(2):195 201, 2006.

[108] Kiefer F. Arnold K. Kunzli M. Bordoli L. Schwede, T. The SWISS MODEL repository and associated resources. *Nucleic Acids Research*, 37(SUPPL. 1):D387 D392, 2009.

[109] M.C. Peitsch. Protein modeling by E mail. *Nature Biotechnology*, 13(7):658 660, 1995.

[110] Grosjean H. Fiers, W. Preferential codon usage in prokaryotic genes: The optimal codon anticodon interaction energy and the selective codon usage in efficiently expressed genes. *Gene*, 18(3):199 209, 1982.

[111] Kuo A. Domene C. Johnson L.N. Doyle D.A. Venien Bryan, C. Two different conformational states of the KirBac3.1 potassium channel revealed by electron crystallography. *Structure*, 13(10):1463 1472, 2005.

[112] GEHealthcare. Superdex 200 10/300 gl instructions and protocols.

[113] Ludwig K. Habbach S. Kriegelstein J. Klumpp S. Konig, S. MALDI-TOF high mass calibration up to 200kDa using human recombinant 16kDa protein histidine phosphatase aggregates. *PLoS ONE*, 6(8), 2011.

[114] Berger B.W. Gendron C.M. Robinson C.R. Kaler E.W. Lenhoff, A.M. The role of protein and surfactant interactions in membrane protein crystallization. *Acta Crystallographica Section D: Biological Crystallography*, 61(6):724 730, 2005.

[115] Marone P.A. Thiyagarajan P. Wagner A.M. Tiede, D.M. Effect of detergent alkyl chain length on crystallization of a detergent solubilized membrane protein: Correlation of protein detergent particle size and particle particle interaction with crystallization of the photosynthetic reaction center from rhodobacter sphaeroides. *Journal of Crystal Growth*, 207(3):214 225, 1999.

[116] D. Linke. Chapter 34 Detergents. An Overview. *Methods in Enzymology*, 463(C):603 617, 2009.

[117] Arakawa T. Timasheff, S.N. The stabilization of proteins by osmolytes. *Biophysical Journal*, 47(3):411 414, 1985.

[118] Hamada H. Arakawa T. Shiraki, K. Effect of additives on protein aggregation. *Current Pharmaceutical Biotechnology*, 10(4):400 407, 2009.

[119] Ito L. Kobayashi T. Shiraki K. Yamaguchi, H. Effect of amino acids and amino acid derivatives on crystallization of hemoglobin and ribonuclease A. *Journal of Synchrotron Radiation*, 15(3):316 318, 2008.

[120] McPherson A. Cudney, B. Searching for silver bullets: An alternative strategy for crystallizing macromolecules. *Journal of Structural Biology*, 156(3):387 406, 2006.

[121] Trakhanov S. Quiocho, F.A. Influence of divalent cations in protein crystallization. *Protein Science*, 4(9):1914 1919, 1995.

[122] Heras B. Martin, J.L. Post crystallization treatments for improving diffraction quality of protein crystals. *Acta Crystallographica Section D: Biological Crystallography*, 61(9):1173 1180, 2005. cited By (since 1996) 64.

[123] Kuo A. Bowler M.W. Zimmer J. Antcliff J.F. Doyle, D.A. Increasing the diffraction limit and internal order of a membrane protein crystal by dehydration. *Journal of Structural Biology*, 141(2):97 102, 2003.

[124] Matar-Merheb R. Rhimi M. Leydier A. Huche F. Galian C. Desuzinges Mandon E. Ficheux D. Flot D. Aghajari N. Kahn R. Di Pietro A. Jault J. M. Coleman A.W. Falson, P. Structuring detergents for extracting and stabilizing functional membrane proteins. *PLoS ONE*, 6(3), 2011.

[125] Caffrey-M. Cherezov, V. Crystallizing membrane proteins using lipidic mesophases. *Nature protocols*, 4(5):706 731, 2009.

[126] Johansson-L.C. Wohri A.B. Katona G. Engstrom S. Neutze, R. Membrane protein crystallization from lipidic phases. *Current Opinion in Structural Biology*, 19(4):372 378, 2009.

[127] Nollert-P. Qiu H. Caffrey M. Rosenbusch J.P. Landau, E.M. Molecular mechanism for the crystallization of bacteriorhodopsin in lipidic cubic phases. *FEBS Letters*, 504(3):179 186, 2001.

[128] Rummel-G. Hardmeyer A. Widmer C. Chiu M.L. Nollert P. Locher K.P. Pedruzzi I. Landau E.M. Rosenbusch, J.P. Lipidic cubic phases: New matrices for the three dimensional crystallization of membrane proteins. *Journal of Structural Biology*, 121(2):82 91, 1998.

[129] Cherezov-V. Rosenbaum D.M. Hanson M.A. Rasmussen S.G.F. Foon S.T. Kobilka T.S. Choi H. J. Kuhn P. Weis W.I. Kobilka B.K. Stevens, R.C. High resolution crystal structure of an engineered human beta 2 adrenergic G protein coupled receptor. *Science*, 318(5854):1258 1265, 2007.

[130] Jaakola-V. P. Griffith M.T. Hanson M.A. Cherezov V. Chien E.Y.T. Lane J.R. Ijzerman A.P. Stevens, R.C. The 2.6 angstrom crystal structure of a human A2A adenosine receptor bound to an antagonist. *Science*, 322(5905):1211 1217, 2008.

[131] DeVree B.T. Zou Y. Kruse A.C. Chung K.Y. Kobilka T.S. Thian F.S. Chae P.S. Pardon E. Calinski D. Mathiesen J.M. Shah S.T. Lyons J.A. Caffrey M. Gellman S.H. Steyaert J. Skiniotis G. Weis W.I. Sunahara R.K. Kobilka B.K., Rasmussen S.G. Crystal structure of the beta 2 adrenergic receptor G protein complex. *Nature*, 477(7366):549 557, 2011.

[132] Faham S. Boulting G.L. Massey E.A. Yohannan S. Yang D. Bowie, J.U. Crystallization of bacteriorhodopsin from bicelle formulations at room temperature. *Protein Science*, 14(3):836 840, 2005.

[133] Ujwal R. Abramson, J. High throughput crystallization of membrane proteins using the lipidic bicelle method. *Journal of visualized experiments : JoVE*, (59):e3383, 2012.

[134] Nishida M. Cadene M. Chait B.T. MacKinnon, R. Crystal structure of a Kir3.1 prokaryotic Kir channel chimera. *EMBO Journal*, 26(17):4005 4015, 2007.

[135] Heginbotham L. Kolmakova Partensky L. Miller, C. Functional reconstitution of a prokaryotic K+ channel. *Journal of General Physiology*, 111(6):741 749, 1998.

[136] C.M. Nimigean. A radioactive uptake assay to measure ion transport across ion channel containing liposomes. *Nature Protocols*, 1(3):1207 1212, 2006.

[137] Epstein W. Kim, B.S. Potassium transport loci in E.coli K 12. *Journal of Bacteriology*, 108(2):639 644, 1971.

[138] Paynter J.J. Andres Enguix I. Fowler P.W. Tottey S. Cheng W. Enkvetchakul D. Bavro V.N. Kusakabe Y. Sansom M.S.P. Robinson N.J. Nichols C.G. Tucker, S.J. Functional complementation and genetic deletion studies of KirBac channels: Activatory mutations highlight gating sensitive domains. *Journal of Biological Chemistry*, 285(52):40754 40761, 2010.

[139] Bavro V.N. De Zorzi R. Schmidt M.R. Muniz J.R.C. Zubcevic L. Sansom M.S.P. Venien Bryan C. Tucker, S.J. Structure of a KirBac potassium channel with an open bundle crossing indicates a mechanism of channel gating. *Nature Structural and Molecular Biology*, 19(2):158 164, 2012.

[140] Krishnan M.N. Bingham J. P. Siew H.L. Trombley P. Moczydlowski, E. Functional role and affinity of inorganic cations in stabilizing the tetrameric structure of the KcsA k + channel. *Journal of General Physiology*, 126(3):271 283, 2005.

[141] Renart M.L. Barrera F.N. Molina M.L. Encinar J.A. Poveda J.A. Fernandez A.M. Gomez J. Gonzolez Ros, J.M. Effects of conducting and blocking ions on the structure and stability of the potassium channel KcsA. *Journal of Biological Chemistry*, 281(40):29905 29915, 2006.

[142] Wang S. Alimi Y. Tong A. Nichols C.G. Enkvetchakul, D. Differential roles of blocking ions in KirBac1.1 tetramer stability. *Journal of Biological Chemistry*, 284(5):2854 2860, 2009.

[143] D'Avanzo N. Cheng W.W.L. Wang S. Enkvetchakul D. Nichols, C.G. Lipids driving protein structure? evolutionary adaptations in Kir channels. *Channels*, 4(3), 2010.

[144] Irizarry S.N. Kutluay E. Drews G. Hart S.J. Heginbotham, L. Opening the KcsA K+ channel: Tryptophan scanning and complementation analysis lead to mutants with altered gating. *Biochemistry*, 41(46):13653 13662, 2002.

[145] Paynter J.J. Sarkies P. Andres Enguix I. Tucker, S.J. Genetic selection of activatory mutations in KcsA. *Channels*, 2(6):413 418, 2008.

[146] Shimomura K. Flanagan S.E. Zadek B. Lethby M. Zubcevic L. Girard C.A.J. Petz O. Mannikko R. Kapoor R.R. Hussain K. Skae M. Clayton P. Hattersley A. Ellard S. Ashcroft, F.M. Adjacent mutations in the gating loop of Kir6.2 produce neonatal diabetes and hyperinsulinism. *EMBO Molecular Medicine*, 1(3):166 177, 2009.

[147] Bushman J.D. Gay J.W. Tewson P. Stanley C.A. Shyng, S. L. Characterization and functional restoration of a potassium channel Kir6.2 pore mutation identified in congenital hyperinsulinism. *Journal of Biological Chemistry*, 285(9):6012 6023, 2010.

[148] Wackett L.P. Dodge A.G. Ellis, L.B.M. Microbial genomics and the periodic table. *Applied and Environmental Microbiology*, 70(2):647 655, 2004.

[149] Bruggemann A. Farre C. Haarmann C. Haythornthwaite A. Kreir M. Stoelzle S. George M. Fertig, N. Planar patch clamp: Advances in electrophysiology. *Methods in Molecular Biology*, 491:165 176, 2008.

[150] Farre C. Haythornthwaite A. Haarmann C. Stoelzle S. Kreir M. George M. Bruggemann A. Fertig, N. Port a patch and patchliner: high fidelity electrophysiology for secondary screening and safety pharmacology. *Combinatorial Chemistry and High Throughput Screening*, 12(1):24 37, 2009.

[151] Clarke O.B. Caputo A.T. Hill A.P. Vandenberg J.I. Smith B.J. Gulbis, J.M. Domain reorientation and rotation of an intracellular assembly regulate conduction in Kir potassium channels. *Cell*, 141(6):1018 1029, 2010.

[152] Cordero-Morales J.F. Jogini V. Lewis A. Vasquez V. Cortes D.M. Roux B. Perozo, E. Molecular driving forces determining potassium channel slow inactivation. *Nature Structural and Molecular Biology*, 14(11):1062 1069, 2007.

[153] Cuello-L.G. Jogini V. Cortes D.M. Perozo, E. Structural mechanism of c type inactivation in K+ channels. *Nature*, 466(7303):203 208, 2010.

[154] Cuello-L.G. Jogini V. Cortes D.M. Pan A.C. Gagnon D.G. Dalmas O. Cordero-Morales J.F. Chakrapani S. Roux B. Perozo, E. Structural basis for the coupling between activation and inactivation gates in K + channels. *Nature*, 466(7303):272 275, 2010.

[155] P. Evans. Scaling and assessment of data quality. *Acta Crystallographica Section D: Biological Crystallography*, 62(1):72 82, 2006.

[156] McCoy-A.J. Grosse Kunstleve R.W. Adams P.D. Winn M.D. Storoni L.C. Read, R.J. Phaser crystallographic software. *Journal of Applied Crystallography*, 40(4):658 674, 2007.

[157] Emsley-P. Cowtan, K. Coot: Model building tools for molecular graphics. *Acta Crystallographica Section D: Biological Crystallography*, 60(12 I):2126 2132, 2004.

[158] Emsley-P. Lohkamp B. Scott W.G. Cowtan, K. Features and development of Coot. *Acta Crystallographica Section D: Biological Crystallography*, 66(4):486 501, 2010.

[159] Blanc-E. Roversi P. Vonrhein C. Flensburg C. Lea S.M. Bricogne, G. Refinement of severely incomplete structures with maximum likelihood in BUSTER TNT. *Acta Crystallographica Section D: Biological Crystallography*, 60(12 I):2210 2221, 2004.

[160] Adams-P.D. Grosse Kunstleve R.W. Hung L. W. Ioerger T.R. McCoy A.J. Moriarty-N.W. Read R.J. Sacchettini J.C. Sauter N.K. Terwilliger, T.C. PHENIX: Building new software for automated crystallographic structure determination. *Acta Crystallographica Section D: Biological Crystallography*, 58(11):1948 1954, 2002.

[161] Adams-P.D. Afonine P.V. Bunkoczi G. Chen V.B. Davis I.W. Echols N. Headd-J.J. Hung L. W. Kapral G.J. Grosse Kunstleve R.W. McCoy A.J. Moriarty N.W. Oeffner R. Read R.J. Richardson D.C. Richardson J.S. Terwilliger T.C. Zwart, P.H. PHENIX: A comprehensive python based system for macromolecular structure solution. *Acta Crystallographica Section D: Biological Crystallography*, 66(2):213 221, 2010.

[162] Moriarty-N.W. Grosse Kunstleve R.W. Adams, P.D. Electronic ligand builder and optimization workbench (eLBOW): A tool for ligand coordinate and restraint generation. *Acta Crystallographica Section D: Biological Crystallography*, 65(10):1074 1080, 2009.

[163] Xu-Y. Shin H. G. Szep S. Lu, Z. Physical determinants of strong voltage sensitivity of K + channel block. *Nature Structural and Molecular Biology*, 16(12):1252 1258, 2009.

[164] Wang-S. Lee S. J. Heyman S. Enkvetchakul D. Nichols, C.G. Structural rearrangements underlying ligand gating in Kir channels. *Nature Communications*, 3, 2012.

[165] Gupta-S. Bavro V.N. D'Mello R. Tucker S.J. Venien Bryan C. Chance, M.R. Conformational changes during the gating of a potassium channel revealed by structural mass spectrometry. *Structure*, 18(7):839 846, 2010.

[166] Bayley-H. Cronin B. Heron A. Holden M.A. Hwang W.L. Syeda R. Thompson-J. Wallace, M. Droplet interface bilayers. *Molecular BioSystems*, 4(12):1191 1208, 2008.

[167] Miller-A.N. Long, S.B. Crystal structure of the human two pore domain potassium channel K2P1. *Science*, 335(6067):432 436, 2012.

[168] Brohawn-S.G. Del Marmol J. MacKinnon, R. Crystal structure of the human K2P TRAAK, a lipid and mechano sensitive K + ion channel. *Science*, 335(6067):436 441, 2012.

[169] Shimamura-T. Shiroishi M. Weyand S. Tsujimoto H. Winter G. Katritch V. Abagyan-R. Cherezov V. Liu W. Han G.W. Kobayashi T. Stevens R.C. Iwata, S. Structure of the human histamine H 1 receptor complex with doxepin. *Nature*, 475(7354):65 72, 2011.